EFFECT OF NITRIC ACID OXIDATION ON VAPOR GROWN CARBON FIBERS (VGCFs). USE OF THESE FIBERS IN EPOXY COMPOSITES

BY

PRIYA V. LAKSHMINARAYANAN

A Thesis
Submitted to the Faculty of
Mississippi State University
in Partial Fulfillment of the Requirements
for the Degree of Master of Science
in Chemical Engineering
in the Dave C. Swalm School of Chemical Engineering

Mississippi State, Mississippi

August 2003

EFFECT OF NITRIC ACID OXIDATION ON VAPOR GROWN CARBON FIBERS (VGCFs). USE OF THESE FIBERS IN EPOXY COMPOSITES

By

Priya V. Lakshminarayanan

Approved:

Hossein Toghiani Associate Professor of Chemical Engineering (Major Professor and co-director of Thesis)	Charles U. Pittman, Jr. Professor of Chemistry (Co-director of Thesis)
Kirk H. Schulz Earnest W. Deavenport Jr. Chair and Director Professor of Chemical Engineering (Committee Member)	Rebecca K. Toghiani Associate Professor of Chemical Engineering (Committee Member)
Mark E. Zappi Texas Olefins Professor of Chemical Engineering (Graduate Coordinator of Dave C. Swalm School of Chemical Engineering)	A. Wayne Bennett Dean of the Bagley College of Engineering

Name: Priya V. Lakshminarayanan

Date of Degree: August 2 , 2003

Institution: Mississippi State University

Major Field: Chemical Engineering

Major Professor: Dr. Hossein Toghiani

Co-Directors of Thesis: Dr. Hossein Toghiani and Dr. Charles U. Pittman, Jr.

Title of Study: EFFECT OF NITRIC ACID OXIDATION ON VAPOR GROWN CARBON FIBERS (VGCFs). USE OF THESE FIBERS IN EPOXY COMPOSITES

Pages in Study: 125

Candidate for Degree of Master of Science

Pyrograf III™ fibers (PR-19-PS, Applied Sciences, Inc.) with 100-300 nm diameters and ~ 10-100 μm lengths were used with a low viscosity aliphatic epoxy resin (Clearstream 9000, Clearstream Products, Inc.) to produce composites. The VGCFs were oxidized in 69-71 wt% nitric acid (115°C) for various times (10 min to 24 h) to modify the surface to enhance fiber/matrix adhesion. Remarkably, little fiber weight loss was detected even after 24 h of oxidation. Composites containing 19.2 volume percent (29.4 weight percent) VGCFs were prepared. Their flexural strengths and flexural moduli were obtained. The flexural strengths did not increase using oxidized VGCFs. Fiber surfaces were characterized using N_2 BET, CO_2 DR, XPS, SEM, TEM and base uptake measurements. Increasing the oxidation time produced only small initial increases in surface area up to a limit. Significant surface oxygen was present before oxidation and the amount increased initially, though not continuously, with nitric acid oxidation.

DEDICATION

To my mother, Mrs. K.N. Vijayam and my father, Mr. K.S. Lakshminarayanan:

"For all those times you stood by me
For all the truth that you made me see
For all the joy you brought to my life
For all the wrong that you made right
For every dream you made come true
For all the love I found in you
I'll be forever thankful
You're the one who held me up
Never let me fall
You're the one who saw me through
Through it all"

- Celine Dion

ACKNOWLEDGEMENTS

I would like to thank Dr. Hossein Toghiani for serving as my major adviser and co-director of my thesis who provided me with guidance throughout my research and thesis.

I would also like to thank Dr. Charles U. Pittman, Jr., for serving as my thesis co-director and committee member. He provided valuable feedback and assistance as well as financial support during early stages of my program of study. Special appreciation to Dr. Kirk H. Schulz for assisting me in analyzing the XPS results and to Dr. Rebecca K. Toghiani for serving as my committee member and providing valuable suggestions during my course of study.

I would also like to thank Dr. Lichang Wang, Hanli Ni, Jun Xu, Venkata R. Chilukuri and Holly Martin for providing valuable help in my research work.

Last, but not the least, my special thanks to my parents Mr. K.S. Lakshminarayanan and Mrs. K.N. Vijayam who gave me the opportunity to fulfill my dream of pursuing my MS degree and encouraging me to do my best, my best buddy, Viswanath Kiran Chittoori for lightening me when I found the going tough and to my spiritual masters Sri Kalki Bhagavan and Amma Bhagavan for helping me complete a 'stress-free' MS.

TABLE OF CONTENTS

CHAPTER Page

LIST OF TABLES

TABLE Page

LIST OF FIGURES

FIGURE Page

FIGURE Page

FIGURE Page

CHAPTER I

INTRODUCTION

History

The earliest known reference to vapor grown carbon fibers (VGCFs) is an 1889 patent by Hughes and Chambers [1] describing the growth of "hair-like carbon filaments" from a mixture of hydrogen and methane in an iron cubicle. These thickened carbon filaments, formed by chemical vapor deposition, were thick enough (~20 μm in diameter) to be observed by the naked eye. It was not until the invention of the electron microscope that Davis, Lawson and Rigby [2] were able to observe nanometer-sized diameter carbon filaments for the first time. This discovery of filamentous carbon inspired a multitude of papers on the observation of carbon filaments [3]. Meanwhile, parallel literature on vapor grown carbon fibers developed [4] without a clear understanding that VGCFs were simply carbon filaments thickened by vapor-deposited carbon. With the development of conventional rayon and polyacrylonitrile (PAN)-based carbon fibers (7-10 μm in diameter), researchers studying VGCF recognized that these fibers could be useful as a reinforcement. Efforts to produce VGCF of approximately 10 μm in diameter with a length longer than 1 mm were published by Koyama and Endo in Japan [5], Benissad et al. [6] in France, and Tibbetts [7] in the USA. Despite the inexpensive feedstocks used by these researchers, the long periods required in the reaction chamber and sparse

product yields produced by these methods proved impractical for most of the applications. Koyama and Endo [8], Hatano, Ohsaki, and Arakawa [9] and others sought to develop a continuous process to produce smaller diameter VGCFs in higher yields by the mid 1980's. Applied Sciences Inc., (ASI) in USA, first marketed VGCFs produced from methane in a tubular furnace.

The carbon fibers are produced by catalytic dehydrogenation of a hydrocarbon (methane, benzene or naphthalene) at high temperatures in a flow system. Small particles of transition metals like iron (10 nm diameter) are heated in an atmosphere of hydrogen and hydrocarbon vapors [10,12]. The iron particle is the nucleation site for the fiber tip. Therefore, the initial carbon filament diameter is directly proportional to the iron particle diameter, i.e. 10 nm [13-15]. The initial iron particle size must be very small (<15 nm) because a considerable decrease in activity is observed when the iron particle diameter exceeds 15 nm [17]. It is very important to retain the small particle size in the flowing gas and to avoid particle coagulation to a larger ineffective diameter [17]. The iron particles may begin extruding long slender filaments of fairly graphitic carbon at over 900°C. Figure 1.1 shows the method by which these fibers are produced. They grow as rapidly as 1 mm/min and lengthen for several minutes until the iron particle is deactivated [10,16]. These filaments may be of several centimeters in length but only 10 nm in diameter. Figure 1.2 illustrates the growth of fibers in a reaction chamber. These filaments can be thickened by chemical vapor deposition of carbon to become macroscopic fibers as shown in Figure 1.5 [10]. This carbon chemical vapor deposition process causes the fibers to develop the morphology shown in Figure 1.5. X-ray and electron diffraction studies by Oberlin et al. have shown that the filaments are comprised of concentric

cylinders of graphitic basal planes and are preferentially oriented parallel or at highly oblique angles to the fiber axis [11].

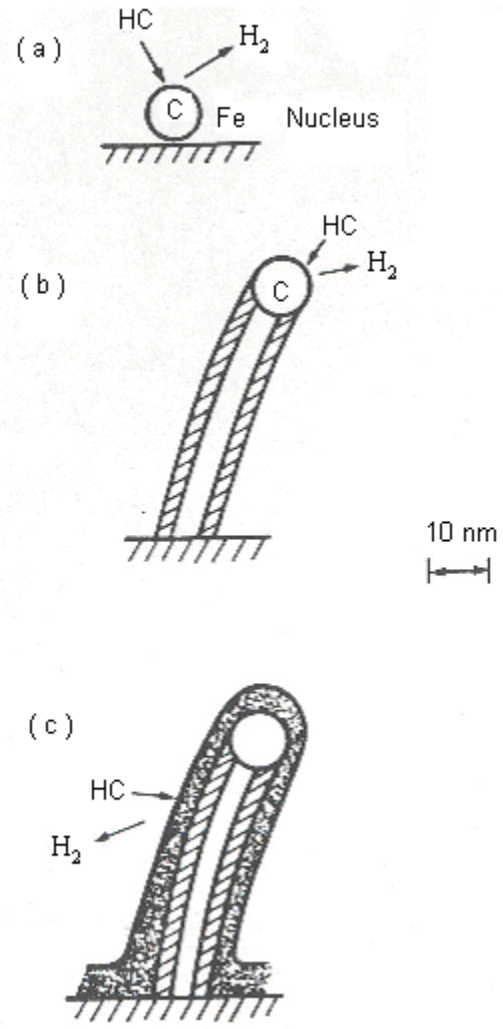

Figure 1.1 Description of the production of VGCF. (a) During the saturation phase an iron particle is loaded with carbon from the gas phase. (b) A carbon filament then precipitates and lengthens as more carbon is supplied by the gas phase. (c) Finally, the filament is thickened by vapor deposited carbon. [c]

[c] Tibbetts, G.G., Endo, M., and Beetz C P Jr., *SAMPE J.*, **1986**, *22*, 30.

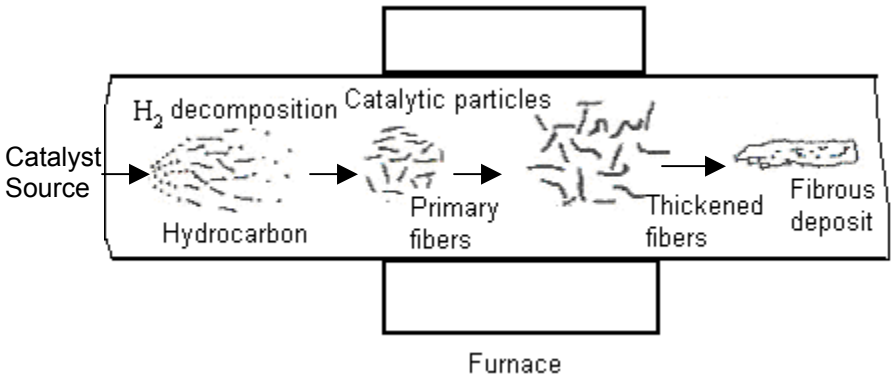

Figure 1.2 Three-dimensional growth of fibers in a reaction chamber.

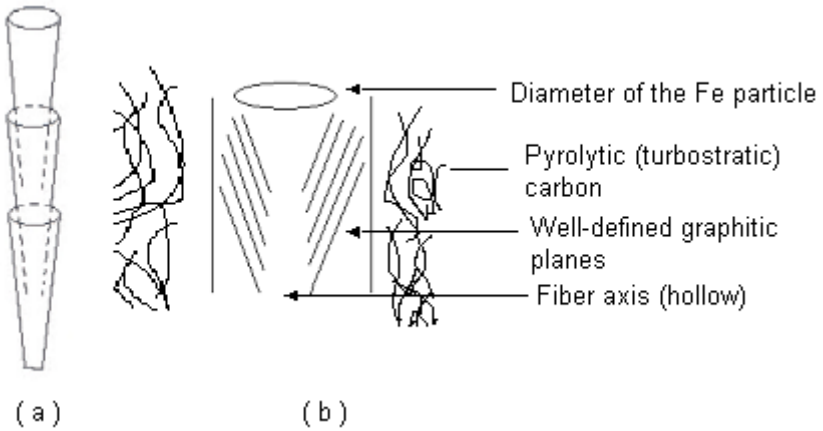

Figure 1.3 Schematic representation of the structure of VGCF: a) Concentric cones of graphitic planes b) Fiber longitudinal section along the fiber axis

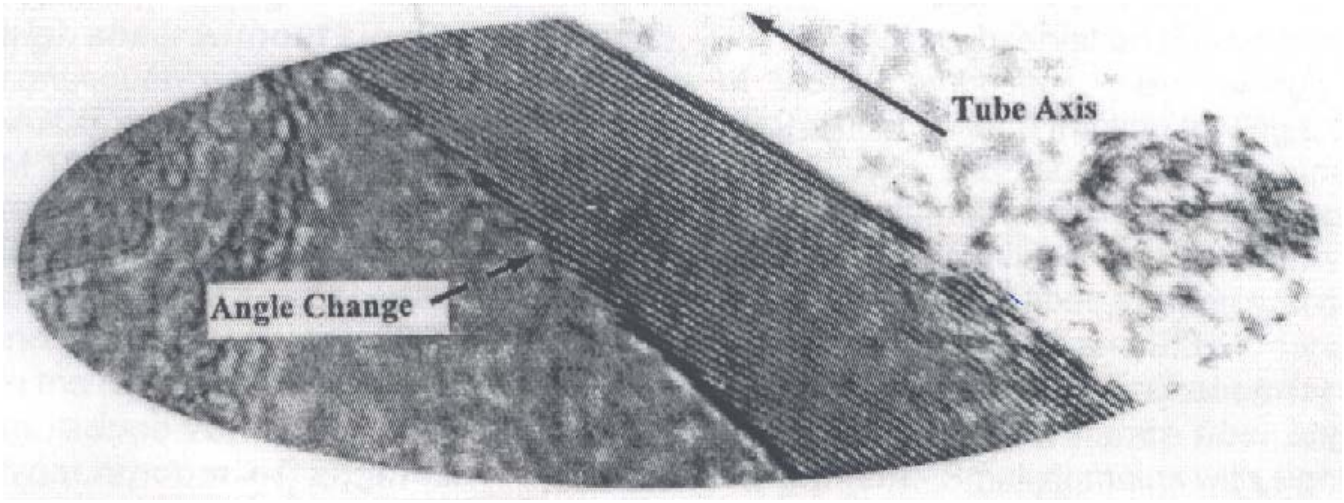

Figure 1.4 TEM image of the wall of a carbon nanotube(VGCF) grown by ASI's Pyrograf III™ process. The light portion to the right is the hollow core. The parallel lines at the center are the graphitic planes of the initially formed filament of the catalytically grown carbon. At left is less orderly CVD pyrolytic (turbostratic)carbon.

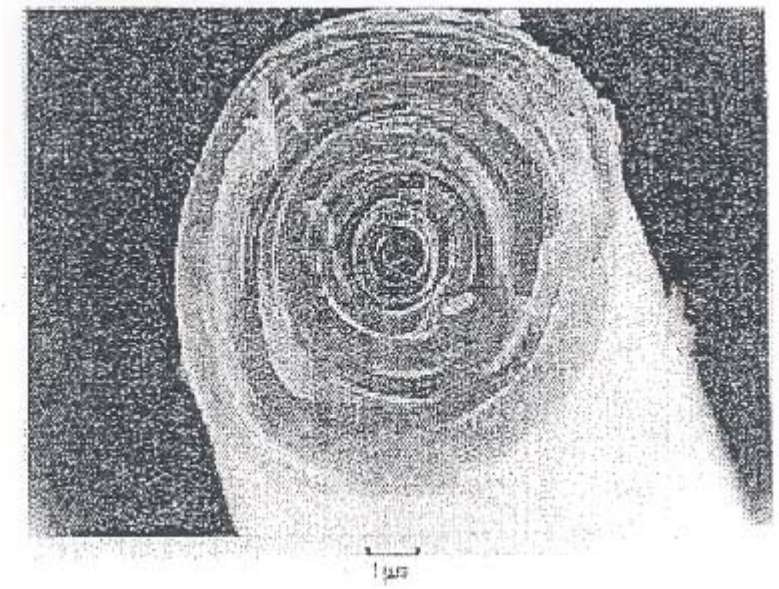

Figure 1.5 Transverse section of large sized (Pyrograf I™-type) VGCF showing tree ring morphology.

Advantages and disadvantages of VGCFs

VGCFs have two main advantages, cost and availability. They can be very inexpensive due to their size and by the use of natural gas as the source of hydrocarbon gas [18,19]. The fiber diameter is a cost driver for VGCF [19]. Smaller fibers like Pyrograf III™ (0.06 - 0.3 μm diameter, 50-100 microns in length) require less time in a continuous flow reaction chamber, thus reducing cost [18,19]. Pyrograf I™, which has a fiber diameter between 1-100 μm (10 to 300 times the size of Pyrograf III™), is much more expensive due to its much greater exposure time in the reactor and also because it is grown from a stationary surface. Thus, this non-continuous process for the manufacture of Pyrograf I results in lower throughput.

The disadvantages associated with Pyrograf III™ VGCFs include obtaining a non-standardized product, lack of a detailed knowledge of its material properties, and fiber packing problems. Since Pyrograf III™ fibers are very small, the individual fiber material properties are extremely difficult to measure [14,18,19]. Patton and Pittman have recently reported lower limits for their flexural moduli and flexural strengths [18,15]. Table 1.1 shows the mechanical property comparison between Pyrograf I™ and Pyrograf III™ [28].

Table 1.1 Mechanical property comparison between Pyrograf I™ and Pyrograf III™ [a]

Property	Pyrograf I™	Pyrograf III™
Diameter	1-100 μm	0.1-0.3 μm
Tensile strength	2.7 GPa	1.70-3.38 GPa [b]
Young's modulus	400 GPa	88-166 GPa [b]

[a] Patton, R.D., Pittman Jr.C.U. and Wang, L.,*Composites: Part A*, **1999**, *30A (9)*,1081.

[b] These values were calculated from the rule of mixtures after measuring the properties of VGCF/epoxy composites with 15% and 19% wt. VGCF, which were mixed in a high speed blender followed by extensive two-roll milling. They represent the lower limits of the properties because these composites have flaws. If they were perfect, the tensile strengths and tensile moduli of these composites (and hence that calculated for the fibers) would be higher.

Mechanical properties have been measured for much smaller carbon nanotubes by atomic force microscopy [20-22]. Due to their size, no testing equipment or techniques exist at this time for measuring the mechanical and thermal properties of Pyrograf III™ fibers. Hence, their material properties are often assumed to be similar to those of Pyrograf I™, since their preparation differs only in the growth time used. Furthermore, approximations of both flexural and tensile moduli and flexural and tensile strength of Pyrograf III™ deduced from composites prepared in our laboratory, and elsewhere, agree with this premise (see Table 1.1). However, the ratio of the pyrolytic carbon outer region to the tubular graphite inner core is different for these two classes of fibers. At present, little data exist for Pyrograf III™ fibers. Table 1.2 lists the material properties for

Pyrograf I™ fibers, under the assumption that the two classes of fibers have similar properties.

Table 1.2 Properties of Pyrograf I™ fibers [a].

Property	Value	Units
Fiber diameter	1-100	μm
Tensile strength	2.7	Gpa
Tensile modulus	400	Gpa
Ultimate strain	1.5	%
Density	1.8	G/cm^3
Coefficient of thermal expansion	-1.0	ppm/°C
Electrical resistance	1000	μΩcm
Thermal conductivity	20	W/mK

[a] Applied Sciences, Inc. (ASI, Cedarville, Ohio)

Mechanical properties of VGCFs

Mechanical properties control many applications of composites, and much research on VGCF composites has focused on determining these properties [23]. Chellappa et al. [24], Shui and Chung [25], as well as Ciminelli et al. [26] obtained poor mechanical properties when testing VGCF composites. Chellappa et al. [24] attributed poor mechanical results in the VGCF composite they prepared to poor fiber/matrix adhesion, poor fiber dispersion, the presence of voids and use of a weak thermoplastic elastomer matrix having a 0.1 MPa ultimate strength. Shui and Chung [25] and Ciminelli et al. [26] attributed the poor mechanical properties to insufficient bonding between the VGCF and the matrix. It also appears that they achieved poor fiber wetting and poor fiber dispersion.

The first strength improvements in VGCF composites were observed by Patton, Pittman and Wang [15,18,19]. The main variable contributing to these strength improvements was the use of pre-cure high shear mixing techniques. These techniques aided in resin infusion, which is one of the two most important problems associated with making VGCF composites. VGCFs were mixed with a low viscosity epoxy resin using a high-speed blender. A two-roll mill was then used to provide high shear mixing. After curing and stress/strain analysis, the values obtained for the flexural moduli and flexural strength of these fibers (Pyrograf III™) were approximated using the rule of mixtures. The lower limits of VGCF's flexural moduli and flexural strength obtained are shown in Table 1.1 [28]. It was observed that composites with high fiber volume fractions did not exhibit any strength improvements. These composites had poor mechanical properties due to their high porosity resulting from fiber packing problems and fiber nesting.

The most striking property improvements yet achieved by using Pyrograf III™ fibers were reported by Kumar et al. [27]. VGCF/poly(propylene) (5/95 wt./wt.) composite fibers were prepared by a twin screw extrusion (high shear mixing) followed by melt spinning and drawing. This produced polypropylene fibers containing highly aligned fibers, which were oriented along the fiber axis and were not aggregated. Property improvements were reported in tensile strength (16.3%), tensile modulus (54.3%) and compressive strength (92%) versus the corresponding properties for 100% Poly(propylene) fibers [27]. Based on rule of mixtures and the tensile strength and tensile modulus of the composite used, the tensile modulus of the fiber was found to be 117 GPa and the tensile strength was found to be 4077 MPa (assuming perfect one dimensional alignment along the fiber axis). According to SEM studies of the composites, Pyrograf

III™ appears to be highly random in a 3-D orientation. This would result in the modulus of the fiber to be greater than 117 GPa. Patton, Pittman and Wang [15,18,19] have reported the modulus of Pyrograf III™ fibers to be between 88 and 166 GPa.

Problem areas

1) Packing and resin infusion

VGCFs present serious packing problems. These fibers are curved and tangled and do not lie down easily into mats. They are difficult to align due to their small size and entanglements. These fibers come in light, fluffy bundles with a density of about 0.01 g/cm^3 (0.5% fiber volume fraction, V_f). Even after standard debulking (wet grinding, compression, etc), the fiber volume fraction could be increased to only about 3%. This creates serious problems during composite fabrication from VGCF, and in shipping VGCFs. The apparent volume of the fibers can be divided into two parts. One part is caused by the elasticity of the fibers. When pressure is applied, this part of the apparent volume is reduced. The other part is caused by the randomness of fiber orientation and by the aspect ratio of the fibers. This part of the apparent volume is not affected by pressure, unless the pressure is great enough either to break the fibers, thus reducing the aspect ratio, or to decrease the average fiber radius of curvature. Since most VGCFs are curved, decreasing the average radius of curvature leads to a decrease in the effective aspect ratio of the fibers.

The maximum packing fraction of cylindrical rods having a random three-dimensional orientation has been investigated both theoretically and experimentally [29].

The packing efficiency varies with the aspect ratio (L/D). The maximum three-dimensional random packing fraction, when L/D >50, yields a fiber volume fraction of only around 10% using both theoretical and experimental approaches [10]. The curvature and entanglements present in the Pyrograf III™ VGCF reduce its effective L/D, while the range of fiber sizes also improves the packing efficiency. There is an upper limit to the fiber volume that can be achieved by pressing the VGCFs before the fibers begin to break. During composite preparation, substantial pressure is needed in order to achieve reasonable fiber loading (>20% V_f for best results). These features make it difficult to obtain VGCF composites with high fiber volume fractions.

As the V_f of VGCF in composites increases, these composite samples exhibit large increases in porosity [15]. This increase in voids lowered the ultimate strength of the samples [15]. The low packing fraction available using random three-dimensional VGCF orientation is a severe limitation on the maximum fiber volume fraction attainable. This limitation could be reduced by moving from a random three-dimensional orientation to a two-dimensional orientation. The use of high shear mixing of VGCF with the matrix resin appears to be one of the more practical approaches possible to achieve this goal. The large surface area of these fibers makes resin infusion very difficult, particularly as V_f increases. The resin at the fiber surfaces forms a surface boundary layer. These boundary layers compose a much larger fraction of the total composite's volume when small-sized VGCFs are used instead of PAN or pitch carbon fibers at the same volume fractions. This makes the distribution of resin to all areas of the composite difficult to achieve. The resin infusion (i.e., the quality of contact between the fibers and resin) cannot be measured directly, although porosity provides an indirect measurement.

Additionally, the distribution of void sizes and incomplete fiber wetting may be as important as the value of total porosity in degradation of composite properties. Thus, even in composites with relatively low porosities, considerable degradation of properties may occur due to pore distribution.

2) Infiltration

It is difficult to form void-free composites with thin fibers because of the high viscous dynamic drag impeding the infiltration of polymer between the fibers [30]. A one-dimensional solution of Darcy's law [31] can be used to calculate the infiltration depth, d. Equation 1.1 describes d in a viscous fluid of viscosity, μ, applied pressure, P_o, and a duration of infiltration, τ, permeating a volume fraction of fibers, V and with the permeability, K, of the preform or mass of fibers.

$$d = \sqrt{\frac{2KP_o}{\mu(1-V)}} \qquad \text{Eq 1.1}$$

For fibrous materials of radius r, equation 1.2 has been shown to represent the permeability fairly well [31].

$$K = \frac{2r^2\sqrt{2}}{gV}\left[1-\frac{\sqrt{4V}}{\sqrt{\Pi}}\right] \qquad \text{Eq 1.2}$$

The dependence of K on r^2 means that K for 0.1 μm fibers is only 10^{-4} times the value for conventional 10 μm fibers. This extremely small value of K leads to very slow infiltration rates. Dispersing and mixing the fibers before infiltration, infiltrating at high

pressures, using less viscous polymers and infiltrating for long periods, can help solve this problem. High shear mixing also assists this goal. It has been reported that one practical solution has been to decrease the average size of the nested clumps of fibers, making resin infiltration of the clumps easier [30].

3) Orientation

Composites formed with randomly oriented fibers have considerably poorer mechanical properties than those in which the fibers are one- or two-dimensionally oriented [32]. This has been explained in detail in section 1 of problem areas.

4) Debulking

During the chemical vapor deposition thickening process of the filaments, the masses of entangled filaments become cemented together in places by the carbon coating, rendering any prospect of ‘combing’ the fibers into a more tractable form very difficult. Applied Sciences, while growing Pyrograf fibers, found that well-formed clumps of long fibers coming out of the reactor have an apparent bulk density less than 0.001 g/cc [30]. It is easy to compress this material to around 0.05 g/cc, but further compression can be destructive to the fibers and diminish the mechanical or electrical properties of the resulting composites [30]. Converting this substance into a dense material, which can be conveniently poured into the hopper of an injection-molding machine, is a challenge, which must be overcome before further applications can be realized.

Surface treatments

Unlike traditional PAN- or pitch-based carbon fibers, the unique growth mechanism that forms VGCFs, results in fibers with a lower concentration of functional groups on the surface [35]. This may result in inadequate bonding between the VGCF and the polymer matrix. Consequently, polymer composites reinforced with VGCF may exhibit mechanical properties that are inferior to those of polymer composites reinforced with commercial PAN or pitch based carbon fibers. To increase the surface concentrations of functional groups, various surface modification methods have been investigated [33], including *in situ* modifications and post-process modifications. Surface spectroscopy indicated that the surface concentrations of various functional groups, especially functional groups containing oxygen, could be increased by these treatments [33]. The chemical nature of the surface carbons such as ratio of aliphatic to aromatic carbon and the size of the aromatic system depends on the surface treatment. Since the average VGCF diameter (0.2 μm) is very small compared to that of PAN- or pitch-based carbon fiber (5-10 μm) [34], these surface treatments are thought by some to also affect the bulk chemistry and structure of VGCF in addition to the surface chemistry [33a].

Interfacial adhesion has been a topic of concern in composites technology for decades [35-37]. Previous studies have attempted to generate strong adhesion between the fiber surface and the matrix [38-41]. Numerous methods have been developed to improve the wetability of the fiber surface or to increase the quantity of the surface functional groups [39,40]. However, the presence of strong interfacial bonding alone may not always lead to satisfactory composite properties. For example, the presence of a tightly bound, but stiff, interface can result in high stress concentrations at the interface,

which result in low impact strength [42]. The introduction of a strongly bound, concentric, elastomeric interphase layer between the matrix and fiber might be expected to improve this situation significantly [43-47]. However, the extent of chemical bonding of this elastomeric interphase to both the matrix and fiber surface will be an important consideration. Without substantial covalent bonding to augment adhesion between the two interfaces (fiber/elastomer and elastomer/matrix), the fiber-to-matrix adhesion could be weak. Rupture of either interface could degrade composite properties. Investigations of composite systems containing such fiber-bound elastomeric interphases have been reported [48-52].

Surface studies of VGCFs

1) Surface chemistry

The functional groups present on the surface of the carbon fibers can enhance the surface chemical bonding between the fibers and the matrix. Therefore, many types of analyses have been employed to characterize the surface functions of PAN-based fibers [53,54]. The traditional analytical methods, such as base neutralization, have been employed to analyze the fiber surface. Previous studies of PAN-based carbon fibers have shown that oxidized carbon surfaces usually contain phenolic, aryl ether, ketone, carboxylic acid, anhydride, and ester groups, etc. [55-57]. Thus, reactions with amines, acids, isocyanates, epoxy resins, alcohol, etc., can be expected.

Many fiber structure models (PAN-/Pitch-based fibers) have been reported in the last two decades [58-61]. None of these models could explain all the fiber properties. Two general types of carbon exist in PAN-based fibers: graphitic sheets and non-

graphitic (amorphous) carbon structures [62]. Moreover, graphite layers exist as basal planes and lateral planes, based on the orientation of graphite layers to the fiber surface. The amorphous regions of PAN-based fibers consist of graphitizable and non-graphitizable carbon. Graphitized carbon can be converted into more stable graphitic structures by heat treatment [63]. The non-graphitized carbon is amorphous and it cannot be converted into graphitic structures even on increasing the temperature to 3500°C.

Vapor grown carbon fibers have a very different morphology and structure than PAN- or pitch- or rayon based fibers. It has been shown that the largest portion of the surface of VGCF consists of graphite-like structures [64]. The central filament of the VGCFs is hollow with the walls comprised of well-organized graphitic planes wrapped as cones along the fiber axis. The central filament is covered by a layer of turbostratic/pyrolytic carbon deposited by CVD once the filament diameter has grown to the diameter of the catalyst particle. About one-fifth of the carbon present in this layer is different from well-ordered graphite (e.g. a twisted graphite-like region with many defects) [33]. The presence of graphite-like structures is important, since they are known to be the active sites for the interaction with polymers [33]. In contrast to PAN-based carbon fibers, these less-ordered carbon structures in VGCFs are stable at higher temperature [64]. The concentration of surface oxygen groups on VGCF is lower than on PAN- or pitch-based carbon fibers, according to the group at ASI, Inc. [64].

Scanning and transmission electron microscopy have also been employed to characterize these VGCFs. Previous research on the behavior of VGCF towards air oxidation has shown that the core of the fibers is more resistant to air oxidation [65]. SEM pictures obtained by Serp et al. [65] on larger diameter VGCFs shows the inner core

of the fiber remains unaffected by air oxidation. Figure 1.6 shows the SEM micrograph obtained by Serp et al. showing the carbon filament present in the inner core. This rationalization sheds light on the surface area results obtained on small Pyrograf III™ VGCFs obtained in this thesis (e.g. increasing oxidation gave only a small increase in fiber surface area). In the present research, a substantial increase in surface area could not be observed with small (200 nm diameter) Pyrograf III™ VGCF even after oxidizing them for 90-minutes (115 °C). It could be inferred that both the core and the outer CVD carbon of the fiber are resistant to nitric acid oxidation. Further explanation is provided in Chapter III.

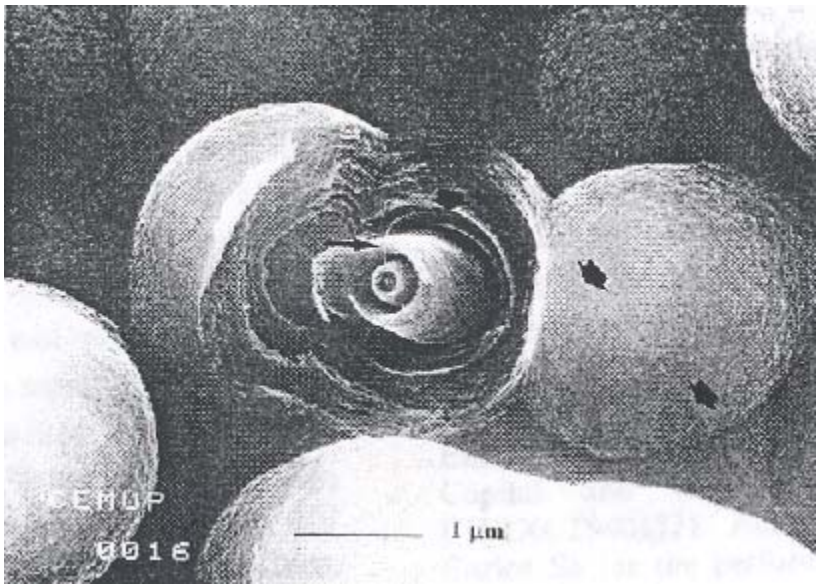

Figure 1.6 SEM micrograph obtained by Serp et al. showing the carbon filament present in the inner core.

Serp.P., Figueiredo, J.L. *Carbon*, **1997**, *35(5)*, 675-683.

XPS measurements have also been used in this thesis to analyze fiber surfaces (oxidized and unoxidized VGCFs). Even though the detection depth of the XPS probes only several tens of Å below the surface, it is a powerful and quick method to obtain information regarding the outer fiber surface region. However, XPS usually suffers from two major problems: (1) XPS is not sensitive enough to give useful information on trace atoms; and (2) the chemical shifts are too small to differentiate all the oxidation states of carbon and oxygen functional groups generated on the fiber surface. This also makes it necessary to use curve fitting operations to approximate the contributions from individual oxidation states.

2) Surface area determination

Both chemical analysis and physical analysis of the surface are important tools used to study the properties of composite material. Increasing the fiber surface area can improve the material-matrix adhesion. Weak surface regions can be removed by cleaning the fibers [69,70]. Increasing the amount of chemical bonding between the fiber and matrix can also greatly improve adhesion [71]. Surface roughness of certain dimensions can cause fiber/matrix mechanical interlocking, which enhances adhesion. Measurements of surface areas are usually performed using the Brunauer, Emmett and Teller (BET) method [72] or the Dubinin-Radushkevich (DR) method [73,74]. Ever since the BET theory was published, it has remained the most widely used procedure for the determination of the surface area of a porous material. This theory was derived from the Langmuir model [75], while considering multilayer adsorption. The BET equation is [76] :

$$\frac{p}{n(p^0 - p)} = \frac{1}{n_m c} + \frac{(c-1)\,p}{(n_m c)\,p^0} \qquad \text{Eq 1.3}$$

Where: p = partial pressure.

p^0 = saturation vapor pressure

c = a constant related to adsorption heat, liquefaction heat and temperature.

n_m = weight of adsorbate constituting a monolayer of surface coverage.

n = weight of gas adsorbed at a relative pressure, p/p^0

A plot of $p/n(p^0-p)$ against p/p^0 should be linear. Generally, nitrogen BET is measured at 77 K [77]. The weight of a monolayer, n_m, is obtained from the slope s and intercept i of the BET plot. From equation 1.3

$$s = \frac{c - 1}{n_m c} \qquad \text{Eq 1.4}$$

$$i = \frac{1}{n_m c} \qquad \text{Eq 1.5}$$

Thus, the weight of monolayer can be obtained by combining Eq 1.4 and Eq 1.5:

$$n_m = \frac{1}{s + I} \qquad \text{Eq 1.6}$$

The total surface area, S_t, of the sample is then expressed as:

$$S_t = \frac{n_m N A_{cs}}{M} \qquad \text{Eq 1.7}$$

where N = Avagadro's number (6.023×10^{23} molecules/g mol)

M = molecular weight of adsorbate

A_{cs} = cross sectional area of adsorbate molecule (16.2 $Å^2$ for nitrogen)

DR theory is based on a relationship between the degree of micropore filling and the Gibbs free energy. It is widely used to describe the adsorption of sub-critical vapors in microporous solids. The usefulness of the equation (See Eq 1.8) lies in the fact that the temperature dependence is reflected in the adsorption potential i.e. if the adsorption data at different temperatures are plotted as the logarithm of the amount of the test compound adsorbed versus the square of adsorption potential, all the data points should fall into one curve (due to the pressure range in which the equation is applicable) called the characteristic curve [98].

$$E = - R \times T \times \ln (p/p_o) \qquad \text{Eq 1.8}$$

where E = adsorption potential

R = universal gas constant

T = absolute temperature.

p = saturated vapor pressure.

po = pressure of the bulk phasae.

The existence of the characteristic curve has been proven in numerous cases by Dubinin and other workers [98]. Dubinin assumed that the adsorption energies of the

adsorption sites on a surface exhibited a Gaussian distribution. The equation employed by DR theory is [73,74]:

$$\log n = \log n_m - k \log^2 (p^0/p) \qquad \text{Eq 1.9}$$

where $k = 2.303\ K\ (RT/\beta)^2$

K = a constant based on the pore size distribution shape

R = universal gas constant

$\beta = E / E_{ref}$ where E is the adsorption potential

T = absolute temperature.

n = weight of gas adsorbed at a relative pressure, p/p^0

Plots of log (n) versus $\log^2(p^0/p)$ should be linear. The value for n_m is then measured from the intercept from which the micropore volume is calculated. The micropore surface area is readily calculated using Eq 1.7. The major difference between these two methods is the operating temperature. The higher temperature used in CO_2-DR measurements provides the required kinetic energy to permit active diffusion of the CO_2 molecules.

Electromagnetic interference (EMI) shielding

Electromagnetic interference (EMI) exists when an electromagnetic disturbance induces undesirable voltages or currents that adversely influence the performance of electronics or electrical devices [82,86]. At present, there are concerns about EMI in three types of environments: radio communications, electronic devices and electromagnetic pollution on human health. To manage EMI, EMI shielding is introduced [87]. EMI shielding refers to the attenuation of electromagnetic radiation by a material through

reflection and/or absorption [87]. This shielding prevents penetration of external electromagnetic radiation through the barrier. There are three types of EMI shielding mechanisms: reflection, absorption and internal re-reflection. When an incident electromagnetic wave hits a shielding material, a part of the incident wave is reflected while the rest of the wave penetrates into the shielding material. The shielding material absorbs a part of this transmitting wave. When the transmitting wave hits the other side of the shielding material, a part of the wave is re-reflected into the shielding material while the rest of the wave emerges out as the transmitted wave. This mechanism is shown in Figure 1.7 [82].

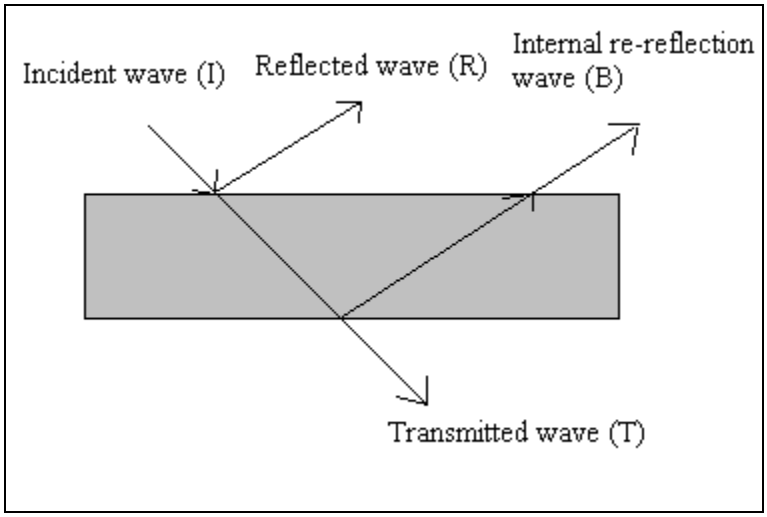

Figure 1.7 EMI shielding mechanism.

The electromagnetic shielding effectiveness (SE) can be defined for plane-waves, electric fields and magnetic fields [82,88]. For plane waves:

$$SE\ (dB) = 10 \log (P_i/P_t) \qquad \text{Eq 1.10}$$

where SE = shielding effectiveness

P_i = incident plane-wave intensity

P_t = transmitted plane-wave intensity

For the electric field, E:

$$SE\ (dB) = 20 \log (E_i/E_t) \qquad \text{Eq 1.11}$$

where E_i = incident electric wave intensity

E_t = transmitted electric wave intensity

For the magnetic field, H:

$$SE\ (dB) = 20 \log (H_i/H_t) \qquad \text{Eq 1.12}$$

where H_i = incident magnetic wave intensity

H_t = transmitted magnetic wave intensity

Consequently, equation 1.12 describes the sum of the three EMI shielding mechanisms [82,89].

$$SE = R + A + B \qquad \text{Eq 1.13}$$

where R = reflection loss

A = absorption loss

B = internal re-reflection loss

The reflection loss, absorption loss and internal re-reflection loss are all frequency dependent. In short, the shielding effectiveness increases with an increase in frequency. Consequently, high frequency electromagnetic waves only penetrate the near surface region of a shielding material [87]. This is called the skin effect. Metals are the best shielding materials. As a result of skin effect, only a very thin layer of metal is needed for EMI shielding purposes [90]. Hence, metal foils or coatings are the most commonly used metal shielding materials. In this research, aluminum foil was used as the shielding material. Further details on EMI shielding are available elsewhere [82].

CHAPTER II

EXPERIMENTAL

Materials used

Unoxidized vapor grown carbon fibers (VGCFs) bought from Applied Sciences, Inc., were used in this research. The grade of VGCFs used along with their properties is shown in Table 2.1. The epoxy resin used was a low viscosity aliphatic epoxy resin containing Bisphenol A epoxide, Bisphenol F epoxide and proprietary aliphatic glycidyl ether (Clearstream 9000, Clearstream Products, Inc., Figure 2.1). The curing agent used in the epoxy resin was a proprietary, aliphatic diamine and proprietary modified amidomine hardener. Table 2.2 shows the components present in the epoxy resin. The general reaction is shown in Figure 2.2. Composites were prepared using vinyl ester resin (Derakane 411-45) containing 45-wt% styrene for the EMI measurements. This resin was purchased from the Dow Chemical Company. The catalyst used was 2-butanone peroxide (~ 35 weight % solution in 2,2,4-trimethyl-1, 3-pentanediol diisobutyrate) and was provided by ATOFINa Chemical Inc. The promoter used was cobalt naphthenate (CoNap) and it was purchased from the Dow Chemical Company.

Table 2.1 Grade of VGCFs used.

Fiber	Surface area m^2/g Total	External	Surface Energy mJ/m^2	Fiber diameter nm	Fiber length μm
PR-19-PS	26	17	133	200	30-100

(a)

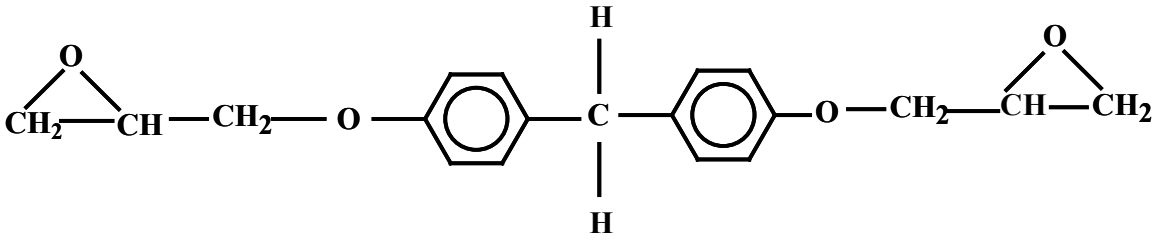

(b)

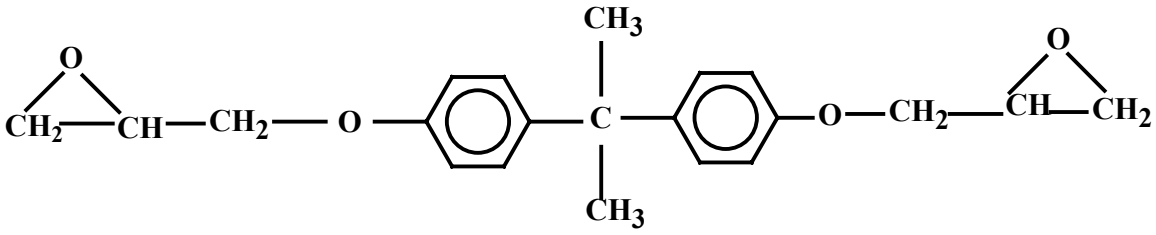

Figure 2.1 Structure of (a) Bisphenol A epoxide (b) Bisphenol F epoxide.

Table 2.2 Components in Clearstream 9000 epoxy resin.

Epoxy resin components	% w/w
Bisphenol A epoxide	70-80
Bisphenol F epoxide	20-30
Proprietary aliphatic glycidyl ether	5-15
Proprietary aliphatic amines	70-80
Proprietary modified amidomine	20-30

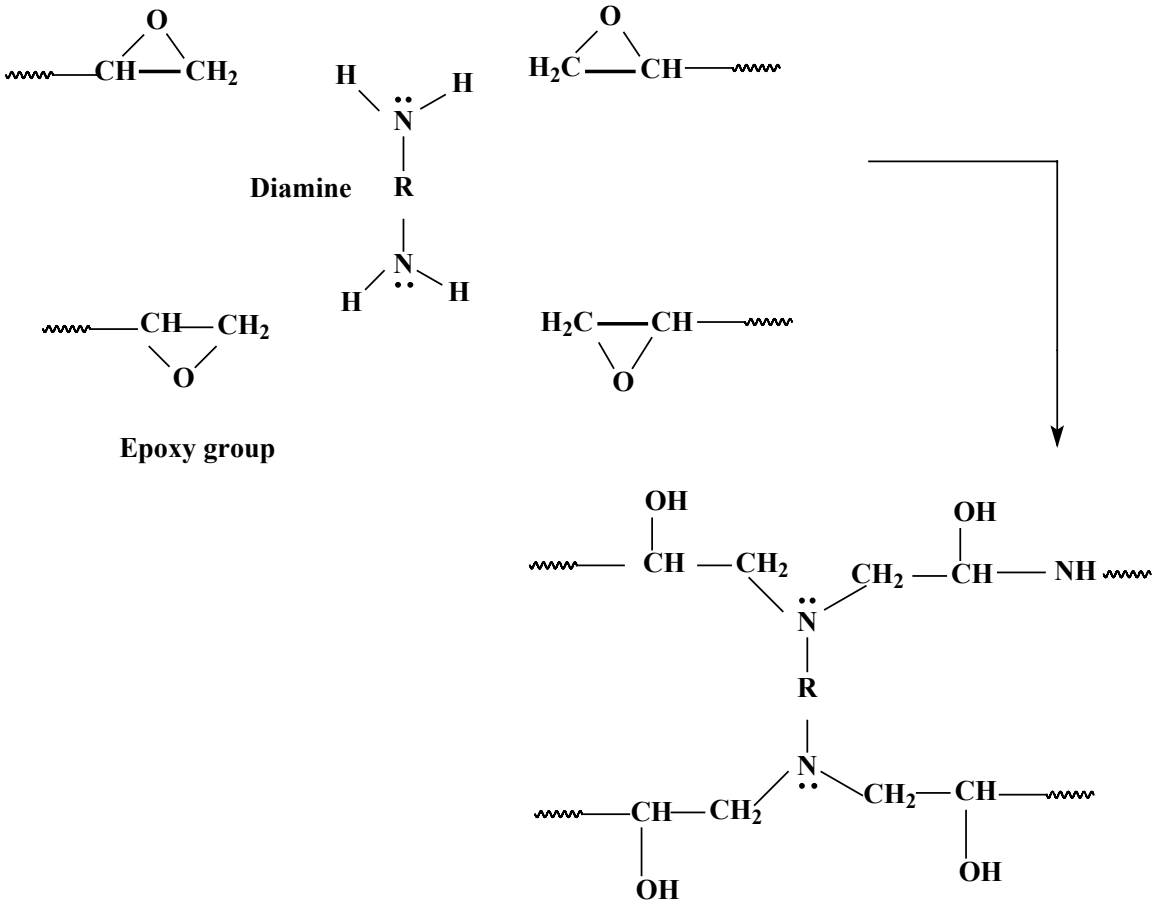

Figure 2.2 General reaction of diamine with epoxy group.

Oxidation of VGCFs

The VGCFs were oxidized with concentrated aqueous nitric acid (69-71 wt%) in a round-bottom flask equipped with a thermometer well. VGCF (40 g) was weighed into a round-bottom flask and approximately 500 ml of concentrated nitric acid was added. Oxidations were conducted at 115 °C for time intervals of 10 minutes, 20 minutes, 30 minutes, 60 minutes and 90 minutes. Approximately 6 g of VGCF was weighed into a small round-bottom flask and 160 ml of concentrated nitric acid was added. Oxidations were conducted for time intervals of 4 h, 10 h and 24 h. These three batches of samples were used only for the base uptake measurements, XPS measurements and surface area measurements. The oxidized fibers were then washed with distilled water to remove residual acid. Washing was performed in a batch process using about 2000 ml of water per batch. The pH of the wash water was measured after each wash. The washing was continued until the pH of the water in which the fibers were immersed was neutral (pH ~ 7). The fibers were then extracted overnight with distilled water in a soxhlet extractor and then dried overnight in an oven at a temperature of 125 ˚C. The oxidized fibers were then stored in an airtight bag and kept in a desiccator until further use.

Composite preparation

Composites were prepared containing 19.2 volume percent (29.4 weight percent) VGCFs in each sample (See Table 2.3). The epoxy resin (Clearstream 9000, proprietary aliphatic diamine or polyamine hardener) was first prepared by mixing the resin and the hardener in a 3:1 ratio, respectively. The resin and VGCFs were first pre-blended in a coffee blender for approximately 10 minutes. The samples were then subjected to high

shear mixing in a two-roll mill (0.2mm roll gap, 5 DC amp current, room temperature). After each pass through the two-roll mill, the resin/fiber sheets were folded and fed through again. The resin/fiber sheets were fed at different angles. After milling for 20 minutes, the fiber/resin sample was put in an aluminum mold (5 inch x 3 inch) and placed in a hot press. A starting pressure of 2 x 10^6 Pa was applied. The temperature was increased slowly in increments of 50 °F (10 °C) until the temperature reached 260 °F (126 °C). At this point, the pressure was 6.1 x 10^6 Pa. The temperature was maintained at 260 °F (120 °C) for one hour. Figure 2.3 shows the curing temperature vs time protocol used for the composite preparation. After one hour, the samples were cooled in the mold to room temperature. The composite sample was then removed from the mold. This identical procedure was repeated for the different VGCF/epoxy resin composites. All the samples were then post-cured overnight at 260 °F (120 °C).

Table 2.3 VGCF/epoxy resin composites.

Sample ID	VGCF loading (Weight %)	Epoxy resin loading [a] (Weight %)
Unoxidized VGCF	29.4	70.6
VGCF (oxidized for10 min)	29.4	70.6
VGCF (oxidized for 20 min)	29.4	70.6
VGCF (oxidized for 30 min)	29.4	70.6
VGCF (oxidized for 60 min)	29.4	70.6
VGCF (oxidized for 90 min)	29.4	70.6

[a] Ratio of resin:hardener = 3:1 (wt/wt)

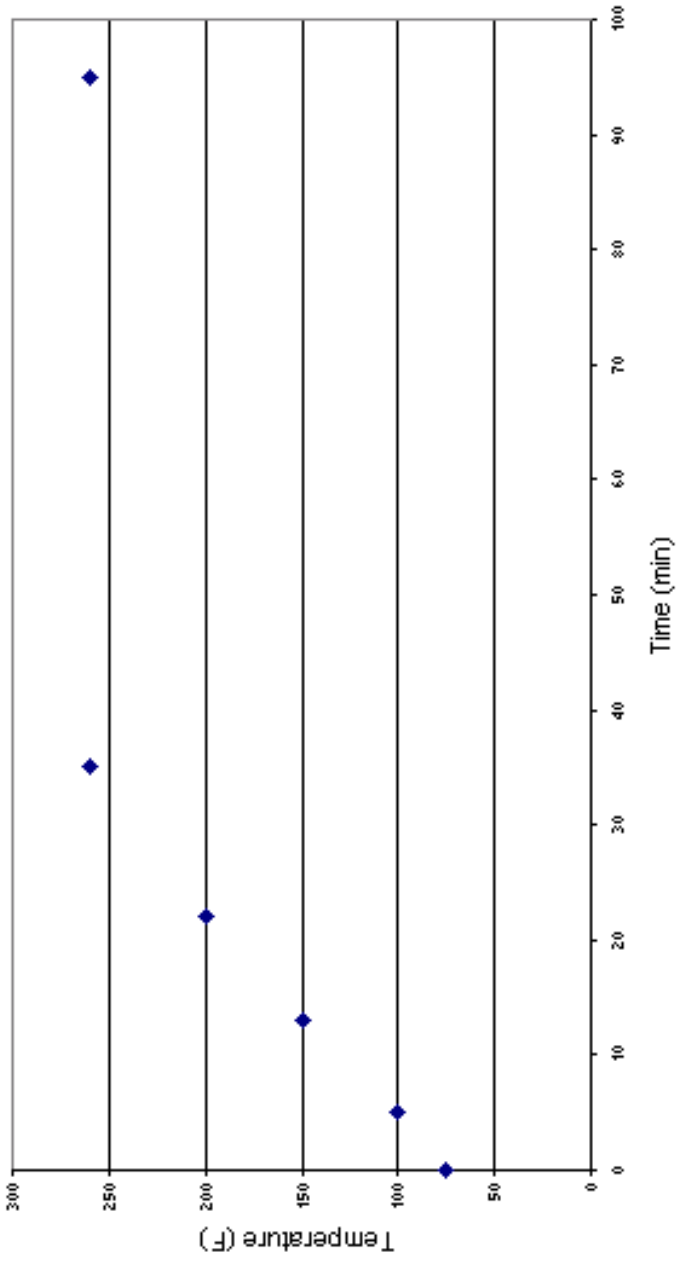

Figure 2.3 Curing temperature vs time protocol for VGCF/epoxy composites.

Three point bend test

The flexural strength and modulus of the VGCF/epoxy composites were found using a Zwick Tensile Testing machine (Model 1435) according to the ASTM standard D 790-62 [78]. Specimens of 70 mm (length) x 10 mm (width) x 2.5 mm (thickness) were used. Flexural strength, FS, is defined as the strength at which the specimen fails in the three-point bend test. It is calculated according to equation 2.1:

$$FS = \frac{3 \times P \times L}{2 \times W \times t^2} \qquad \text{Eq 2.1}$$

where P = breaking force of the specimen

L = span support (60 or 30 mm)

t = sample thickness (2.5 mm)

W = sample width (10 mm)

The flexural modulus, FM, is calculated by drawing a tangent to the steepest initial straight line portion of the load deflection curve. It is calculated according to equation 2.2:

$$FM = \frac{L^3 \times M}{4 \times W \times t^3} \qquad \text{Eq 2.2}$$

where M = slope of the tangent of the initial straight line portion of the load deflection curve.

L = span support (60 or 30 mm)

t = sample thickness (2.5 mm)

W = sample width (10 mm)

Five composite samples in each batch were tested by the above methods and the average values are reported.

Determination of base uptake

The acidic functionality of the carbon fibers surfaces was determined by neutralization with sodium hydroxide (NaOH). Fresh aqueous NaOH stock solution was prepared with boiled distilled water (to remove dissolved carbon dioxide). The initial concentration of the NaOH used was 0.4936 N. VGCF sample (1 g) was placed in a 100 ml polyethylene bottle. NaOH stock solution (50 ml) was added to the sample. The bottle was capped airtight and the samples were agitated in a mechanical agitator (Gyrotory water bath shaker, model G76). The pH values of the samples were measured using a pH/ion analyzer (Denver Instrument model 215). The analyzer was first calibrated with pH 4.00 (± 0.02 at 25°C) and pH 10.00 (± 0.01 at 25°C) buffer solutions (Fisher Scientific). The pH 4.00 buffer was made using potassium biphthalate and the pH 10.00 buffer was made using potassium carbonate-potassium borate-potassium hydroxide (Fisher Scientific). The pH value of the sample was then measured by immersing the glass electrode into the sample. Care was taken to immerse the electrode through a sealed cap so that any contact between carbon dioxide in the air and the sample was prevented. The number of μmoles of NaOH in the sample was calculated based on the pH value measured and the volume of the sample according to equation 2.3:

$$\text{NaOH Uptake } (\mu\text{moles/g of fiber}) = \frac{V \times [10^{(pHo-14)} - 10^{(pH-14)}] \times 1000}{W} \qquad \text{Eq 2.3}$$

where V = sample volume (ml)

pHo = pH of the blank solution

pH = pH value obtained

W = fiber sample weight (1 g)

The above procedure was repeated with various oxidized VGCF samples. The difference between the number of μmoles of NaOH in the blank solution and that in the sample was assumed to be equal to the number of μmoles of NaOH neutralized by the acidic functional groups on the surface of the fiber [51].

Density and void measurements

The densities of the composite samples were determined using an electronic densimeter (ED – 120T). Using these densities, the void content of each sample was found using the following formulas:

$$\text{Void content (\%)} = \frac{V_c - V_o}{V_c} \qquad \text{Eq 2.4}$$

$$\text{Volume of composite } (V_c) = \frac{W_{comp}}{\rho_{comp}} \qquad \text{Eq 2.5}$$

$$\text{Total volume (Vo)} = \frac{W_{CF}}{\rho_{CF}} + \frac{W_{resin}}{\rho_{resin}} \qquad \text{Eq 2.6}$$

where W_{comp} = weight of the composite sample

ρ_{comp} = density of the composite sample

W_{CF} = weight of the carbon fiber

ρ_{CF} = density of the carbon fiber (2.1 g/cc)

W_{resin} = weight of the resin

ρ_{resin} = density of the resin (1.158 g/cc)

Determination of surface area by nitrogen BET

The surface areas of the unoxidized and oxidized VGCFs were measured using a Quantasorb dynamic flow analyzer (Quantachrome, Inc.) by nitrogen BET at 77 K. VGCFs of approximately 0.125 grams were taken in a small, round-bottomed, long-stemmed glass tube. The samples were first out-gassed for ~5 hours at 140 °C. The autosorb measured the variation in gas pressure (nitrogen only). Since the BET equation is usually applied under nitrogen relative pressures of 0.05 – 0.35, an N_2 / He gas mixture (70:30 w/w) was used. This procedure was repeated for three different batches. A sample of VGCFs (unoxidized) was analyzed at Quantachrome using the latest software.

Determination of surface area by carbon dioxide DR adsorption method

The surface areas of the unoxidized and oxidized VGCFs were measured using a Quantasorb dynamic flow analyzer (Quantachrome, Inc.) by the carbon dioxide DR method. VGCFs (0.135 g) were weighed into a small, round-bottomed, long stemmed glass tube. The samples were first out-gassed for ~10 hours at 140 °C under a vacuum of 10^{-6} torr. The testing was done at 273 K in the relative p/p^o range of 0-0.3 and absolute pressure range of 0-1 atm [79]. The data were monitored and plotted as logW vs. $\log^2(p^o/p)$, according to the Dubinin - Radushkavich (DR) method [80,81]. This gives the amount of carbon dioxide adsorbed onto each sample. This procedure was repeated for

three different batches. Two samples of VGCFs (unoxidized and oxidized for 10 h) were analyzed at Quantachrome Inc., (May 2003) using their software.

X-ray Photoelectron Spectroscopy (XPS) studies

X-ray Photoelectron Spectroscopy (XPS) spectra were obtained on a Physical Electronics Model 1600 surface analysis system (Perkin Elmer). The equipment was operated with an achromatic Mg Kα X-ray source operating at a working power of 300 W (15kV). The instrument was calibrated using the Au $4f_{7/2}$ spectrum, which was assumed to occur at 84 eV [83]. The full width at half maximum of each deconvoluted C1s spectra is 1.6eV. An electron take off angle of 30 degrees was used to acquire data during XPS analyses. During all XPS experiments, the pressure inside the analysis chamber was maintained at 5×10^{-9} torr. The atomic ratio of any two elements, A and B, was calculated from the respective peak areas and the elemental sensitivity factors for the signal Perkin-Elmer Spherical Capacitor Analyzer (SCA) [83].

$$\frac{A}{B}\ \text{atomic ratio} = \frac{\text{peak area of A}}{\text{peak area of B}} \times \frac{\text{sensitivity factor of B}}{\text{sensitivity factor of A}} \qquad \text{Eq 2.7}$$

For carbon and oxygen, the sensitivity factors employed were 0.3 and 0.71, respectively.

Scanning Electron Microscope (SEM) studies

SEM pictures were taken using a Leo/Leica/Cambride S360 SEM. The samples were first mounted on a grid using carbon tape. The grids were then placed in the SEM

scope. The VGCF/epoxy samples had to be sputter-coated because they charged under vacuum in the scope when they were not coated. An Au/Pd sputter coating was used and the coating operation was performed for 30 seconds. Figure 2.4 shows the Magnetron sputtering device used. An accelerating voltage of 15 kV was used. Figure 2.5 shows an example of the diffusion of the incident electrons and Figure 2.6 shows the effect of the accelerating voltage on a sample [84]. SEM photos of the VGCF/epoxy composites will be discussed in Chapter III.

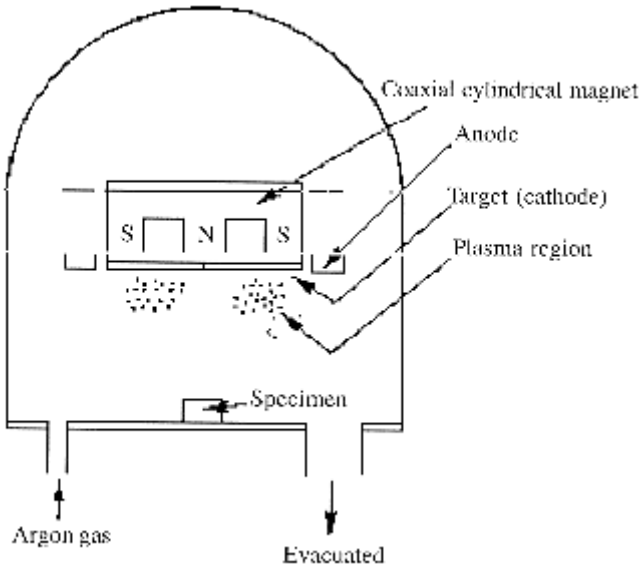

Figure 2.4 Magnetron sputtering device.

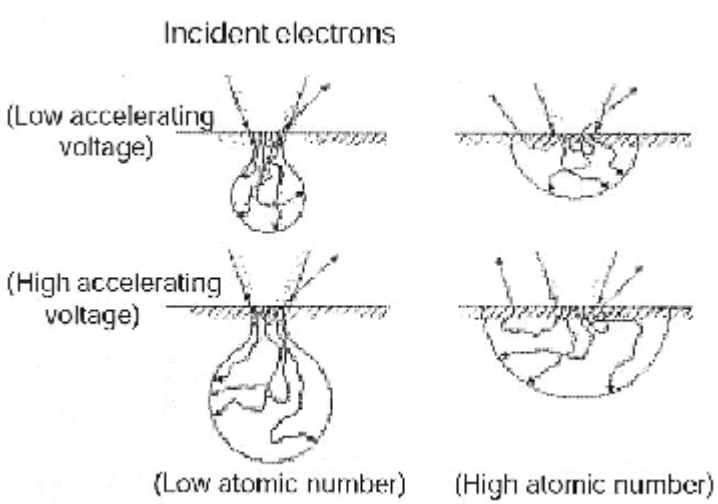

Figure 2.5 Diffusion of the incident electrons.

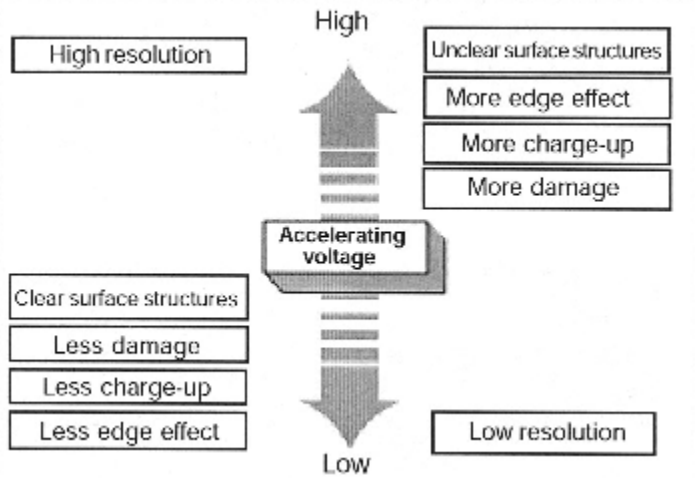

Figure 2.6 Effect of accelerating voltage.

Transmission Electron Microscope (TEM) studies

TEM pictures were taken using a JOEL JEM – 100CX II TEM. Figure 2.7 shows an external view of the TEM used [85]. All the TEM samples were prepared to contain 5-weight percent of VGCF in the VGCF/epoxy resin composite (since the composites containing 19.2 volume% VGCF proved too difficult to cut even with a diamond knife). An epoxy resin (Clearstream 9000, proprietary aliphatic diamine or polyamine hardener) was used to prepare the VGCF/epoxy resin composites. The samples were first cut into 5 mm trapezoids using a razor blade. The cut edge was then smoothed using a glass knife. Finally, the thin sections were cut using an ultra-mictrotome. A diamond knife was used to cut a series of uniform ultra-thin sections (~50 μm). These ultra-thin sections were then mounted on a grid, which was placed in the TEM. Photographs were taken and the negatives were developed in the dark room.

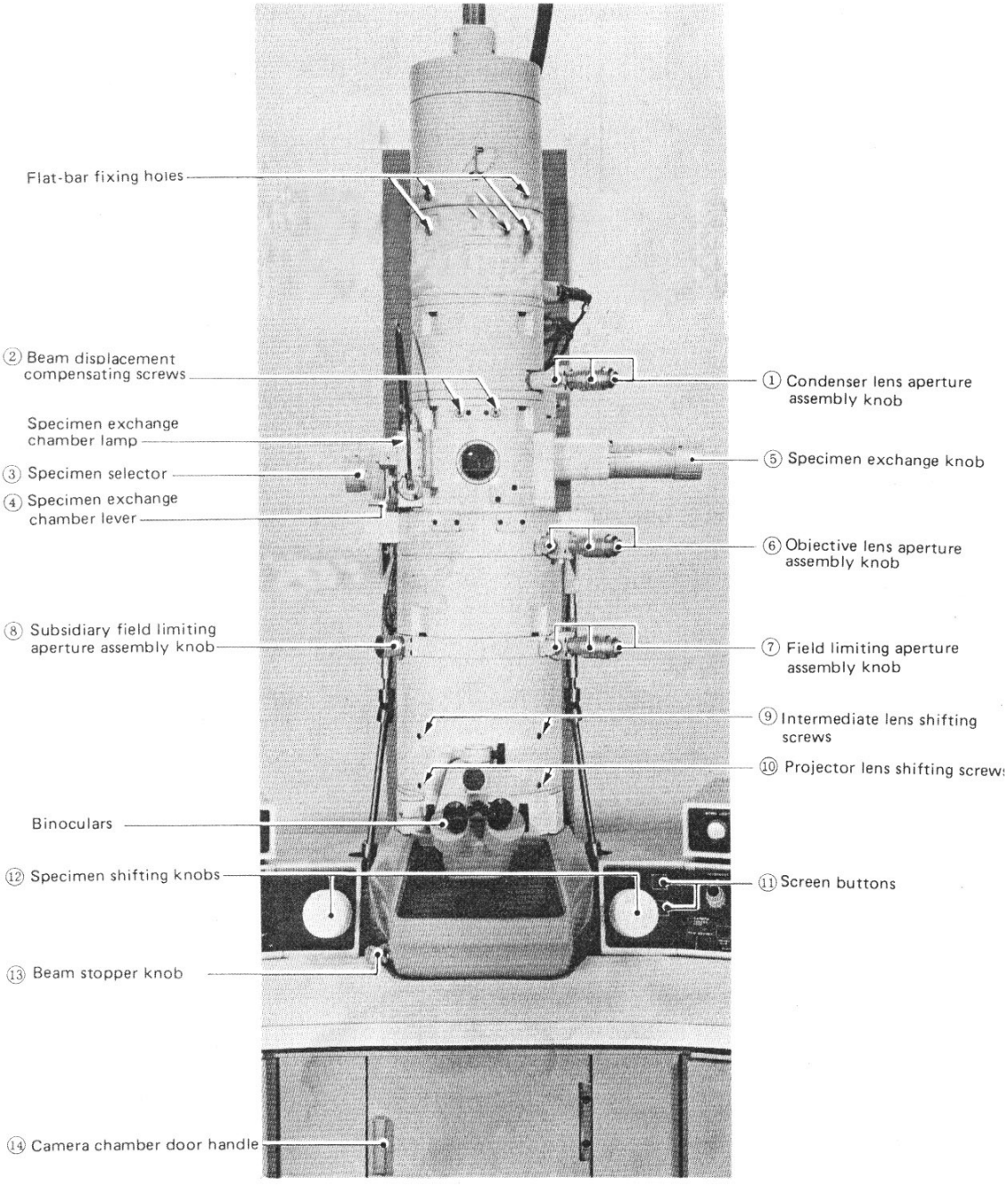

Figure 2.6 External view of the column of the JOEL JEM – 100CX II TEM.

Preparation of VGCF/Vinyl ester composites

A series of composites were prepared by J.Xu using PR-19-PS fibers and Derakane 411-45 vinyl ester (VE) resin (See Table 2.4). The curing temperature versus time protocol shown in Figure 2.8 was used to prepare the composites. The catalyst (0.8 wt%) and promoter (0.2 wt%) mixture were first mixed and then added into the vinyl ester resin (See Table 2.4). A 33.3 weight % (VGCF/VE) pre-mixture was prepared by mixing VGCFs with a calculated amount of vinyl ester resin containing the catalyst and the promoter [82]. The amount of VGCFs used was half the weight of the resin. High speed mechanical blending at 3,000 RPM was performed to mix the VGCF/VE mixture. This blending was continued for about 3 minutes. After the pre-mixture was prepared, the remaining amount of the vinyl ester resin containing the catalyst and the promoter was mixed with the pre-mixture. This mixing was done by hand for one minute. The mixture was kept at room temperature for one hour. It was then poured into an aluminum mold (4 inch x 5 inch) and placed in a hot press at room temperature for a period of 1.5 hours. The initial pressure in the hot press was 7.6 x 10^5 Pa and this was gradually increased to 45.6 x 10^5 Pa over a period of 1.5 hours. The temperature of the hot press was then increased to 100 °F (~38 °C). After 16 hours, the temperature was further increased to 200 °F (~93 °C) and held for 5 hours. The mold was then transferred into an oven at 150 °F (~66 °C) and left for another 1.5 hours. Finally, the mold was removed from the oven and cooled to room temperature. Only two samples were prepared. One had a 7-weight % fiber loading, and the other, a 15-weight % fiber loading. These preparations are shown

in Table 2.2. The same procedure was used to prepare another series of composites with the VGCF, which had been oxidized for 90 minutes.

Table 2.4 VGCF/ Derakane 411-45 vinyl ester composites

Sample ID	Fiber loading (Weight %)	Resin loading (Weight %)	Catalyst loading (Weight %)	Promoter loading (Weight %)
Unoxidized VGCF	7	93	0.8	0.2
Unoxidized VGCF	15	85	0.8	0.2
90 minute oxidized VGCF	7	93	0.8	0.2
90 minute oxidized VGCF	15	85	0.8	0.2

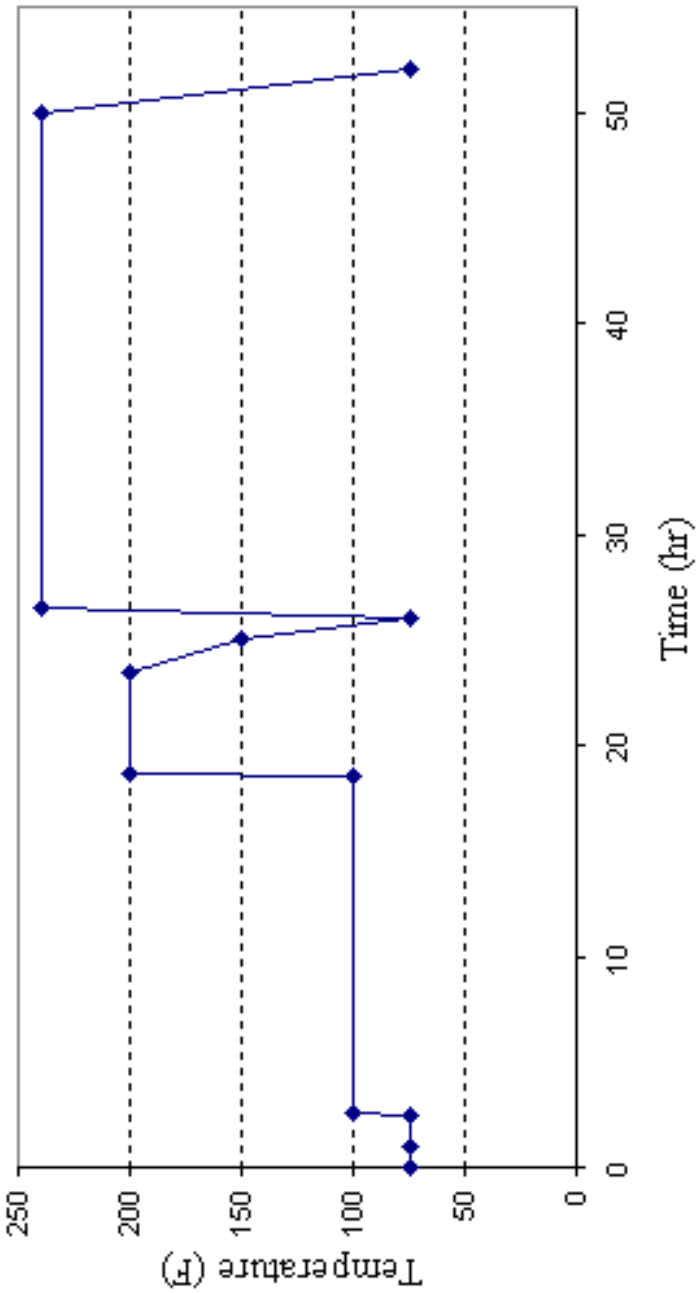

Figure 2.8 Curing temperature vs time protocol for VGCF/ Derakane 411-45 vinyl ester composites.

Electromagnetic interference (EMI) shielding measurements.

Electromagnetic shielding measurements were performed by J.Xu for the samples shown in Table 2.4. Two kinds of electromagnetic shielding, namely electric field insert loss (ILe) and magnetic field insert loss (ILm), were measured. The apparatus used was a Hewlett Packard 8753D Network Analyzer connected to a test chamber (Dual TEM cell by VHS Tech, Inc., State College, PA). To control the network analyzer and to automatically collect the resulting data, a laptop was connected to the Network Analyzer. The samples were held in the test chamber to minimize the environmental noise. Figure 2.9 shows the experimental apparatus [82]. A total of 401 data points were collected over frequency range of 30 KHz and 1000 MHz. Each data point is the average of 64 tests. All the samples were tested for EMI shielding both before and after the samples were polished.

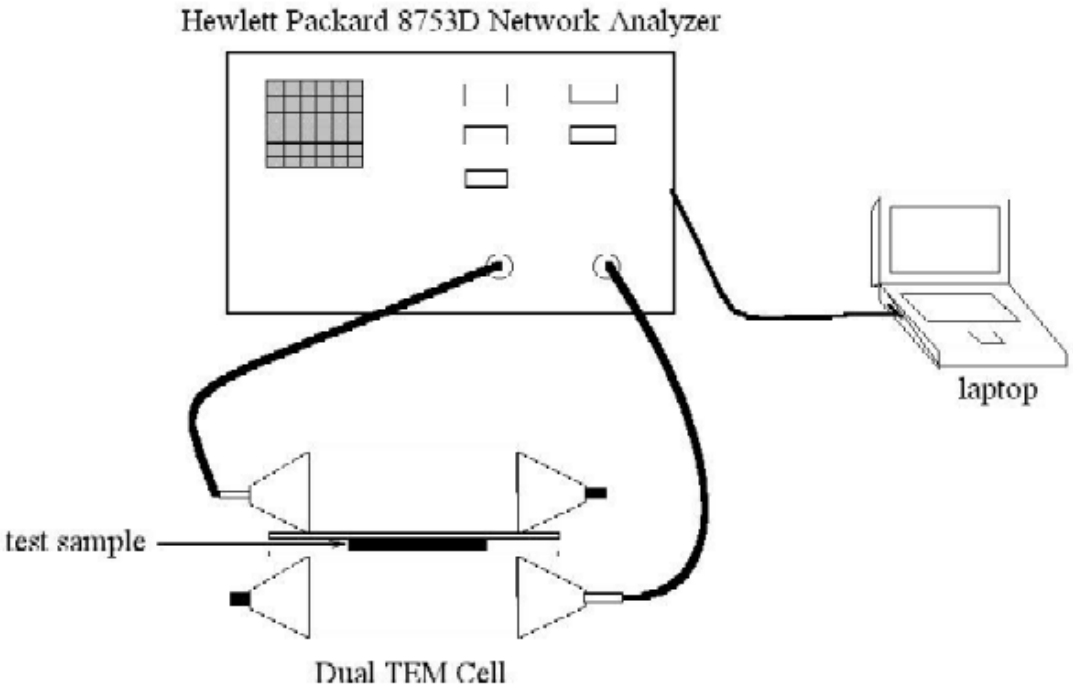

Figure 2.9 Electromagnetic shielding test equipment

Volume electrical resistivity measurements

Volume electrical resistivity measurements were performed by J.Xu for the samples shown in Table 2.4. A Monroe Electronics Model 271 Resistivity meter was used for the measurements of volume electrical resistivities higher than 1 x 10^{10} Ω cm. In order to provide a low noise environment, a guarded electrode (Model 96101A-1 surface test electrode) was used. Figure 2.10 shows the apparatus used [82].

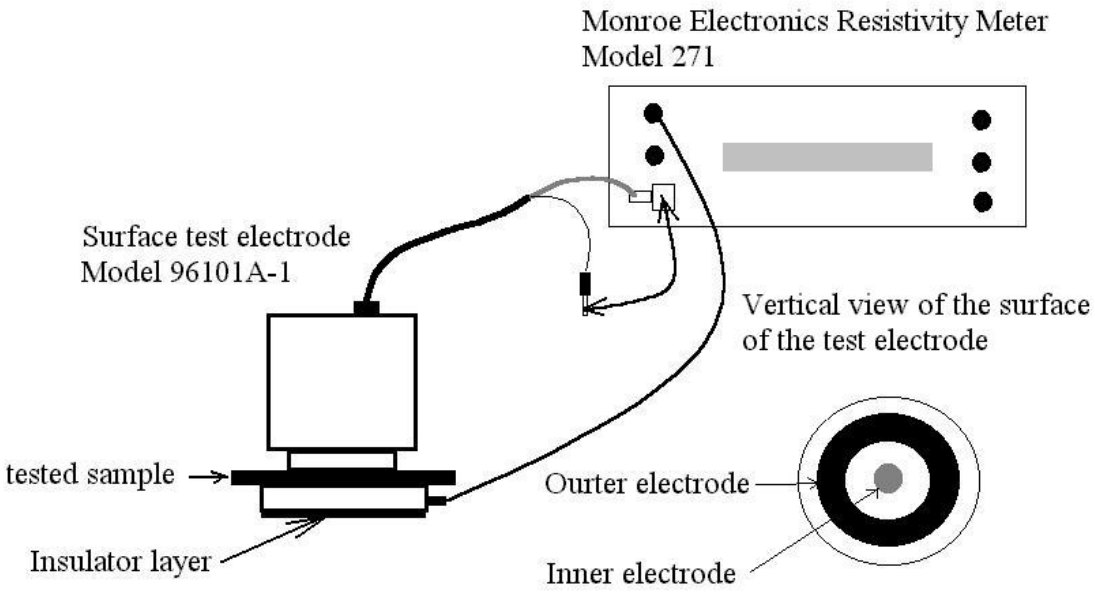

Figure 2.10 Equipment for volume electrical resistivity measurements using a surface test electrode.

Volume electrical resistivities lower than 1 x 10^{10} Ω cm were measured using a parallel capacity device connected to a Simpson Model 464 Digital Multimeter (Simpson Electric Company, Elgin, IL). Figure 2.11 shows this device [82].

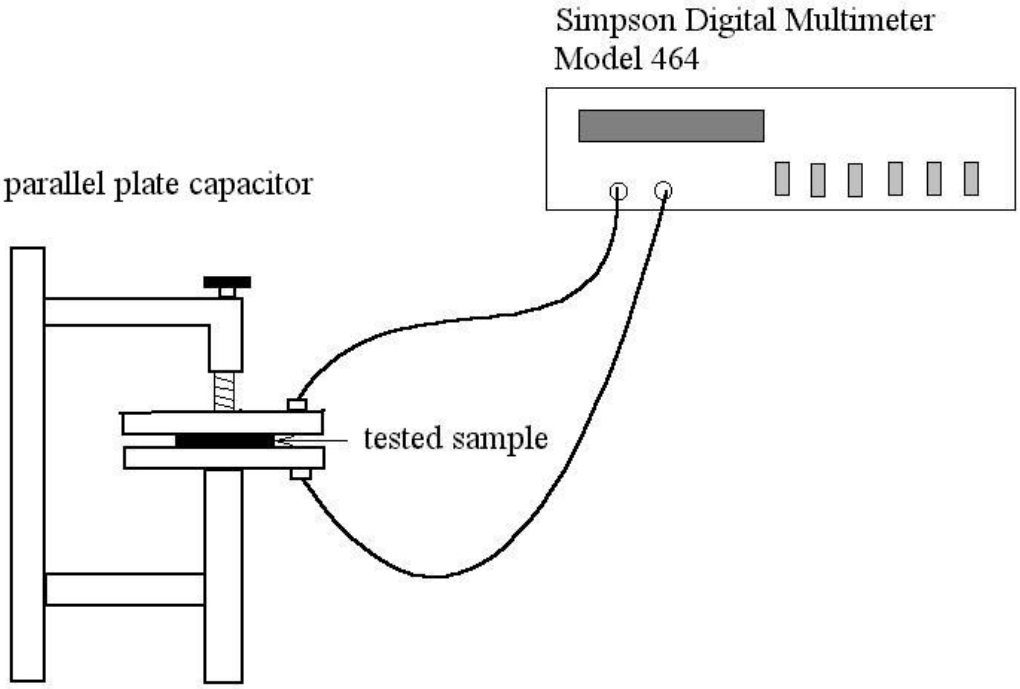

Figure 2.11 Parallel capacity device used for volume resistivity measurements.

Both the model 96101A-1 surface test electrode and the parallel capacity device were used to obtain the bulk resistivity. The volume resistivity (ρ_v) was calculated from equation 2.8:

$$\rho_v = \frac{R \times A}{L} \qquad \text{Eq 2.8}$$

where ρ_v = volume resistivity (Ω cm)

R = bulk resistivity (Ω)

L = sample thickness (cm)

A = tested surface area (cm^2) (surface area of the sample which was tested by parallel capacity device and 21.535 cm^2 when using the Model 96101A-1 surface test electrode).

All samples were tested for volume resistivity before and after the samples were polished.

CHAPTER III

RESULTS AND DISCUSSIONS

Three point bend test

The flexural strengths and flexural moduli were obtained for a series of VGCF/epoxy composites according to the ASTM D 790-92 standards [10] using a Zwick Tensile Testing machine (Model 1435). All the composite samples were prepared to contain 19-volume % of VGCF. The sizes of the composite samples were 70 mm (width) x 10 mm (length) x 2.5 mm (thickness). Table 3.1 shows the flexural testing results.

Table 3.1 Flexural strengths and flexural moduli of the VGCF/Epoxy composites [a].

Composite ID	Average Flexural Modulus (MPa)	Average Flexural Strength (MPa)
Pure epoxy resin composite	3980 [b] ± 199	90 [b] ± 5
Unoxidized VGCF/Epoxy composite	5890 [c] ± 1103	104 [c] ± 11
VGCF (oxidized for10 min)/epoxy composite	7475 [d] ± 1646	104 [d] ± 14
VGCF (oxidized for 20 min)/epoxy composite	4175 [c] ± 946	104 [c] ± 10
VGCF (oxidized for 30 min)/epoxy composite	3683 [b] ± 439	110 [b] ± 9
VGCF (oxidized for 60 min)/epoxy composite	7039 [c] ± 392	95 [c] ± 7
VGCF (oxidized for 90 min)/epoxy composite	4770 [c] ± 817	102 [c] ± 9

[a] The epoxy resin used was a low viscosity aliphatic epoxy resin containing Bisphenol A epoxide, Bisphenol F epoxide and proprietary aliphatic glycidyl ether (Clearstream 9000, Clearstream Products Inc.). The curing agent used in the epoxy resin was a proprietary aliphatic diamine and modified amidomine hardeners. Ratio of resin: curing agent = 3:1.This resin system was blended with 29.4 weight percent (19-volume %) VGCF (PR-19-PS) and cured.
[b] Average of 4 values
[c] Average of 3 values
[d] Average of 2 values

.

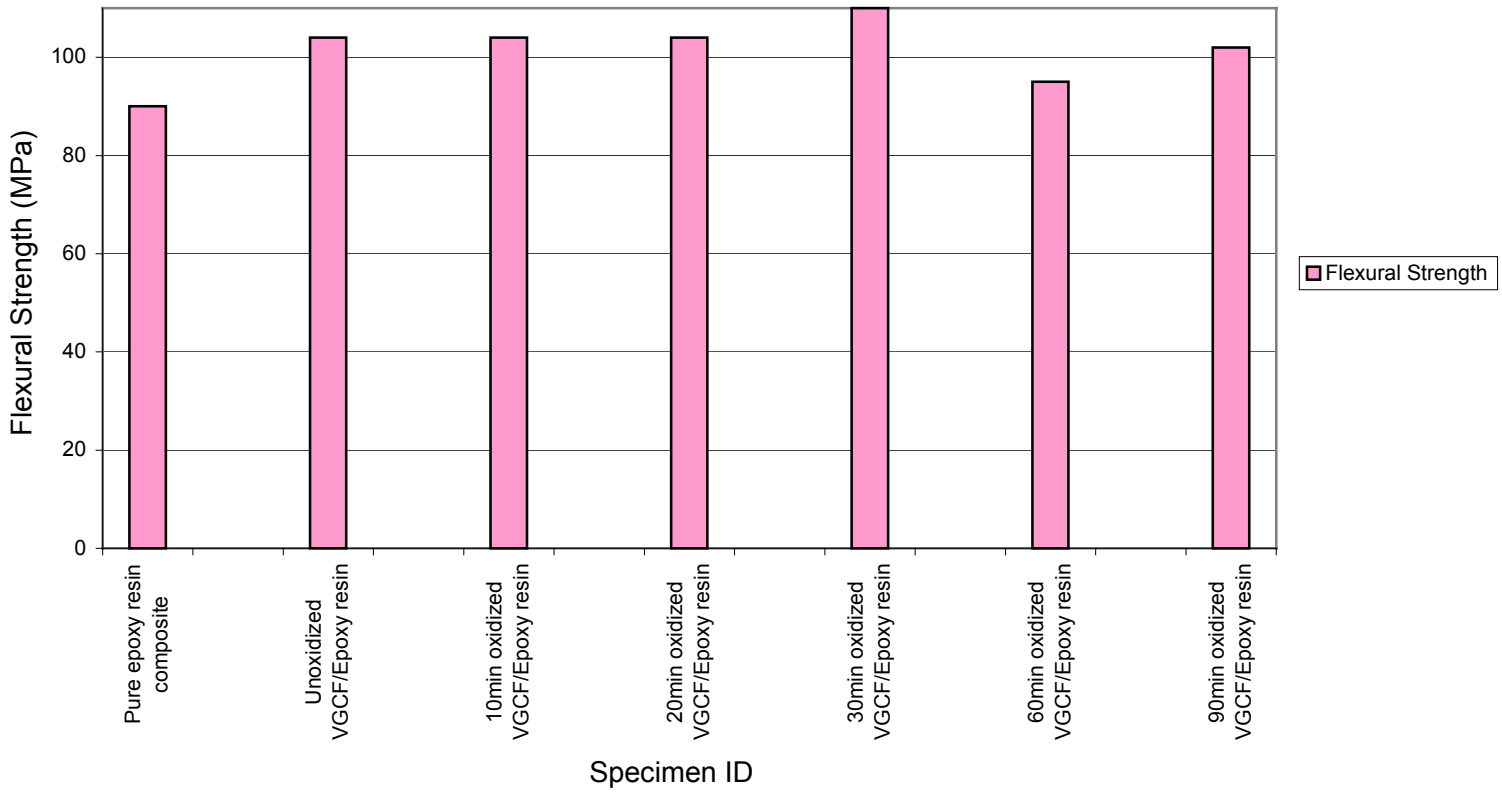

Figure 3.1 Flexural strength distributions of the various VGCF/ epoxy resin composites.

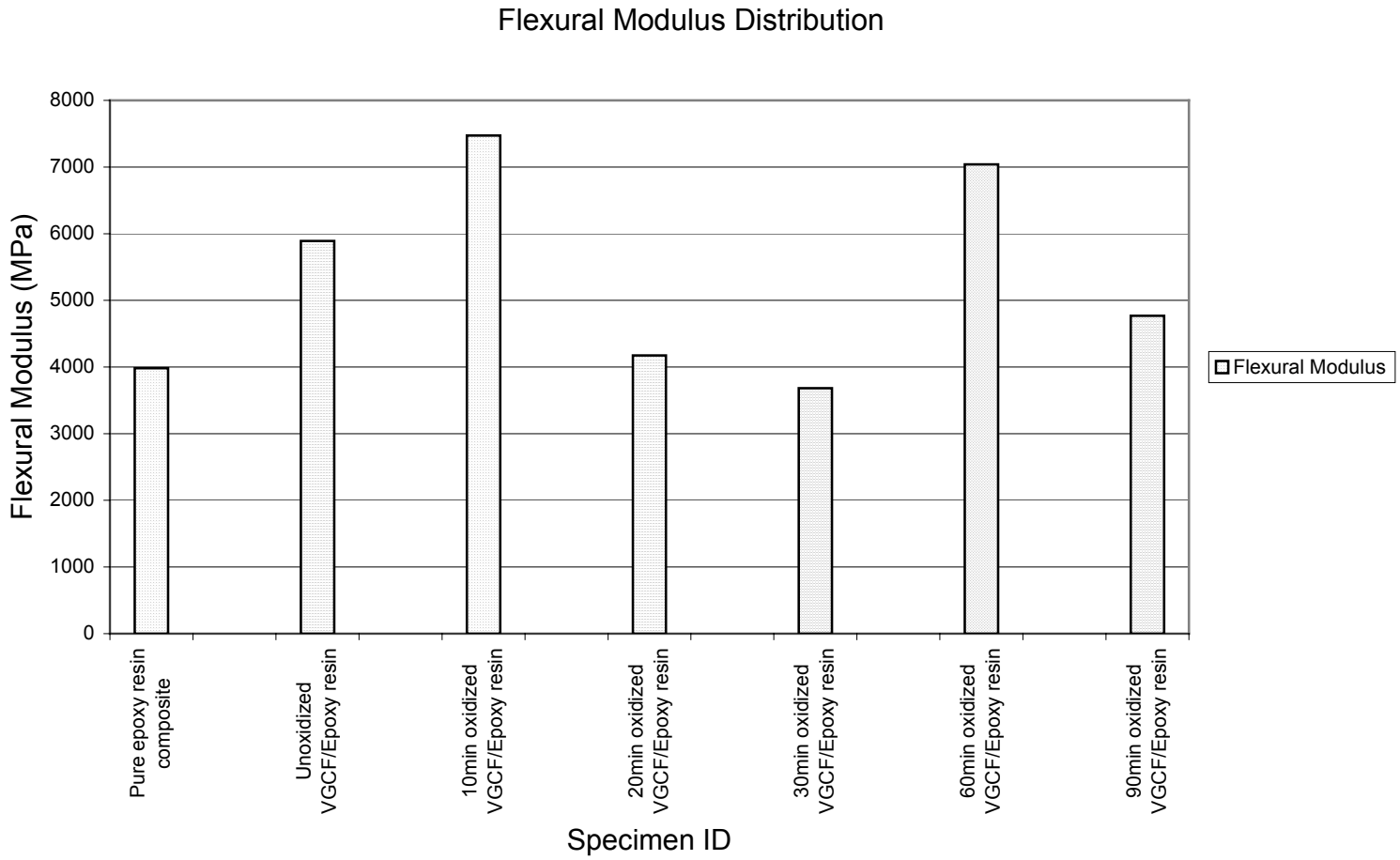

Figure 3.2 Flexural modulus distributions of the various VGCF/ epoxy resin composites.

The flexural strength was the highest for the VGCF (oxidized for 30 min)/epoxy composite. There were no large differences between the flexural strength values obtained for the various composites. Previous studies of carbon-carbon composites have shown that strong chemical bonding between the fiber and matrix results in lower flexural strength [66,91,92]. No studies of this issue have been reported for VGCF/epoxy composites.

Acidic functionality

The number of μmoles of NaOH neutralized by the acidic surface functional groups on a sample of VGCFs was determined by titration with NaOH (see page 31 and equation 2.3). Table 3.2 shows the acidic capacities of the VGCF samples (calculated with the corresponding pH value of the blank solution at various time intervals. See Appendix A for further information). The acidic capacity of the unoxidized fibers was less than that of the oxidized fibers. No significant difference in acidic capacity was noticed among the oxidized VGCFs. Figure 3.3 shows a schematic representation of the surface chemistry during neutralization with NaOH.

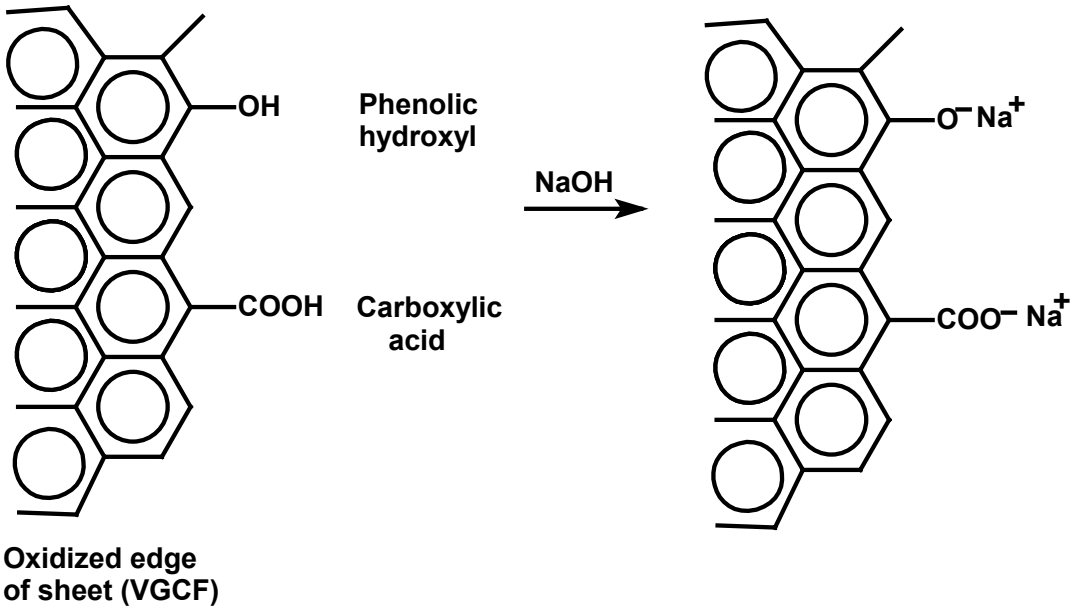

Figure 3.3 Schematic representation of the surface chemistry.

Table 3.2 NaOH uptake of the unoxidized and oxidized VGCFs.

Sample ID	After 1 hr [a] (μmoles / g of fiber)	After 12 hrs [a] (μmoles / g of fiber)	After 24 hrs [a] (μmoles / g of fiber)
Unoxidized VGCF	26.3	26.8	21.8
VGCF oxidized for10 min	95.3	75.7	70.6
VGCF oxidized for 20 min	95.2	75.7	70.6
VGCF oxidized for 30 min	95.3	75.7	70.6
VGCF oxidized for 60 min	94.1	75.2	70.5
VGCF oxidized for 90 min	95.3	75.7	70.6
VGCF oxidized for 4 hr	95.3	75.7	70.6
VGCF oxidized for 10 hr	95.3	75.7	70.6
VGCF oxidized for 24 hr	95.3	75.7	70.6

[a] VGCF sample (1 g) was placed in a 100 ml polyethylene bottle. NaOH stock solution (50 ml) was added to the sample. The bottle was capped airtight and the samples were agitated in a mechanical agitator (Gyrotory water bath shaker, model G76). The values shown were measured (using a pH/ion analyzer, Denver Instrument model 215) after 12 and 24 hours of agitation.

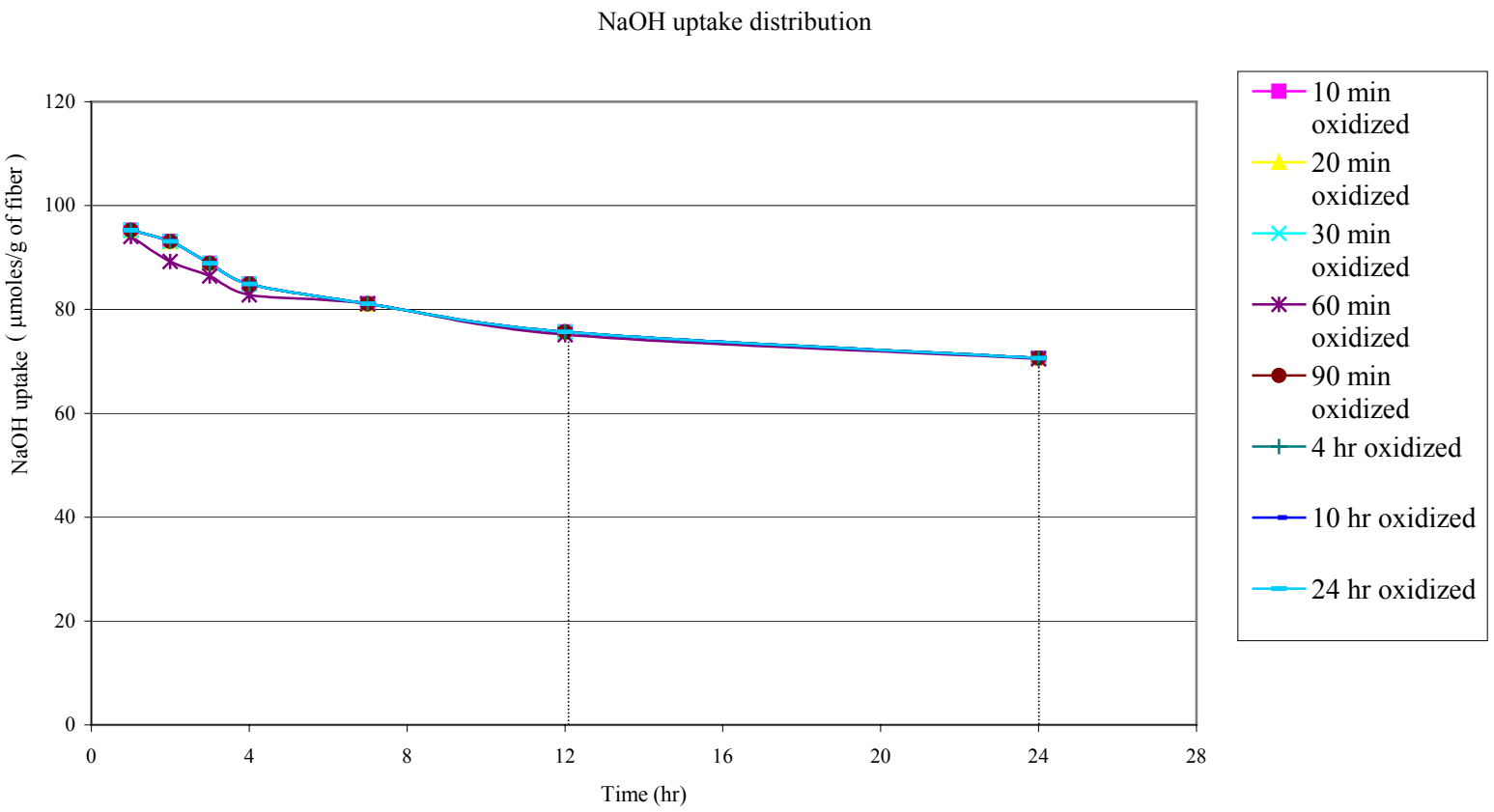

Figure 3.4 NaOH uptake vs agitation time for the various VGCF samples.

Density and void content measurements

The densities of the various VGCF/Epoxy resin composites were determined using an electronic densimeter (ED-120T). The densities of the VGCF/Epoxy resin composites were between 1.299 g/cc and 1.308 g/cc. The density of the pure cured epoxy resin was 1.158 g/cc. The void content of each composite sample was calculated using equations 2.4 to 2.6. The results obtained are shown in Table 3.3. The void content decreased with increasing oxidation time. Figure 3.5 shows the void content of the samples.

Table 3.3 Void content and densities of the various VGCF/epoxy resin composites. [a]

Sample ID	Average Void Content [b] (%)	Average density [b] (g/cc)
Unoxidized VGCF/Epoxy composite.	2.51 ± 0.01	1.299
VGCF (oxidized for 10 min)/epoxy composite	2.45 ± 0.01	1.301
VGCF (oxidized for 20 min)/epoxy composite	2.42 ± 0.01	1.302
VGCF (oxidized for 30 min)/epoxy composite	2.24 ± 0.01	1.304
VGCF (oxidized for 60 min)/epoxy composite	1.99 ± 0.01	1.307
VGCF (oxidized for 90 min)/epoxy composite	1.96 ± 0.01	1.308

[a] The epoxy resin used was a low viscosity aliphatic epoxy resin containing Bisphenol A epoxide, Bisphenol F epoxide and proprietary aliphatic glycidyl ether (Clearstream 9000, Clearstream Products Inc.). The curing agent used in the epoxy resin was a proprietary aliphatic diamine and modified amidomine hardeners. Ratio of resin: curing agent = 3:1.This resin system was blended with 29.4 weight percent (19-volume %) VGCF (PR-19-PS) and cured.

[b] Average of 5 trials.

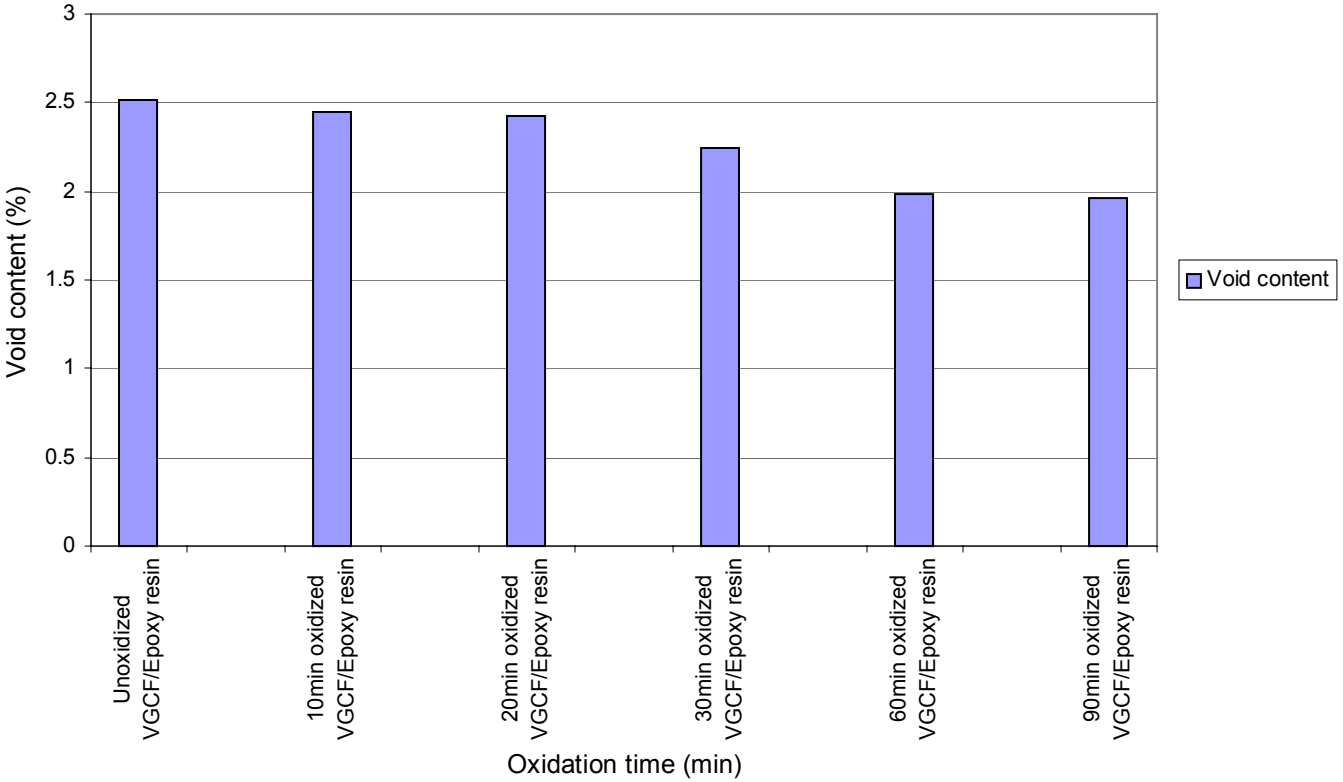

Figure 3.5 Average void content of the various VGCF/Epoxy resin composites.

Surface area determination by nitrogen BET

Nitrogen BET surface areas for the unoxidized and oxidized VGCFs samples are shown in Table 3.4. The nitrogen BET surface areas were quite low. The surface areas slowly increased with further oxidation up to 30 minutes and then decreased a little. VGCFs oxidized for 30 minutes had the highest surface area (27.8 m^2/g). The flexural strength values were also the highest (110MPa) for composites containing VGCF, which had been oxidized for 30 minutes. However, the major conclusion is that very little change in surface area occurred during these oxidations. The range of surface areas, from 21.3 to 27.8 m^2/g (up to 90 min oxidation) is very small considering the enormous oxidizing conditions these fibers were exposed to (69-71 wt% nitric acid, 115 °C). Even after 10 h of oxidation, the surface area did not change much.

Table 3.4 Nitrogen BET surface areas of the unoxidized and oxidized VGCFs.

Sample ID	N_2 BET [a] (m^2/g)
Unoxidized VGCF	21.3[b]
VGCF oxidized for10 min	22.4
VGCF oxidized for 20 min	24.1
VGCF oxidized for 30 min	27.8
VGCF oxidized for 60 min	25.0
VGCF oxidized for 90 min	26.0
VGCF oxidized for 10 h	34.6[cd]

[a] Average surface area values of two trials.
[b] This sample exhibited a CO_2-DR surface area of 20.5 m^2/g (See table 3.6)
[c] Surface area value of 1 trial. Measured at Quantachrome.
[d] This sample gave a CO_2-DR surface area of 23.1 m^2/g (See Table 3.6)

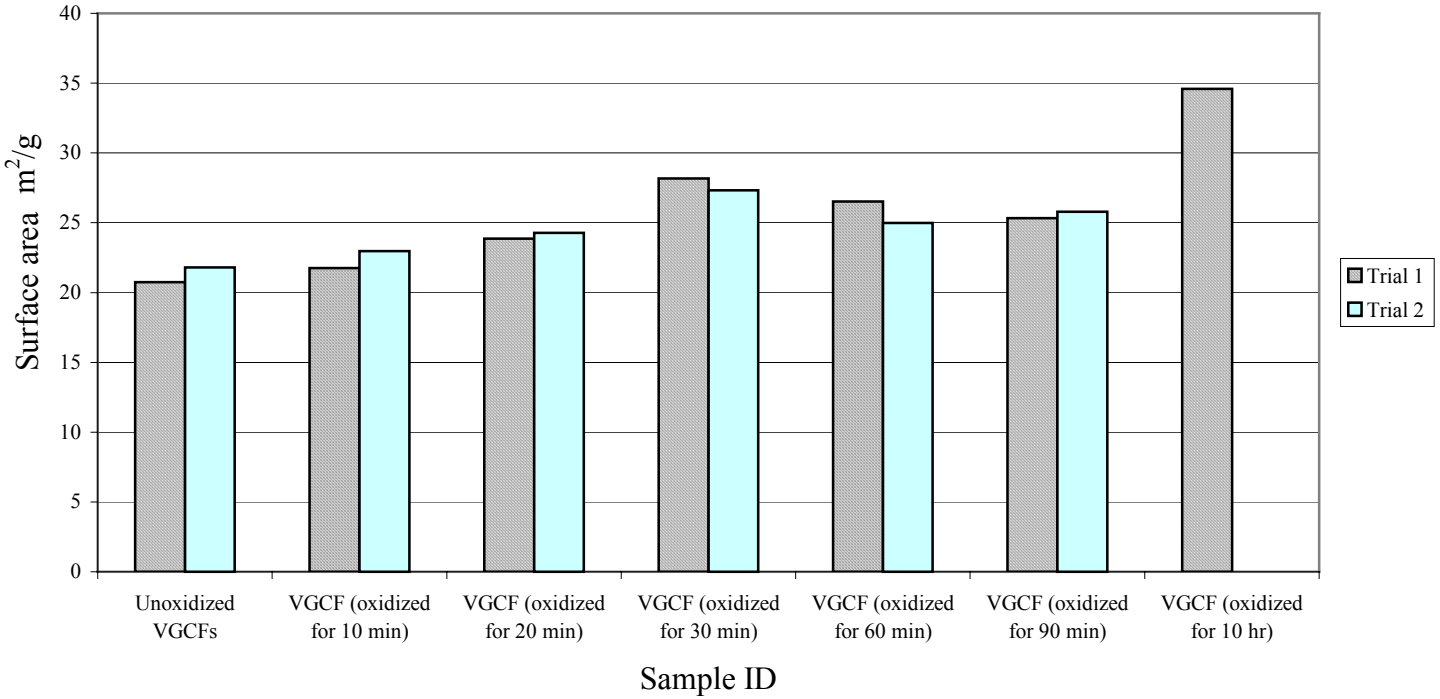

Figure 3.6 N_2 BET surface area of unoxidized and oxidized (concentrated nitric acid, 115 °C) VGCFs.

Previous studies by our research group on polyacrylonitrile (PAN)-based carbon fiber, which were oxidized in concentrated nitric acid oxidation, 115 °C, showed a continually increasing surface area with oxidation time using nitrogen BET measurements [79a]. These results are shown in Figure 3.8 and Table 3.5. After 60 minutes of oxidation, the surface structure of the fibers was heavily damaged. After 105 minutes of oxidation, the surface area of PAN fibers had increased 29-fold! Furthermore, the rate of surface area increase was accelerating! The results obtained for the oxidized VGCFs did not show a similar pattern. Using a cylindrical model, and assuming the diameter of PAN fibers to be 7.5 μm and that of VGCF to be 200 nm, the surface area of an equal weight of VGCFs is 37.5 times greater than PAN fibers. This comparison shows that the VGCFs are more resistant to oxidation compared to PAN fibers. Thus, if VGCFs underwent oxidation as rapidly as PAN fibers, we might have expected a surface area of 37.5 x 18.8 = 705 m^2/g (after 105 min of oxidation).

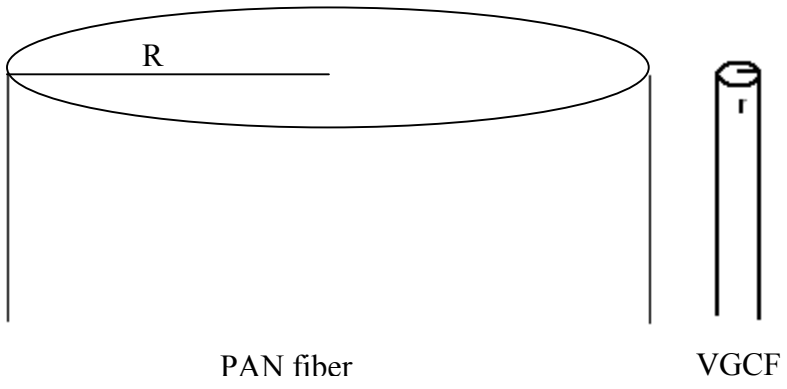

Figure 3.7 Schematic representation of PAN vs VGCFs.

Table 3.5 N_2 BET specific areas of PAN fibers. [a b]

Fiber oxidation time (min)	N_2 BET specific area (m^2/g)	PAN fiber surface area x 37.5[c]
0	0.65	24
20	0.73 (1.1 fold)	27
40	1.65 (2.5 fold)	62
60	2.09 (3.2 fold)	78
90	12.4 (19 fold)	465
105	18.8 (29 fold)	705

[a] These PAN fibers were oxidized in concentrated nitric acid at 115 °C.
[b] Pittman,Jr.C.U., Jiang,W., Yue,Z.R., Leon y Leon, C.A., *Carbon*, **1999**, *37*, 85-96
[c] Expected VGCF surface area if they behaved like PAN fibers.

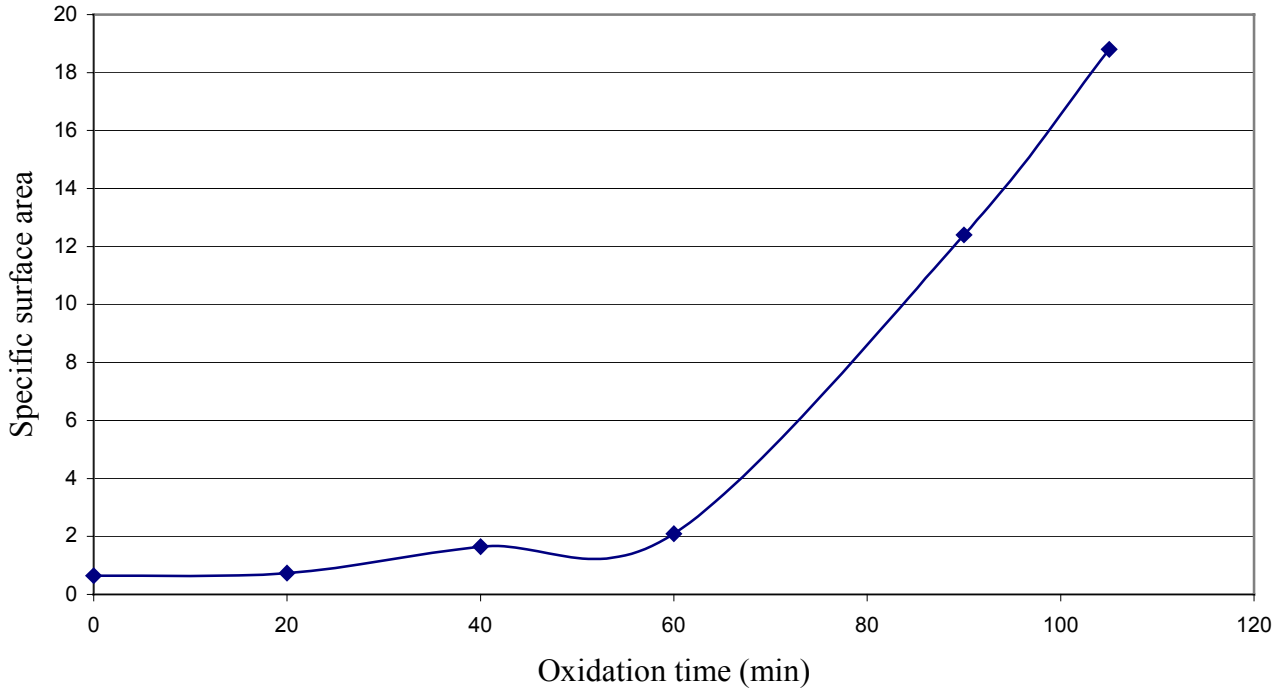

Figure 3.8 Nitrogen BET specific area of nitric acid oxidized (115 °C) PAN carbon fibers.

Pittman,Jr.C.U., Jiang,W., Yue,Z.R., Leon y Leon, C.A., *Carbon*, **1999**, *37*, 85-96

Surface area determination by carbon dioxide DR adsorption method

The surface area values for the unoxidized and oxidized VGCFs obtained by carbon dioxide Dubinin-Radushkevich (DR) method are given in Table 3.6. The surface area increased as oxidation increased to 30 minutes and then decreased a little at longer oxidation times. The differences in surface areas measured by nitrogen BET versus carbon dioxide DR are substantial. Carbon dioxide DR measured surface areas are more than twice those measured by nitrogen BET. Thermal activation is required for both nitrogen and carbon dioxide molecules to migrate through small pores. The operating temperatures used for the two measurements were different. The carbon dioxide DR measurements were done at 273 K while nitrogen BET was performed at 77 K. The higher temperature used in carbon dioxide DR measurements provided enough kinetic energy to permit activated diffusion of carbon dioxide [79,93,94]. Thus, carbon dioxide molecules can overcome the energy barriers associated with being adsorbed near the entrance in very narrow pores. The low temperature used in nitrogen BET does not provide the required thermal activation for migration throughout small pores whereas carbon dioxide can better fill the pore surfaces of small pores.

Like nitrogen BET measurements, the carbon dioxide DR measurements showed that increasing nitric acid oxidation of the fibers did not lead to progressive increases in the surface area. In fact, little or no further change in the surface area occurred after 10-minute oxidation. Thus, VGCFs are exceptionally resistant to oxidation. Previous carbon dioxide DR measurements done on PAN fibers (electrochemically oxidized with KNO_3) by our research group showed a significant increase in surface area compared to nitrogen

BET measurements [79a]. This further proves that carbon dioxide DR method gave better results compared to nitrogen BET method because CO_2-DR can access pores with tiny diameters.

Table 3.6 CO_2 -DR surface areas of the unoxidized and oxidized VGCFs.

Sample ID	CO_2 DR [a] (m^2/g)
Unoxidized VGCF	20.48
VGCF oxidized for 10 min	59.54
VGCF oxidized for 20 min	53.34
VGCF oxidized for 30 min	67.37
VGCF oxidized for 60 min	41.8
VGCF oxidized for 90 min	67.30
VGCF oxidized for 10 h	23.12 [b]

[a] Average surface area values of two trials.
[b] Measured at Quantachrome.

A schematic diagram showing the adsorption of gaseous molecules diffusing into a micropore is shown in Figure 3.10 [79].

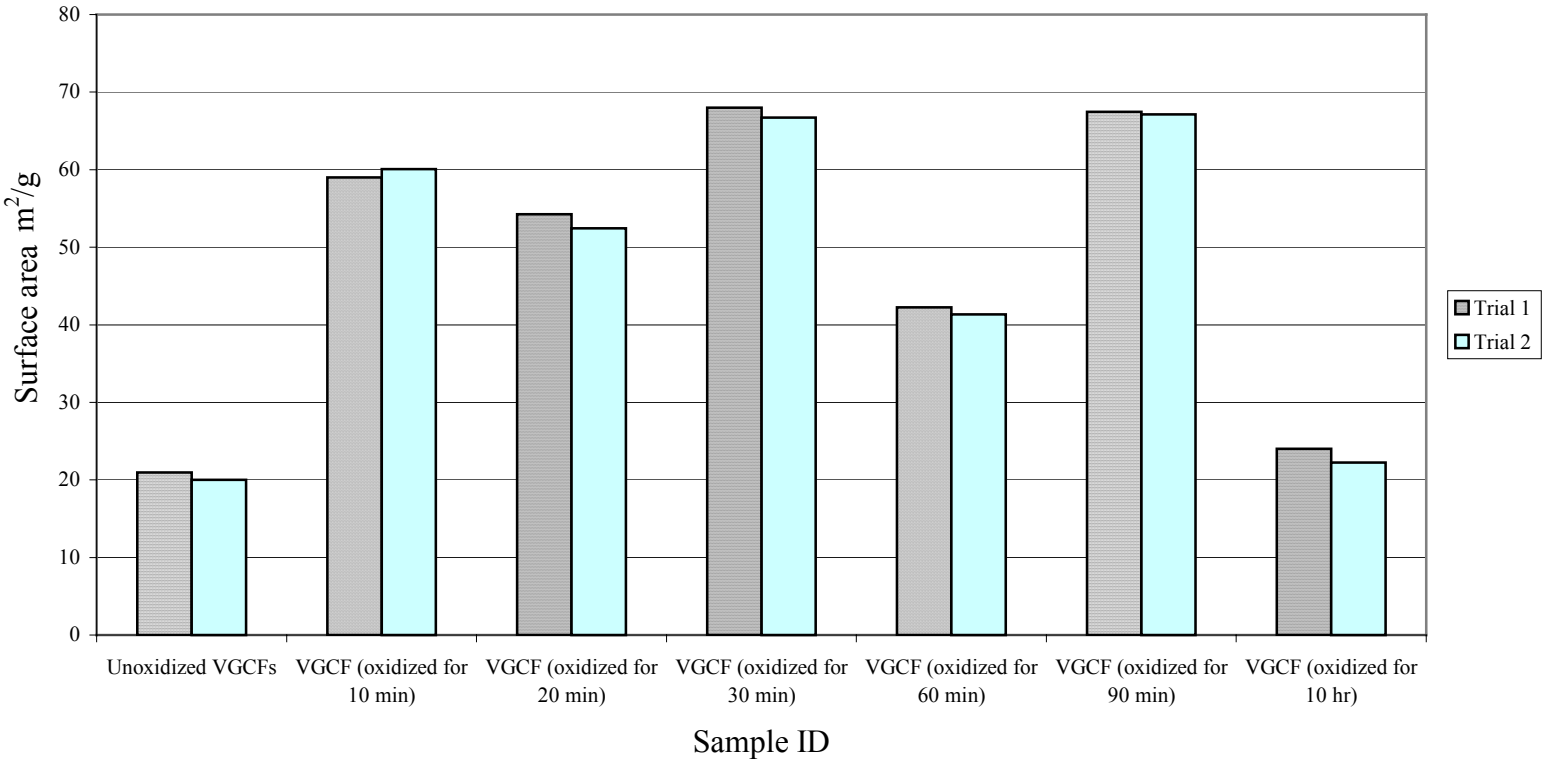

Figure 3.9 CO_2 DR surface area distributions of unoxidized and oxidized (concentrated nitric acid, 115 °C) VGCFs

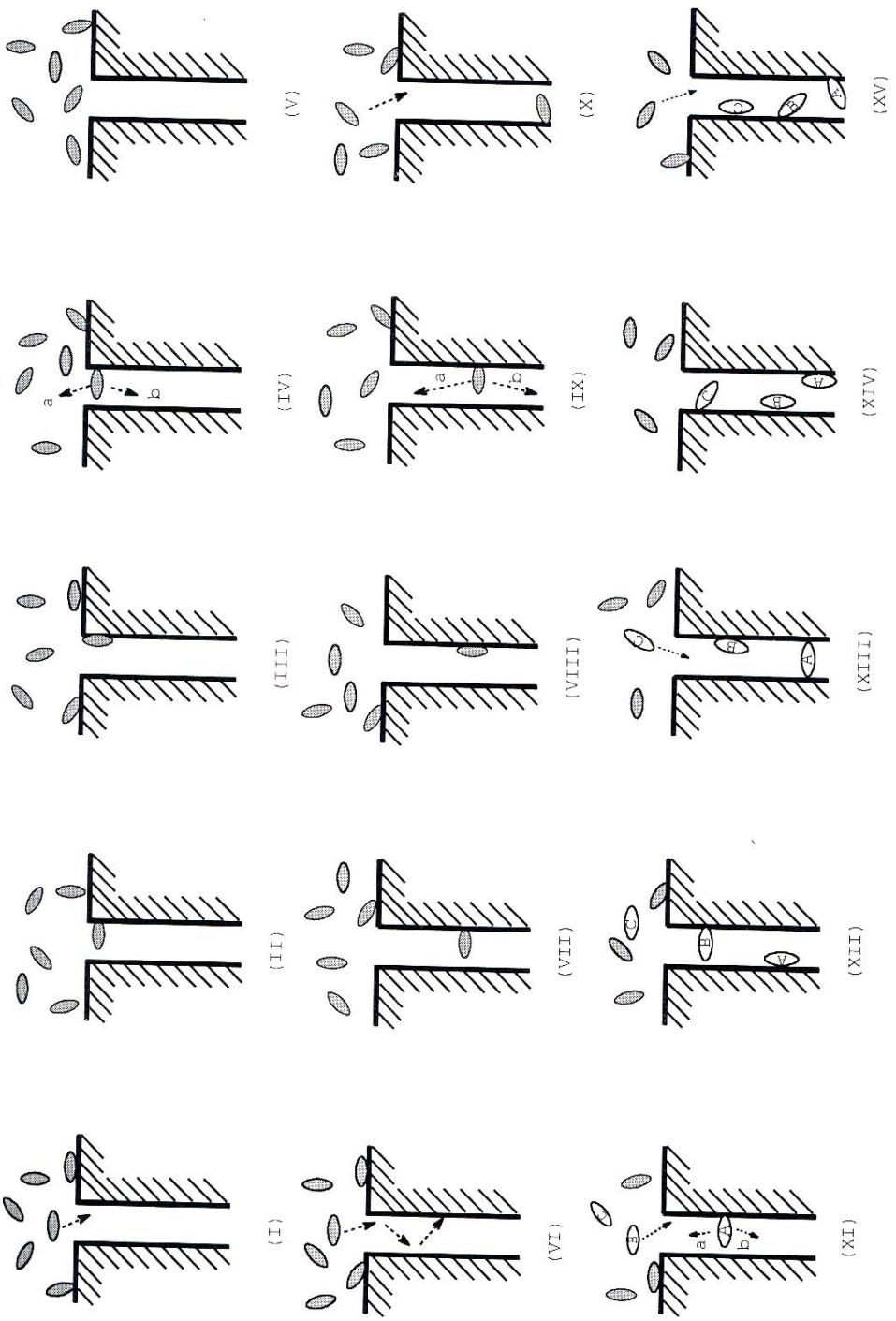

Figure3.10 Adsorption diagram of gaseous molecules diffusing into a micropore.

At low temperature, the adsorbate molecule has a low kinetic energy (I). It can only diffuse a very short distance into the micropore (II) before it is adsorbed by the surface (III). Later, the adsorbed molecule may gain enough energy to escape from that specific adsorption site (IV). There are two escape pathways: pathway ‘a’, with a low energy barrier, is back into the gaseous phase. In pathway ‘b’, deeper penetration of the molecule into the micropore may occur if the molecule overcomes the higher energy barrier associated with this process. At low temperatures, the molecule has a low kinetic energy. Therefore, it travels by pathway ‘a’ to reenter its gaseous phase (V). Large inner surface areas are not detected by the adsorbate. At 273 K, an adsorbate molecule has higher kinetic energy (VI). It can penetrate deeply into the micropore (VII) by a series of jumps on and off shallower adsorption sites before it is adsorbed by the surface (VIII). When the adsorbate re-escapes from the adsorption site (IX), the difference of the energy barriers between the two pathways becomes smaller, and the kinetic energy of the adsorbate molecule becomes bigger. The adsorbate can further diffuse into the micropore (X).

In ultramicropores, (pores < 1 nm in diameter) the adsorption of N_2 or CO_2 near the pore opening blocks the access of any other adsorbate molecule (XI). Hence, adsorbed molecule A prevents entry of molecule B. At low temperature, path ‘a’ (lower energy) is greatly favored over path ‘b’ (higher energy). The small pore diameter will not accommodate both molecule A and molecule B. At higher temperature, path ‘b’ is populated leading to (XIII) where molecule A is adsorbed more deeply in the pore. Thus molecule B can also diffuse into the pore (XII) and adsorb (XIII). Now both molecules A and B block further entry of other adsorbate molecules. At higher temperatures, further

sequential penetrations occur opening an adsorption site for molecule C (XIV). This picture clearly points out why CO_2-DR method can more accurately measure surface areas within smaller pores (typically below 5 nm) than N_2 BET.

Pore size distribution models assume that the stronger the adsorption site, the stronger the molecules are adsorbed. Adsorption is strongest in the smallest pores where walls surround all sides of the CO_2 molecule [79]. Thus, the small pores are filled first compared to the larger pores. Using the isotherm data and the DR results, the pore size distribution is computed. This, of course, depends on the model assumptions. The DR method assumes all pores to be flat slits of average width. The DR method correctly measures the pore size distribution (calculated from density functional theory) but may slightly overestimate the true micropore volume.

XPS analysis of VGCFs

The different functional groups present on the surface of the unoxidized and oxidized VGCFs were determined using XPS (Perkin Elmer, Physical Electronics Model 1600 surface analysis system, 30° take-off angle). The surface O1s/C1s atomic ratios of the different VGCFs are shown in Table 3.6 and Figure 3.11. The O1s/C1s atomic ratio is the smallest for the unoxidized VGCFs. On oxidation, the O1s/C1s atomic ratio increases, though not continuously. Deconvolution of the C1s spectra gave 3 peaks designated as Peak A (at 284.6 eV assigned to graphitic carbon), Peak B (at 286.1-286.3 eV, carbons bonded to phenolic or alcoholic hydroxyls or ether oxygens) and Peak C (at 287.7-288.6 eV, carbonyl, quinone, carboxyl or ester groups). From this deconvoluted

spectra, the ratio of graphitic carbon and the carbon bonded to different oxygenated groups were calculated and are given in Table 3.7.

Table 3.7 XPS O1s/C1s atomic ratio of VGCFs taken at a 30° take-off angle.

Sample ID	O1s/C1s atomic ratio
Unoxidized VGCF	0.059
VGCF oxidized for 10 min	0.177
VGCF oxidized for 20 min	0.181
VGCF oxidized for 30 min	0.256
VGCF oxidized for 60 min	0.232
VGCF oxidized for 90 min	0.238
VGCF oxidized for 4 hr	0.200
VGCF oxidized for 10 hr	0.154
VGCF oxidized for 24 hr	0.167

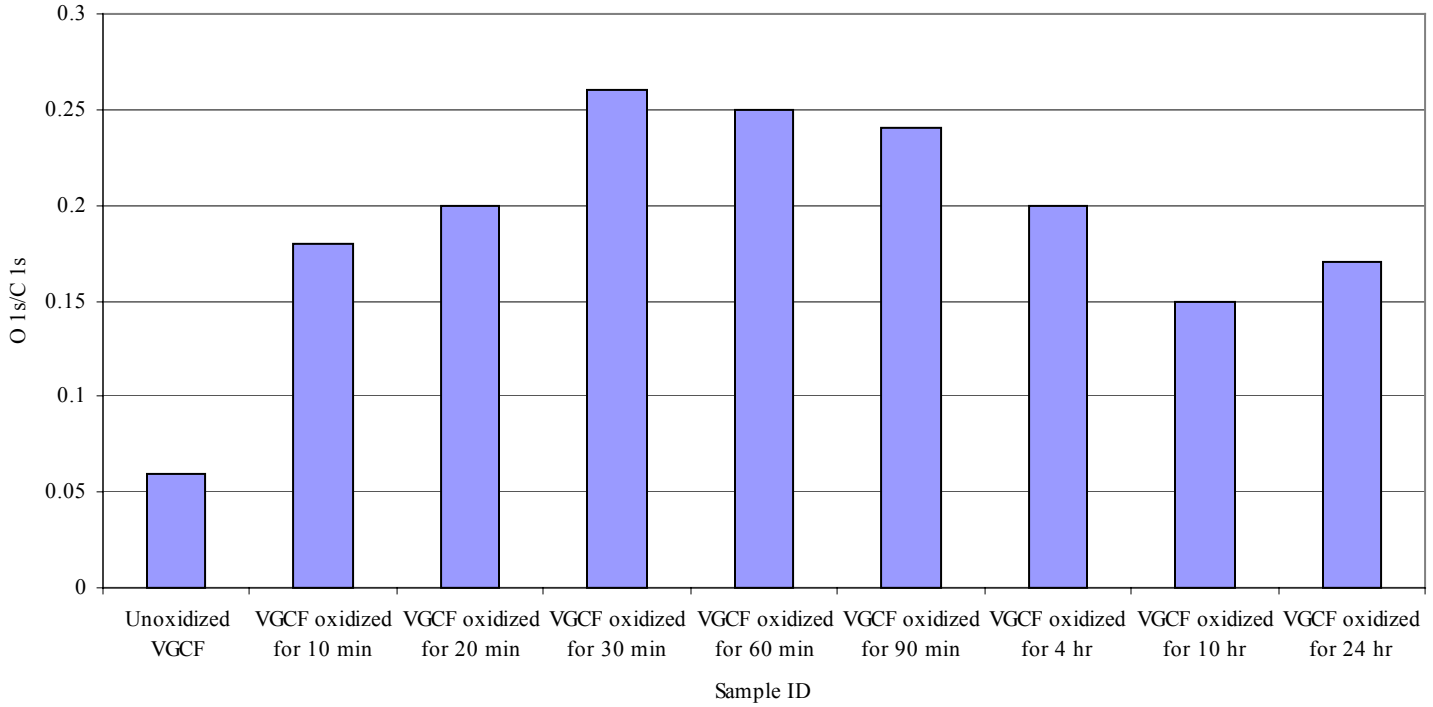

Figure 3.11 XPS O1s/C1s atomic ratio of VGCFs taken at a 30° take-off angle.

Table 3.8 Relative content of functional groups in C1s spectra from XPS at a 30° take-off angle.

Sample ID	Percentage area of functional groups in C1s spectra (%)		
	Peak A [a] 284.6 (eV)	Peak B [b] 286.1 – 286.3 (eV)	Peak C [c] 287.7 – 288.6 (eV)
Unoxidized VGCF	75.09	24.91	------
VGCF oxidized for 10 min	73.35	19.13	7.52
VGCF oxidized for 20 min	81.00	13.12	5.87
VGCF oxidized for 30 min	78.7	12.19	9.11
VGCF oxidized for 60 min	76.71	13.72	9.57
VGCF oxidized for 90 min	76.93	12.65	10.42
VGCF oxidized for 4 hr	76.92	13.81	9.27
VGCF oxidized for 10 hr	83.79	11.3	4.91
VGCF oxidized for 24 hr [d]	83.55	16.45	------

[a] Peak A (at 284.6 eV assigned to graphitic carbon)
[b] Peak B (at 286.1-286.3 eV, phenolic, alcoholic hydroxyls or ether oxygens)
[c] Peak C (at 287.7-288.6 eV, carbonyl, quinone, carboxyl or ester carbons)
[d] The increase in peak B and the absence of peak C may be an artifact of the deconvolution mathematics. Various peaks were seen in the O1s XPS spectra (see page 71) suggesting that some functions belonging to peak C should be present.

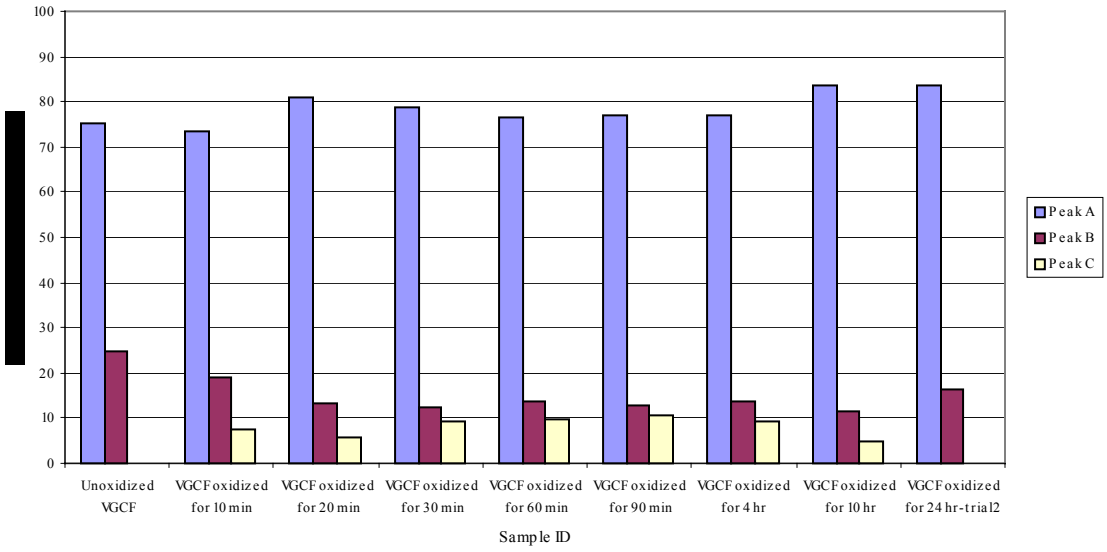

Figure 3.12 Distribution of functional groups in C1s spectra from XPS at a 30° take-off angle

The XPS results indicate that Peak B (carbons bonded to phenolic or alcoholic hydroxyls or ether oxygens) decreased on oxidation. Also, no Peak C (carbonyl, quinone, carboxyl or ester carbons) was observed in the unoxidized VGCF. Oxidation of VGCFs resulted in the rise of peak C through the production of carbonyl, quinone, carboxyl or ester groups on the fiber surfaces. The high-resolution C1s spectra for the different samples of VGCFs are shown in Figures 3.13 to 3.21.

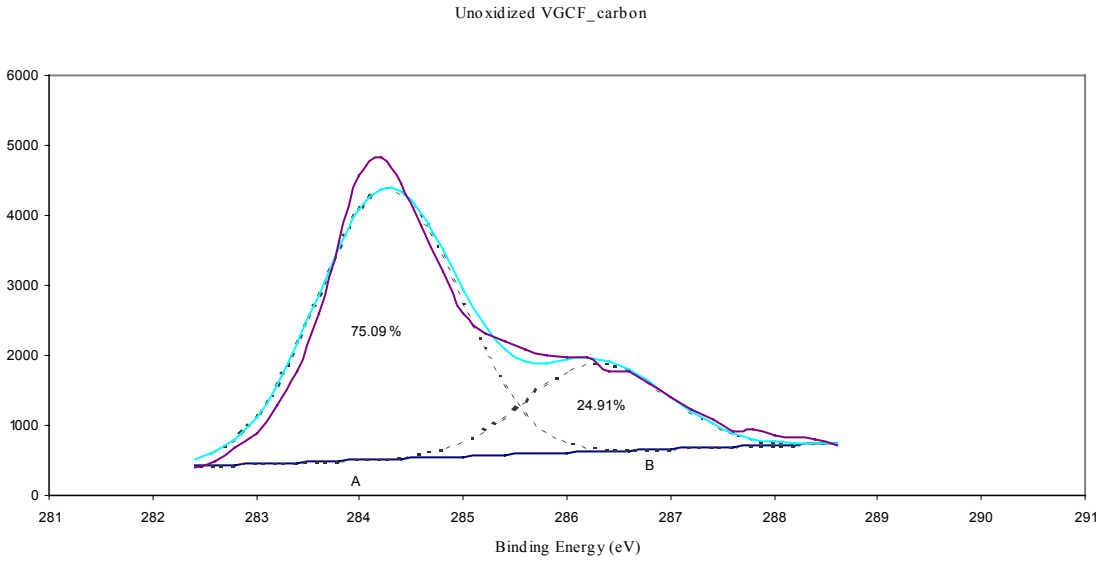

Figure 3.13 High-resolution XPS C1s spectra of unoxidized VGCF taken at a 30° take-off angle.

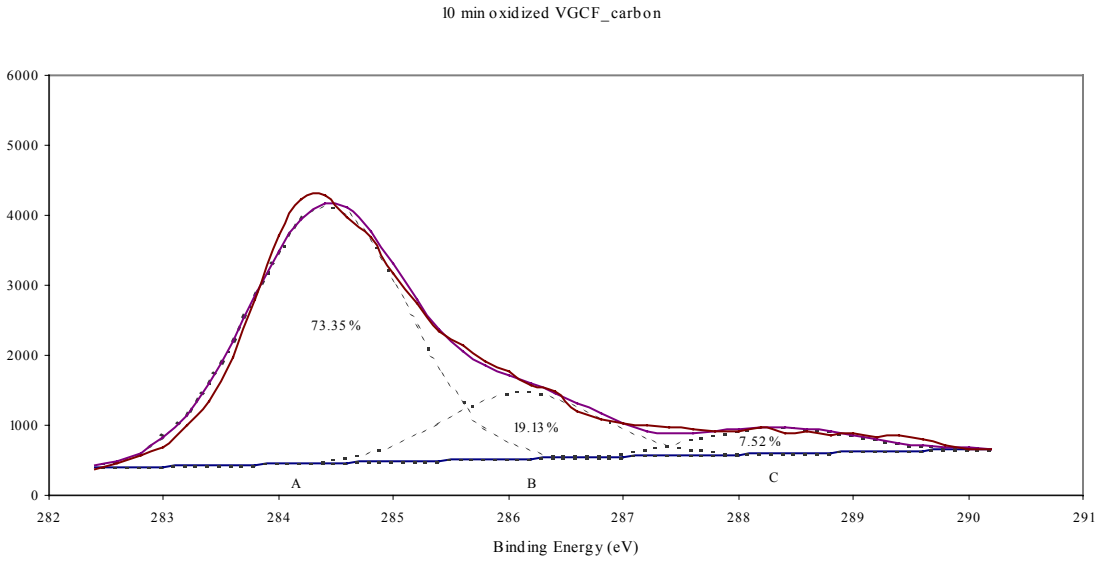

Figure 3.14 High-resolution XPS C1s spectra of VGCF (oxidized for 10 min) taken at a 30° take-off angle.

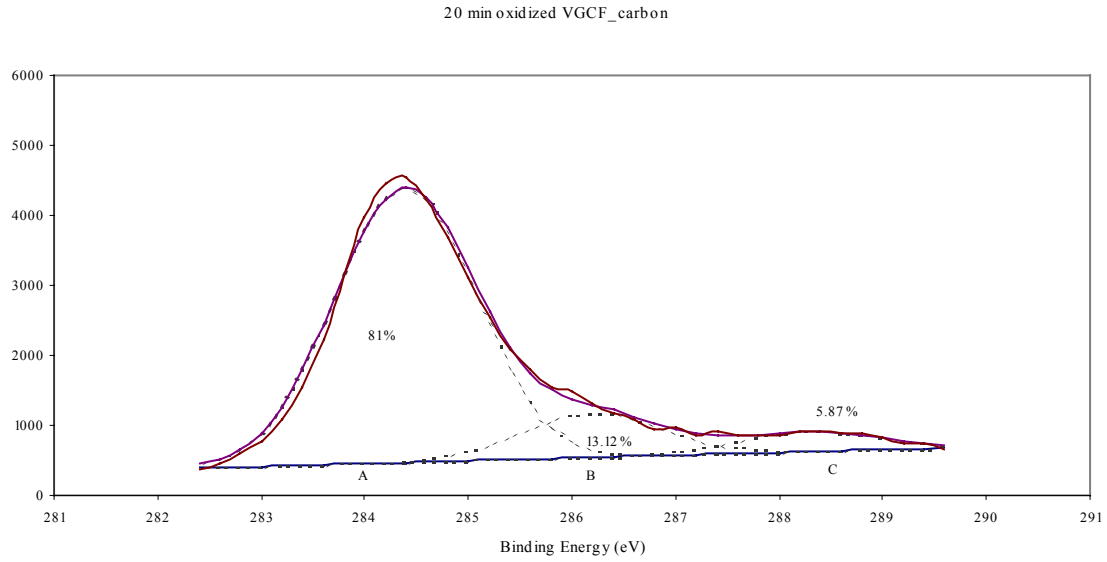

Figure 3.15 High-resolution XPS C1s spectra of VGCF (oxidized for 20 min) taken at a 30° take-off angle.

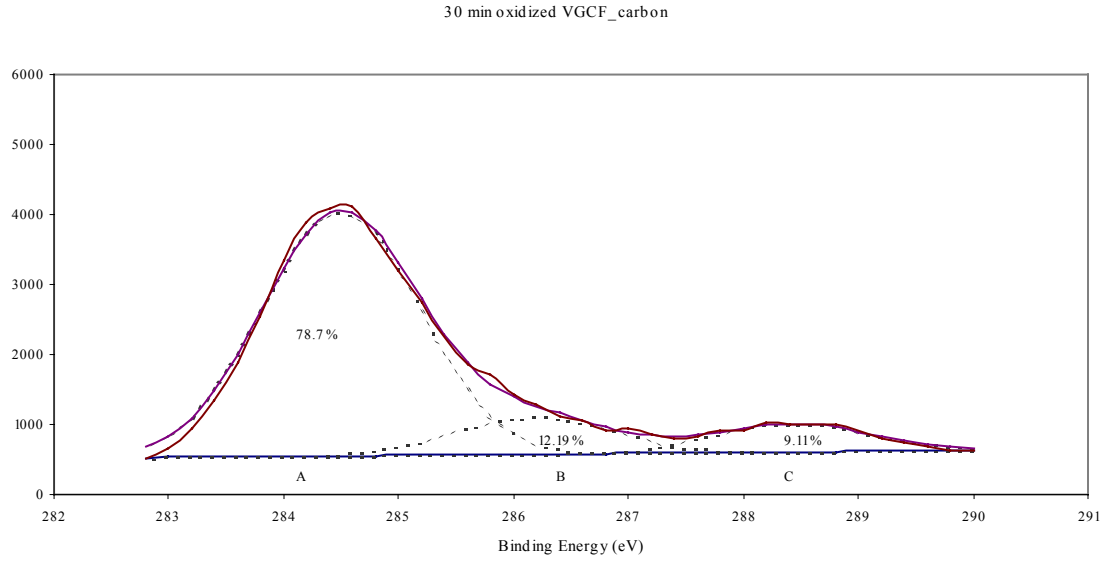

Figure 3.16 High-resolution XPS C1s spectra of VGCF (oxidized for 30 min) taken at a 30° take-off angle.

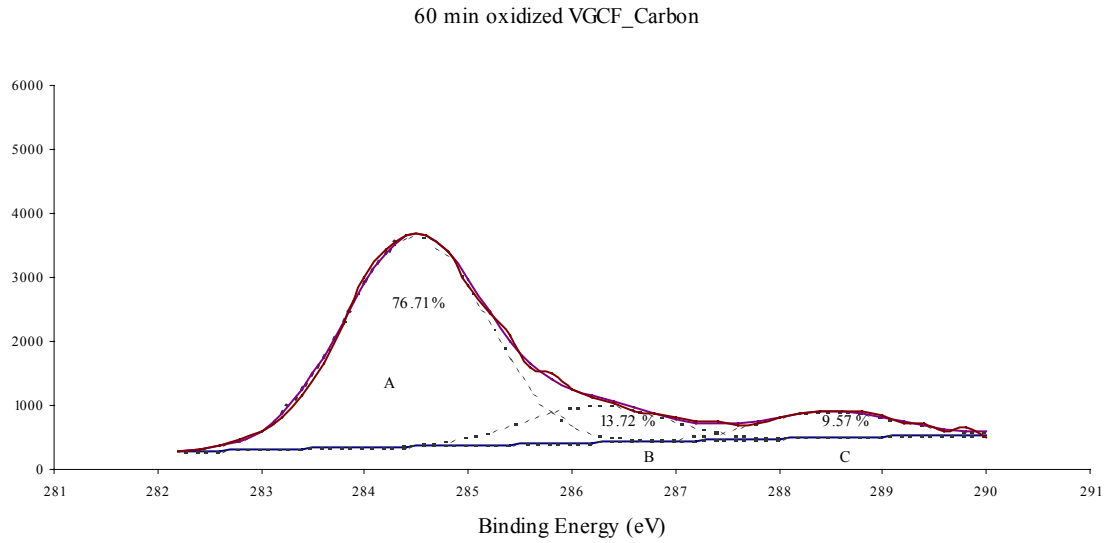

Figure 3.17 High-resolution XPS C1s spectra of VGCF (oxidized for 60 min) taken at a 30° take-off angle.

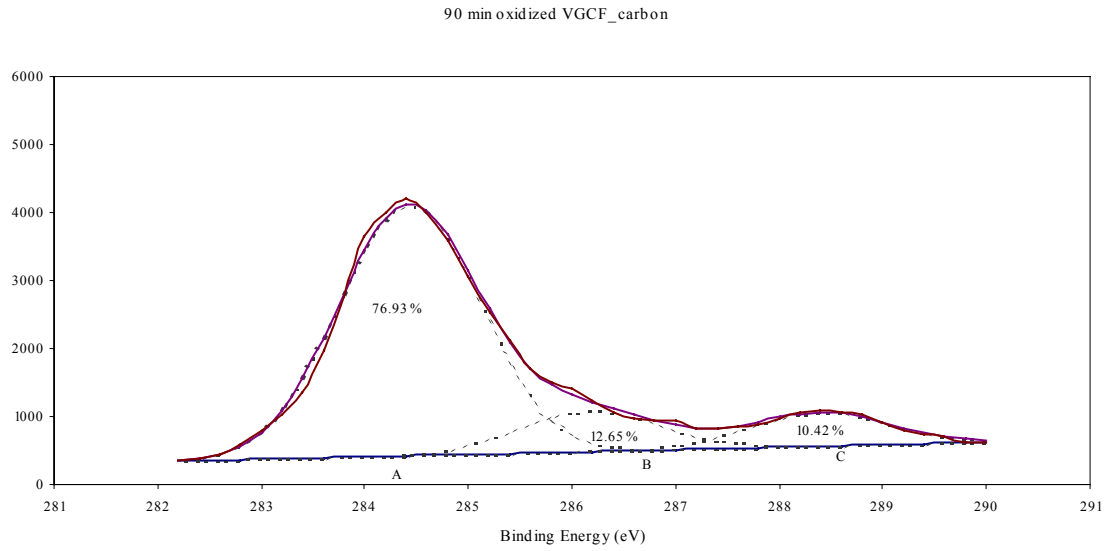

Figure 3.18 High-resolution XPS C1s spectra of VGCF (oxidized for 90 min) taken at a 30° take-off angle.

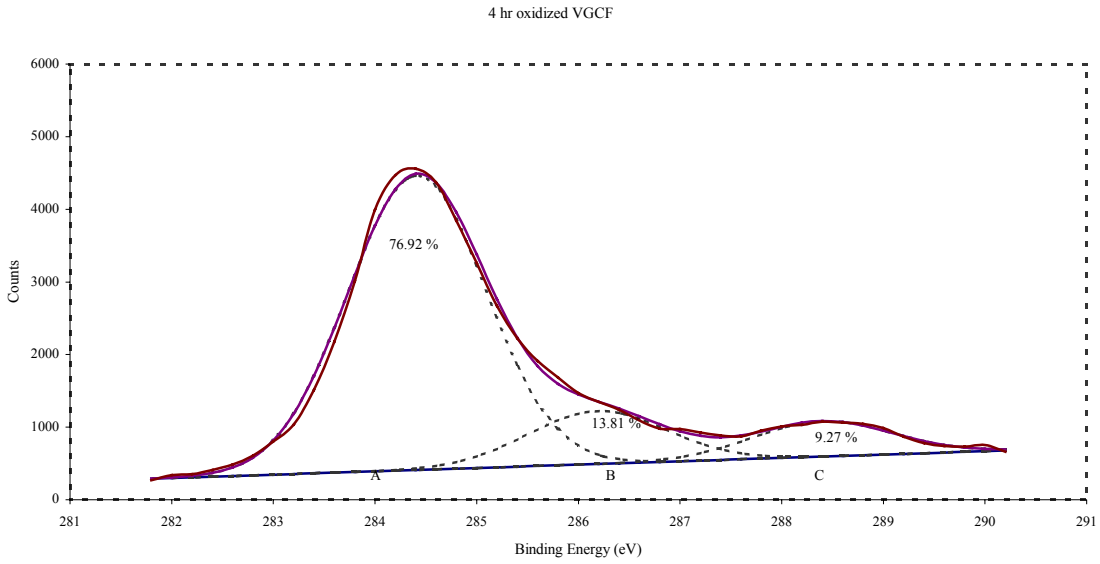

Figure 3.19 High-resolution XPS C1s spectra of VGCF (oxidized for 4 hr) taken at a 30° take-off angle.

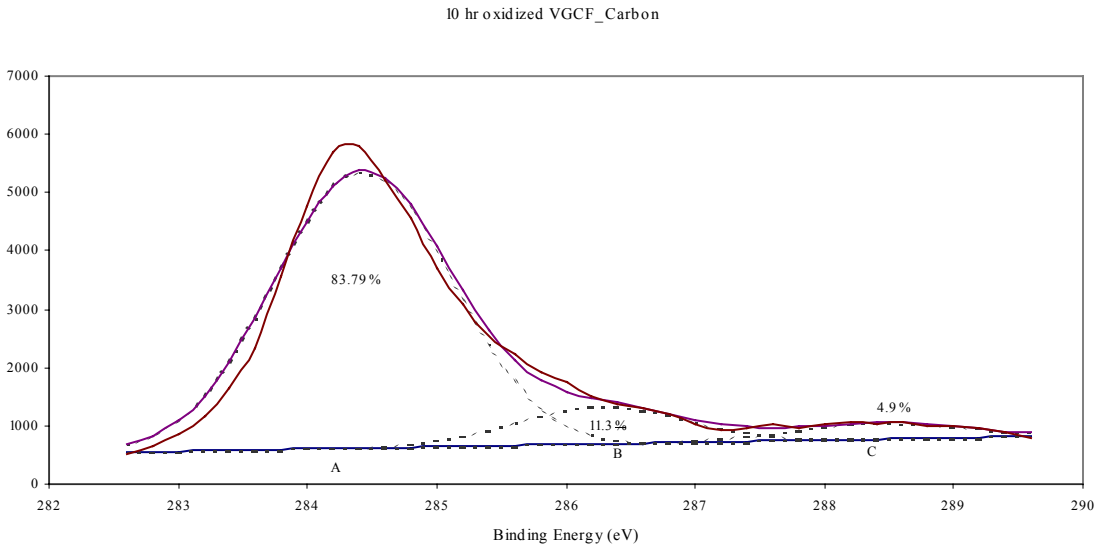

Figure 3.20 High-resolution XPS C1s spectra of VGCF (oxidized for 10 hr) taken at a 30° take-off angle.

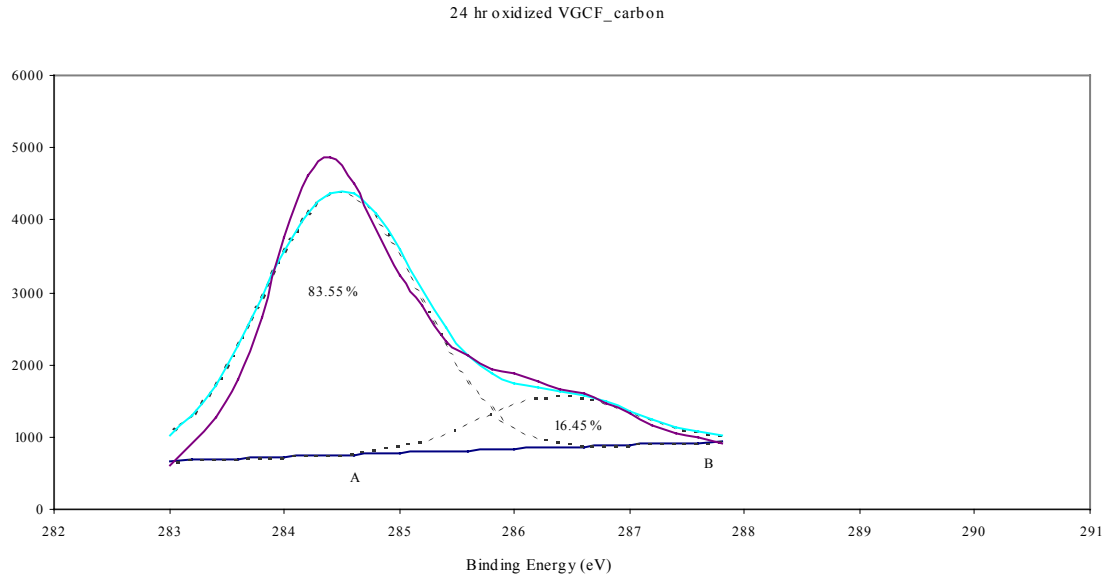

Figure 3.21 High-resolution XPS C1s spectra of VGCF (oxidized for 24 hr) taken at a 30° take-off angle.

Similar deconvolution of the O1s spectra of the VGCF gave 4 peaks designated as Peak I (at 530.97-531.94 eV, quinoid carbonyl), Peak II (at 532.33-532.82 eV, carbonyl oxygen atoms in esters, anhydrides and oxygen atoms in hydroxyls or esters), Peak III (at 533.13-533.81 eV, ether oxygen atoms in esters and anhydrides) and Peak IV (at 534.97 eV, oxygen atoms in carboxyl groups). From this, the distribution of the functional groups on the O1s spectra was calculated as shown in Table 3.8. Figure 3.22 shows a schematic representation of the functional groups present in the different peaks (peak I – IV).

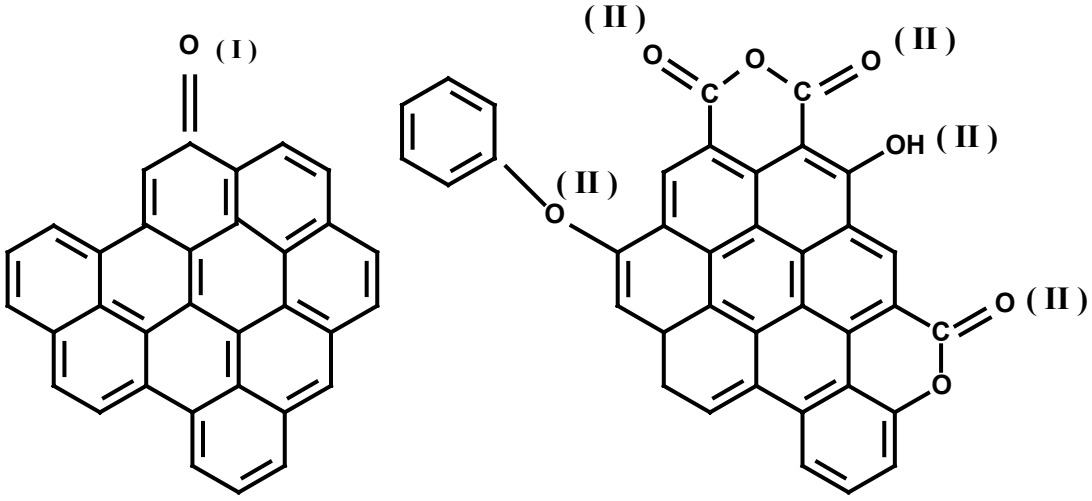

Peak I (at 530.97-531.94 eV, quinoid carbonyl)

Peak II (at 532.33-532.82 eV, carbonyl oxygen atoms in esters, anhydrides and oxygen atoms in hydroxyls or esters)

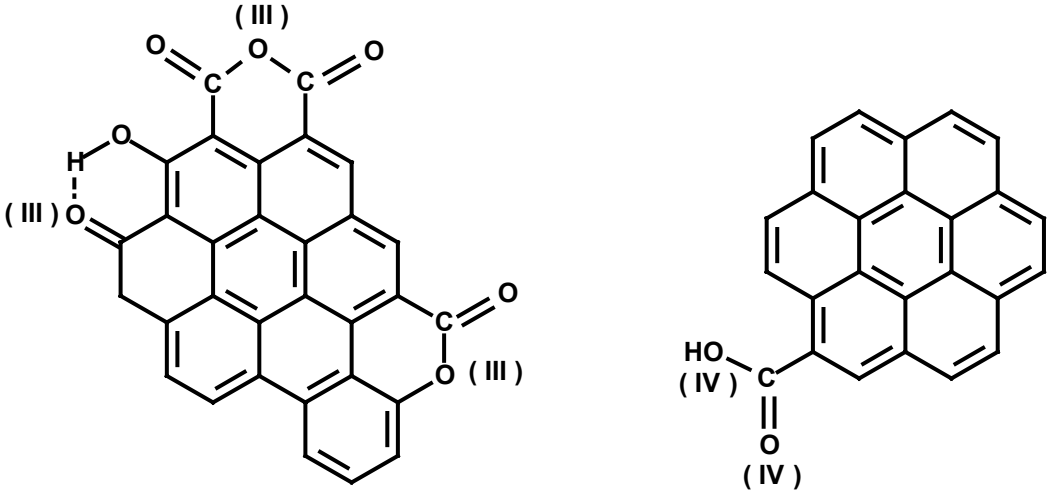

Peak III (at 533.13-533.81 eV, ether oxygen atoms in esters and anhydrides)

Peak IV (at 534.97 eV,oxygen atoms in carboxyl groups)

Figure 3.22 Schematic representation of the functional groups present in the O1s spectra.

Table 3.9 Relative content of functional groups in O1s spectra from XPS at a 30° take-off Angle.

Sample ID	Percentage area of functional groups in O1s spectra			
	Peak I 530.97 - 531.94 (eV)	Peak II 532.33 - 532.82 (eV)	Peak III 533.13 - 533.81 (eV)	Peak IV 534.97 (eV)
Unoxidized VGCF	16.05	-----	49.14	34.81
VGCF oxidized for 10 min	35.54	33.62	30.84	-----
VGCF oxidized for 20 min	37.34	37.22	25.44	-----
VGCF oxidized for 30 min	43.13	37.98	18.89	-----
VGCF oxidized for 60 min	19.83	40.14	40.03	-----
VGCF oxidized for 90 min	42.18	40.77	17.05	-----
VGCF oxidized for 4 h	34.07	32.08	33.85	-----
VGCF oxidized for 10 h	19.44	34.13	46.43	-----
VGCF oxidized for 24 h	40.11	45.55	14.34	-----

[a] Peak I (at 530.97-531.94 eV, quinoid carbonyl)
[b] Peak II (at 532.33-532.82 eV, carbonyl oxygen atoms in esters, anhydrides and oxygen atoms in hydroxyls or esters)
[c] Peak III (at 533.13-533.81 eV, ether oxygen atoms in esters and anhydrides)
[d] Peak IV (at 534.97 eV, oxygen atoms in carboxyl groups)

Table 3.10 Amount of oxygen present in each peak of oxidized VGCFs relative to oxygen present on the unoxidized VGCFs.

Sample ID	Area percent [e]			
	Peak I [a] 530.97 - 531.94 (eV)	Peak II [b] 532.33 - 532.82 (eV)	Peak III [c] 533.13 - 533.81 (eV)	Peak IV [d] 534.97 (eV)
Unoxidized VGCF	16.05	-----	49.14	34.81
VGCF oxidized for 10 min	104.5	98.8	90.67	-----
VGCF oxidized for 20 min	109.78	109.43	74.79	-----
VGCF oxidized for 30 min	126.80	111.66	55.54	-----
VGCF oxidized for 60 min	58.30	118.01	117.69	-----
VGCF oxidized for 90 min	124.01	119.86	50.13	-----
VGCF oxidized for 4 h	100.17	94.32	99.52	-----
VGCF oxidized for 10 h	57.15	100.34	136.50	-----
VGCF oxidized for 24 h	117.92	133.92	42.16	-----

[a] Peak I (at 530.97-531.94 eV, quinoid carbonyl)
[b] Peak II (at 532.33-532.82 eV, carbonyl oxygen atoms in esters, anhydrides and oxygen atoms in hydroxyls or esters)
[c] Peak III (at 533.13-533.81 eV, ether oxygen atoms in esters and anhydrides)
[d] Peak IV (at 534.97 eV, oxygen atoms in carboxyl groups)
[e] Unoxidized VGCF is used as the reference

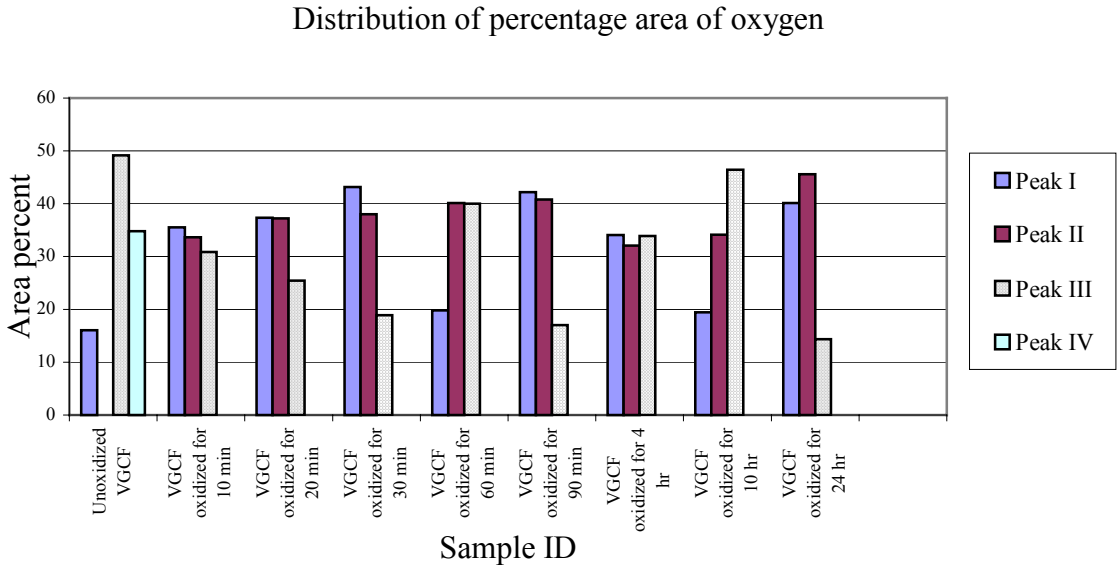

Figure 3.23 Distribution of functional groups in O1s spectra from XPS at a 30° take-off angle.

The XPS results indicate an initial increase in oxygen content with nitric acid oxidation (though not continuously). It was observed that oxidation caused peak IV (oxygen atoms in carboxyl groups) to disappear. Thus, carboxyl functions are on the surface of the as-received fibers. Remarkably, at 115 °C in 69 - 71 wt% nitric acid these groups are decarboxylated. Nitric acid oxidation promotes the growth of peak II (carbonyl oxygen atoms in esters, anhydrides and oxygen atoms in hydroxyls or esters) at the surface. Also, there was an increase in the ester/anhydride and quinone groups in the oxidized fibers. Table 3.11 shows the atomic concentrations of the C1s and O1s spectra on the surface of VGCFs.

Table 3.11 Atomic concentration of C1s and O1s spectra obtained from XPS.

Sample ID	C1s spectra	O1s spectra
Unoxidized VGCF	93.7	6.3
VGCF oxidized for 10 min	81.5	18.5
VGCF oxidized for 20 min	83.7	16.3
VGCF oxidized for 30 min	78.8	21.2
VGCF oxidized for 60 min	78.8	21.2
VGCF oxidized for 90 min	77.5	22.5
VGCF oxidized for 4 hr	81.1	18.9
VGCF oxidized for 10 hr	85.3	14.7
VGCF oxidized for 24 hr	85.6	14.4

A three-fold increase in surface oxygen was observed in oxidized VGCFs compared to the unoxidized VGCFs. Correspondingly, the surface carbon content decreased in oxidized VGCFs compared to the unoxidized VGCFs. This accounts for the increase in base uptake values obtained (oxidized VGCFs showed a double base uptake value compared to the unoxidized VGCFs). The phenolic hydroxyl groups present on the oxidized VGCFs react with the base (NaOH). The XPS analysis of the unoxidized fiber showed the absence of phenolic groups, which accounts for the lower base uptake value obtained despite the presence of –COOH functions. Figure 3.24 shows a schematic representation of the chemistry of the unoxidized and oxidized edge of the VGCFs.

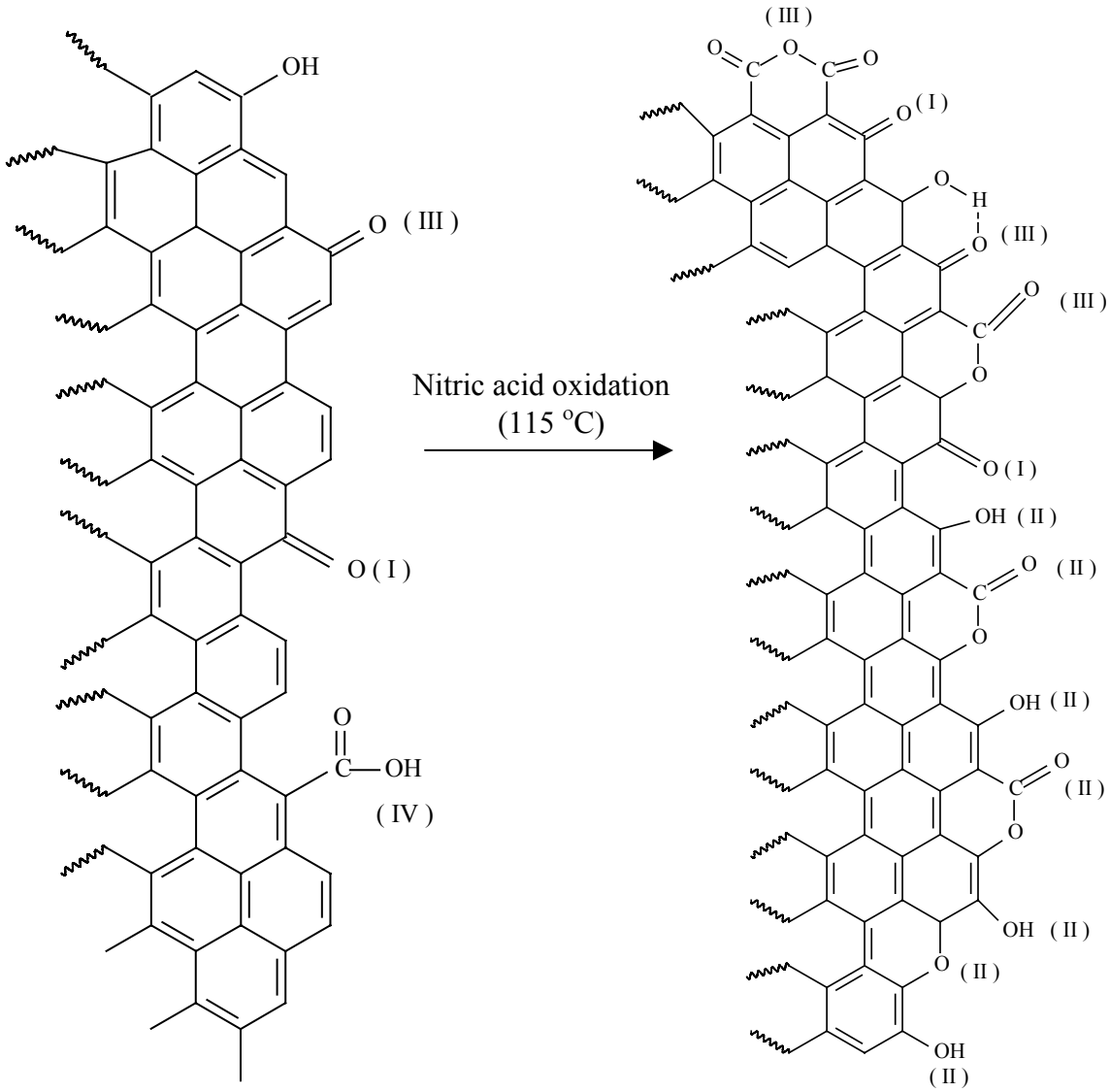

Unoxidized edge of VGCF

Oxidized edge of VGCF

Figure 3.24 Schematic representation of the chemistry of unoxidized and oxidized edge of VGCF.

The high-resolution O1s spectra for the different samples of VGCFs are shown in Figures 3.25 to 3.33.

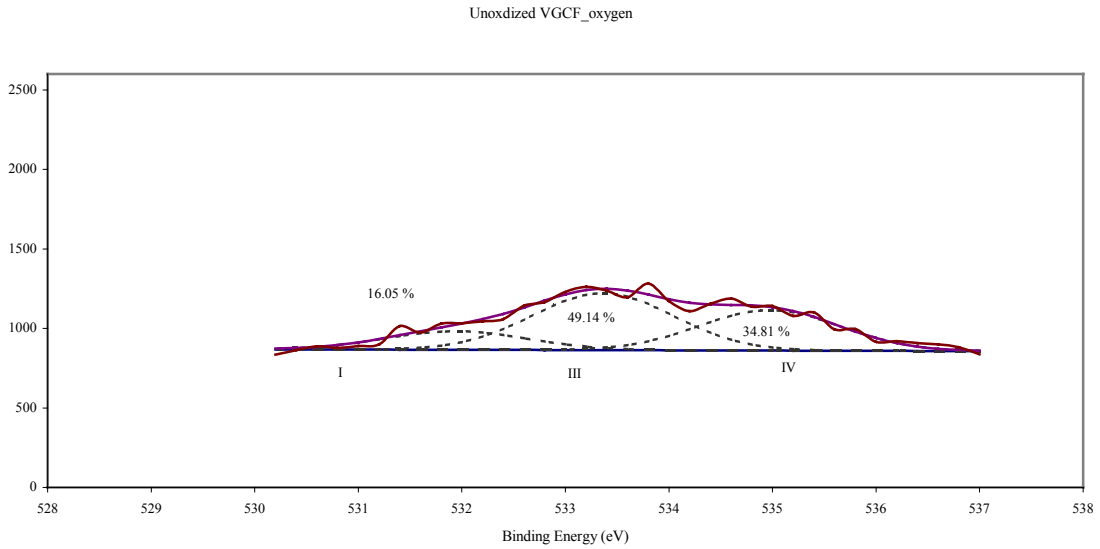

Figure 3.25 High resolution XPS O1s spectra of unoxidized VGCF taken at a 30° take-off angle.

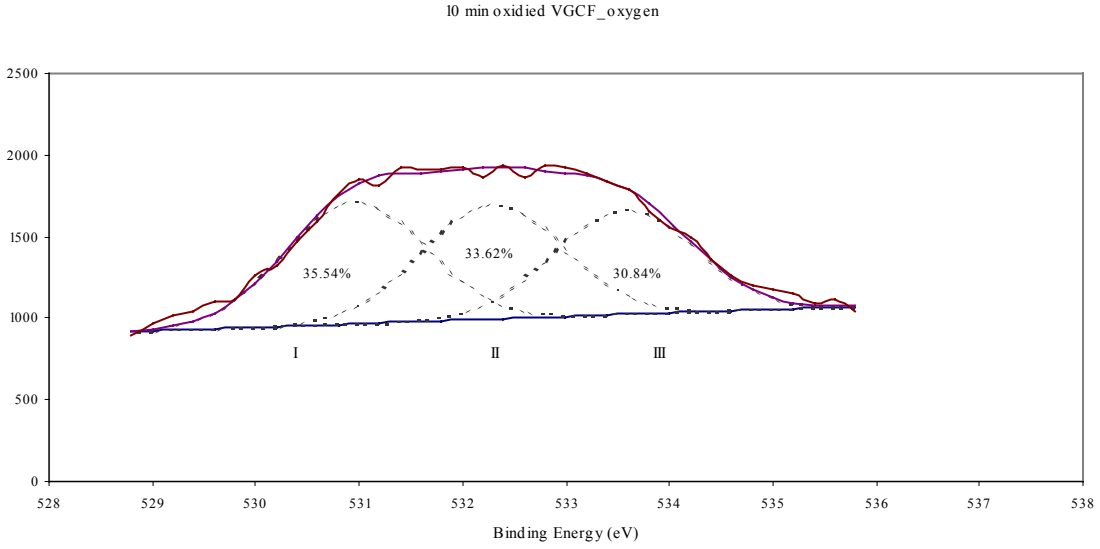

Figure 3.26 High resolution XPS O1s spectra of VGCF (oxidized for 10 min) taken at a 30° take-off angle.

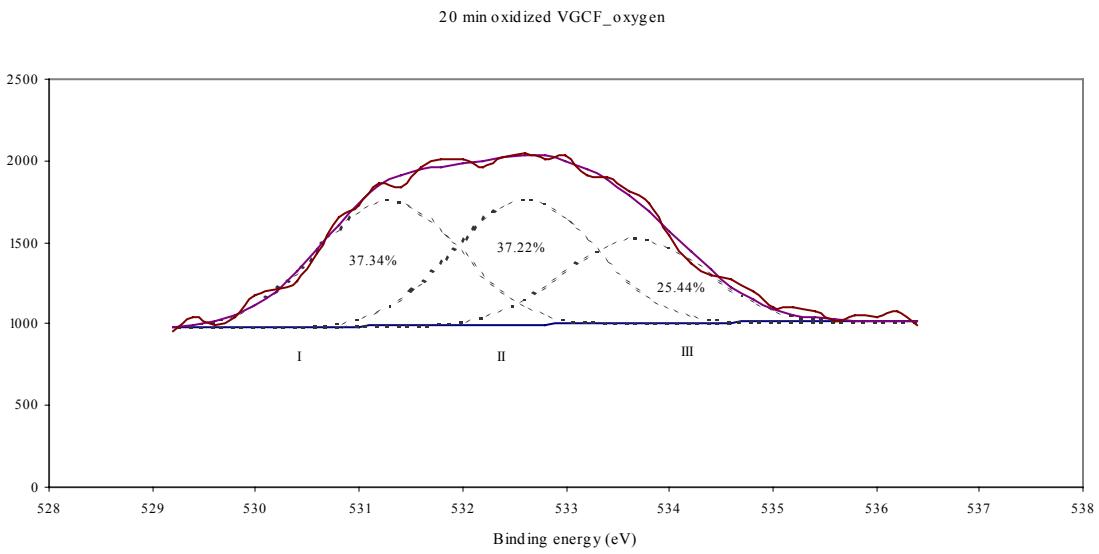

Figure 3.27 High resolution XPS O1s spectra of VGCF (oxidized for 20 min) taken at a 30° take-off angle.

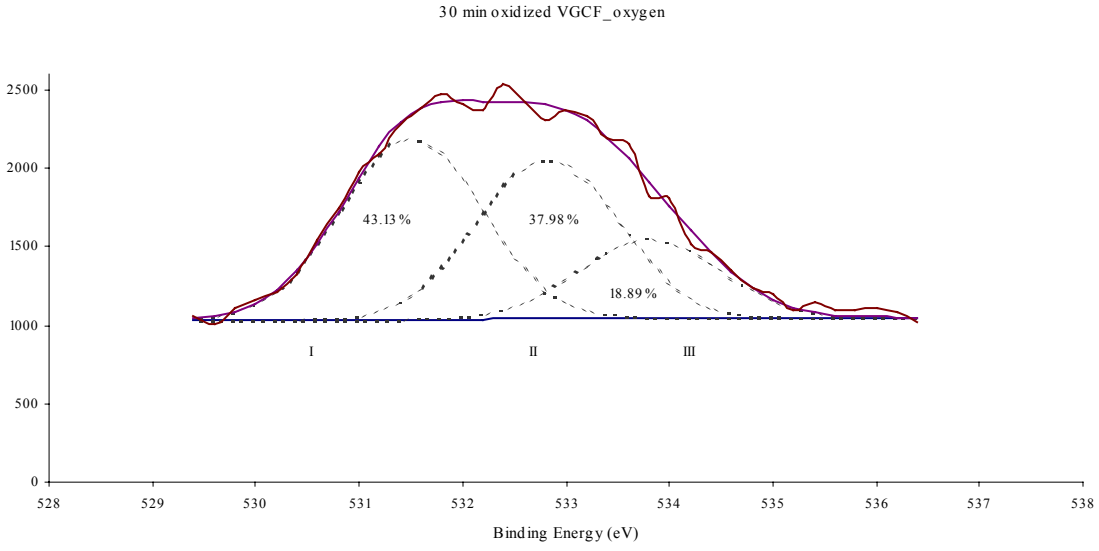

Figure 3.28 High resolution XPS O1s spectra of VGCF (oxidized for 30 min) taken at a 30° take-off angle.

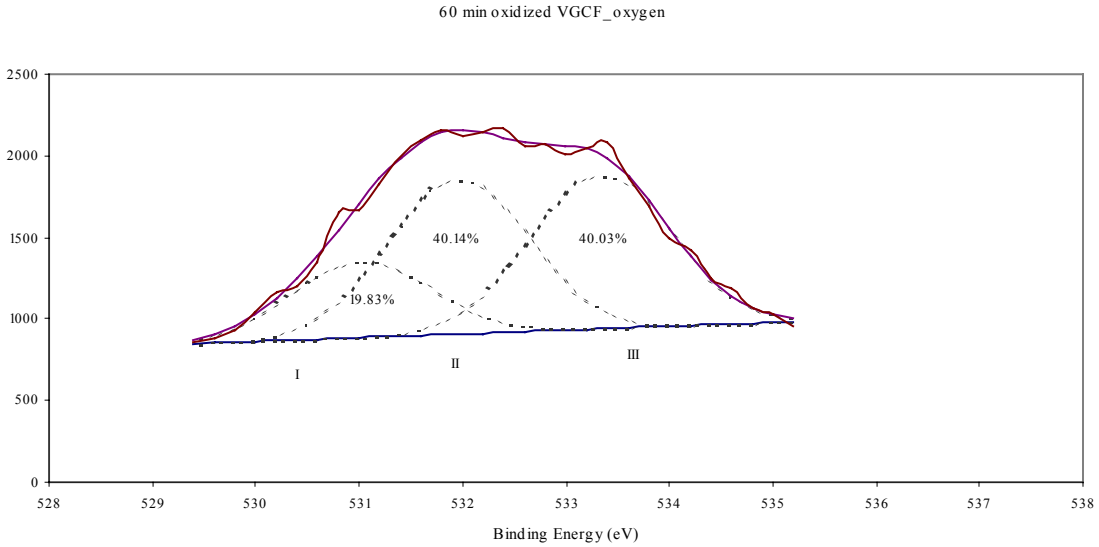

Figure 3.29 High resolution XPS O1s spectra of VGCF (oxidized for 60 min) taken at a 30° take-off angle.

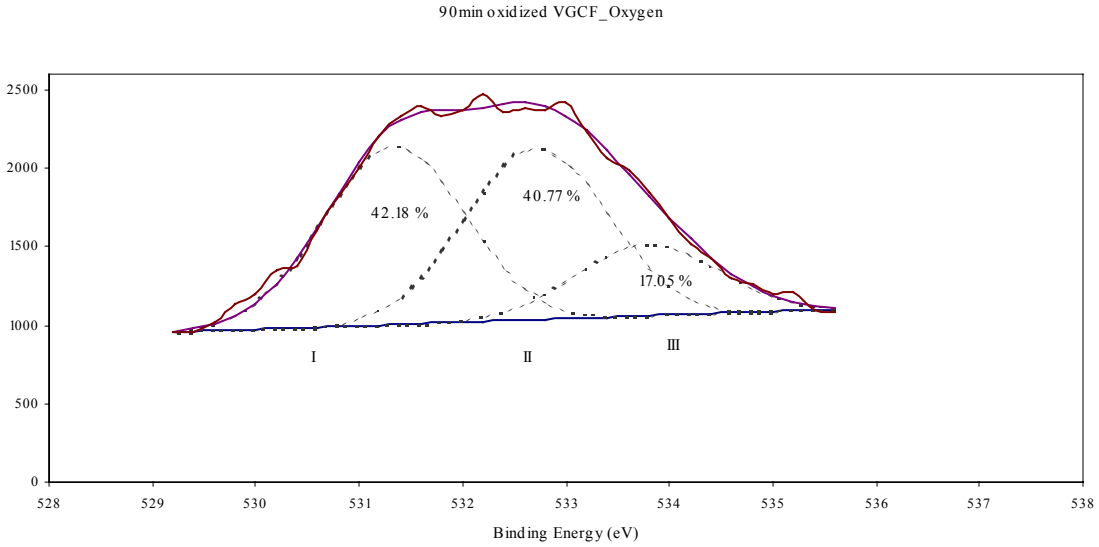

Figure 3.30 High resolution XPS O1s spectra of VGCF (oxidized for 90 min) taken at a 30° take-off angle.

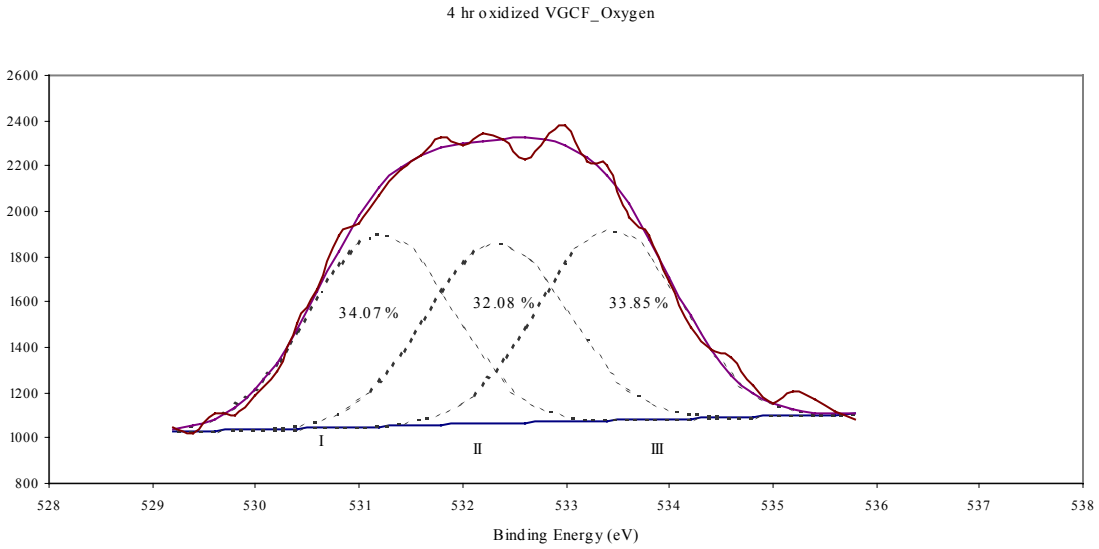

Figure 3.31 High resolution XPS O1s spectra of VGCF (oxidized for 4 hr) taken at a 30° take-off angle.

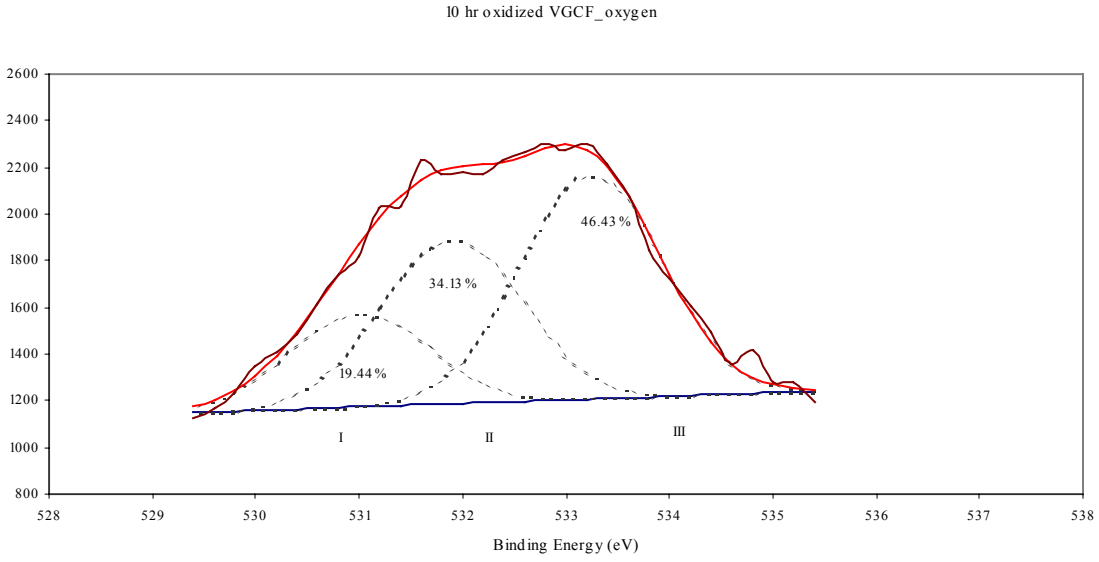

Figure 3.32 High resolution XPS O1s spectra of VGCF (oxidized for 10 hr) taken at a 30° take-off angle.

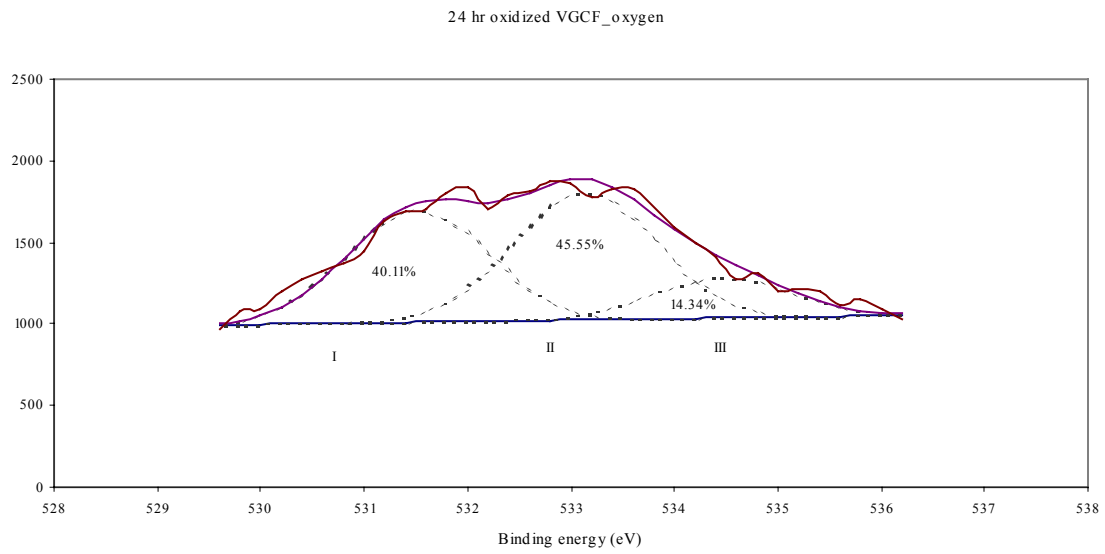

Figure 3.33 High resolution XPS O1s spectra of VGCF (oxidized for 24 hr) taken at a 30° take-off angle.

The XPS survey spectra of the various VGCFs are shown in Figures 3.34 to 3.42. There was a 3-fold increase in the surface O1s functional groups of the oxidized VGCFs compared to unoxidized VGCFs (from 6.3 atom % to 21.2 atom %). Nitric acid oxidation produces more oxygen containing groups on the surface. This increase was not continuous and dropped somewhat to 14.4 atom % for VGCFs, which were oxidized for 24 h.

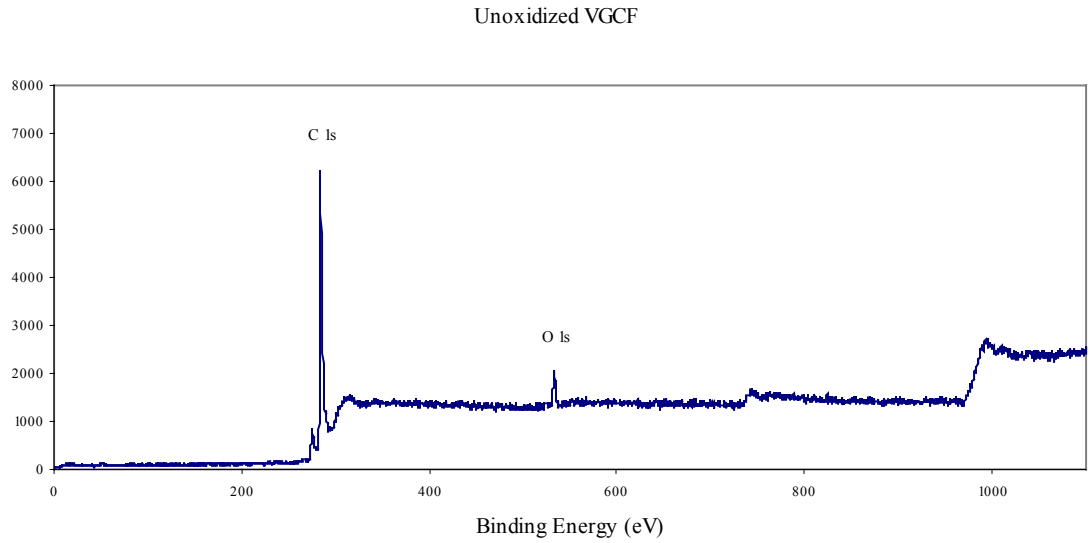

Figure 3.34 XPS survey spectra of unoxidized VGCF taken at a 30° take-off angle.

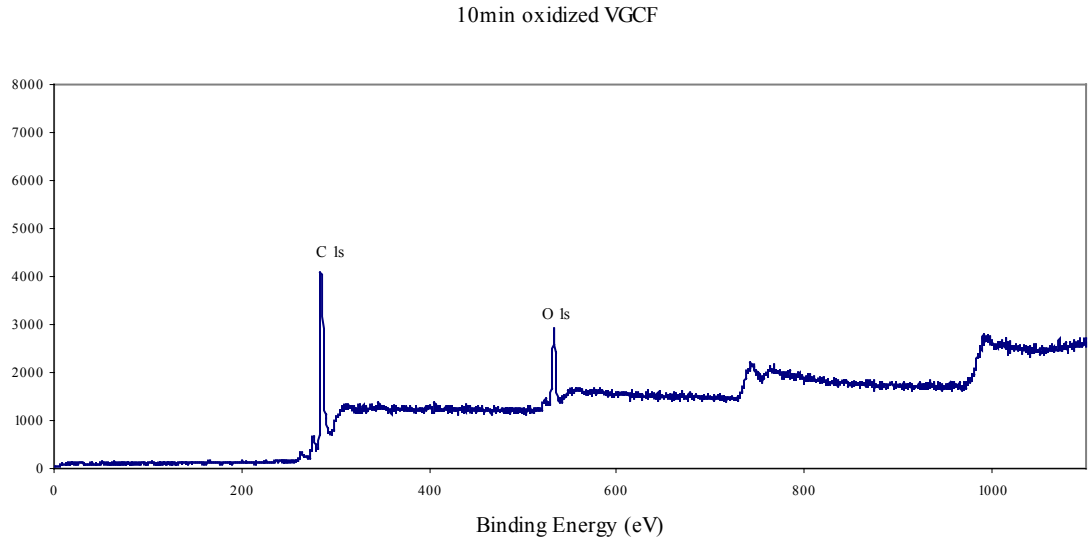

Figure 3.35 XPS survey spectra of VGCF (oxidized for 10 min) taken at a 30° take-off angle.

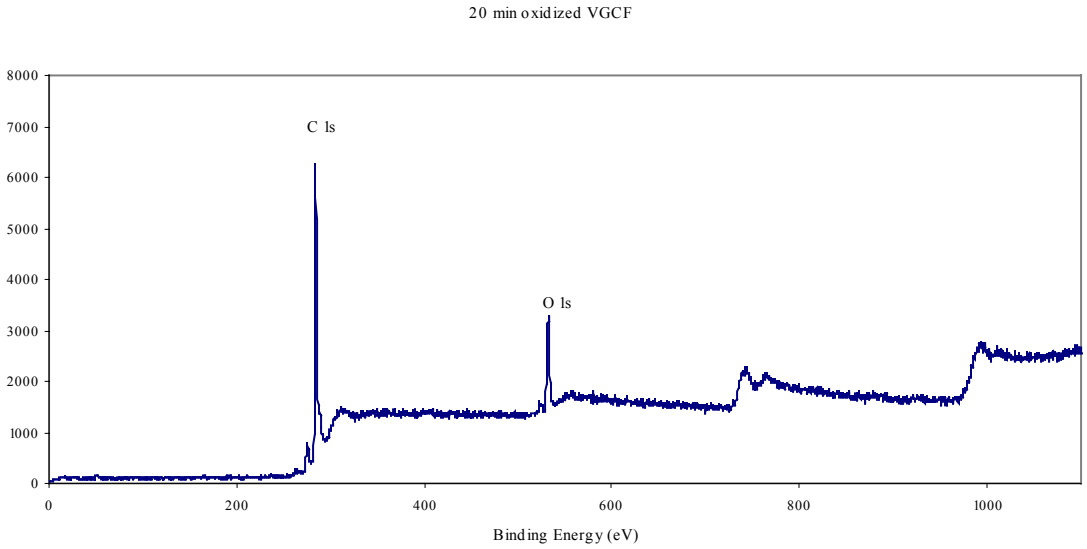

Figure 3.36 XPS survey spectra of VGCF (oxidized for 20 min) taken at a 30° take-off angle.

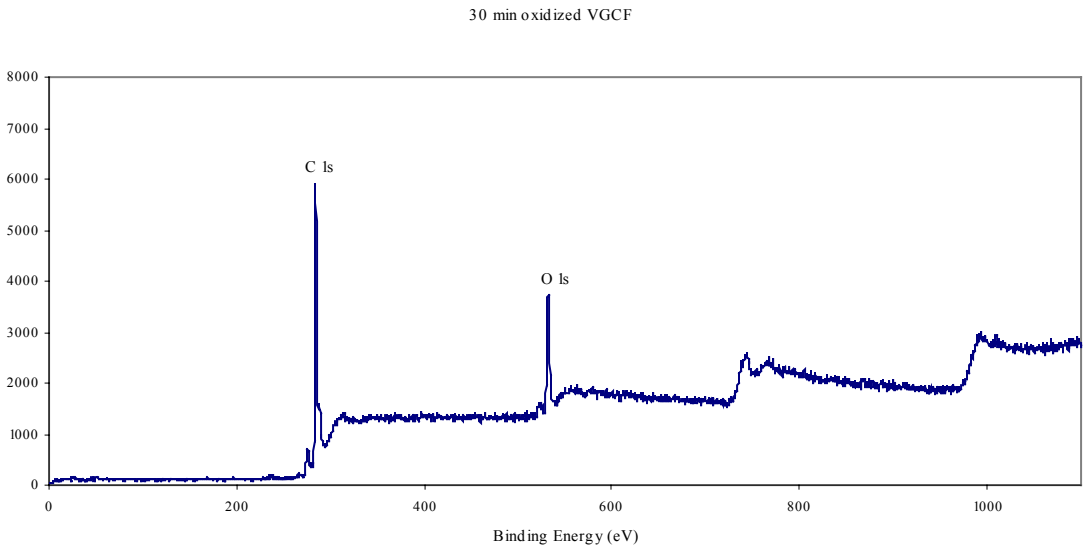

Figure 3.37 XPS survey spectra of VGCF (oxidized for 30 min) taken at a 30° take-off angle.

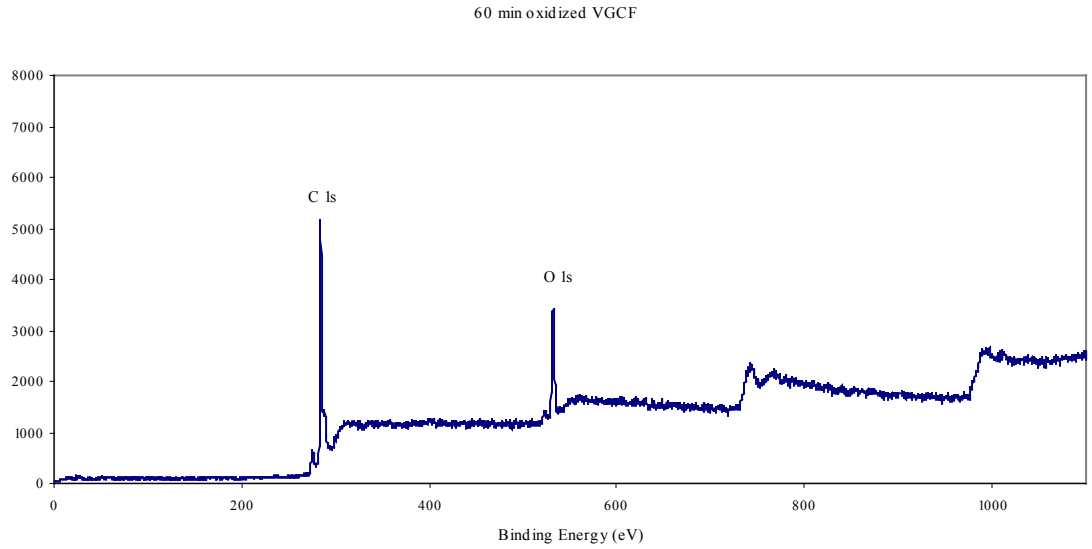

Figure 3.38 XPS survey spectra of VGCF (oxidized for 60 min) taken at a 30° take-off angle.

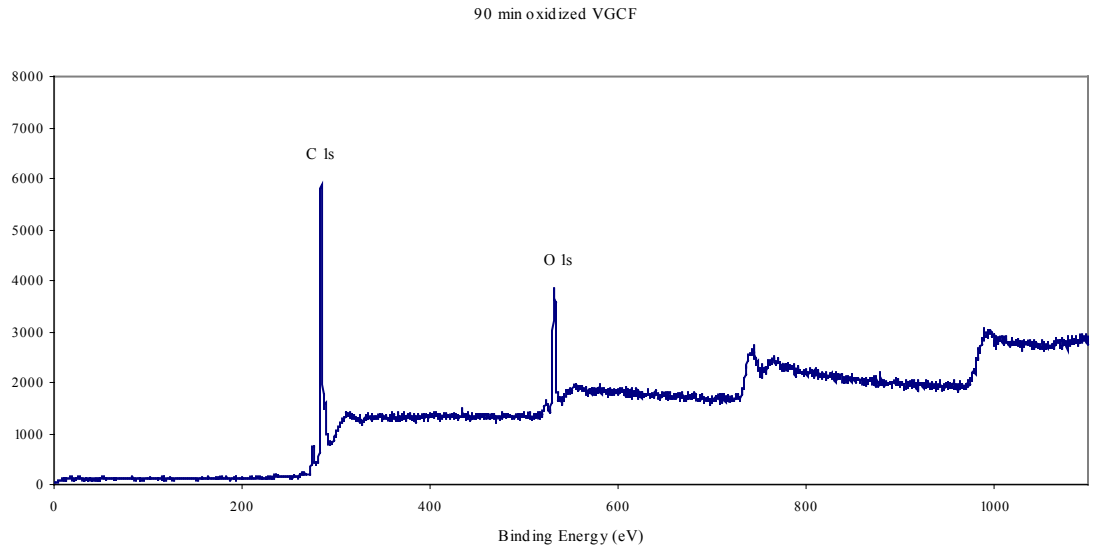

Figure 3.39 XPS survey spectra of VGCF (oxidized for 90 min) taken at a 30° take-off angle.

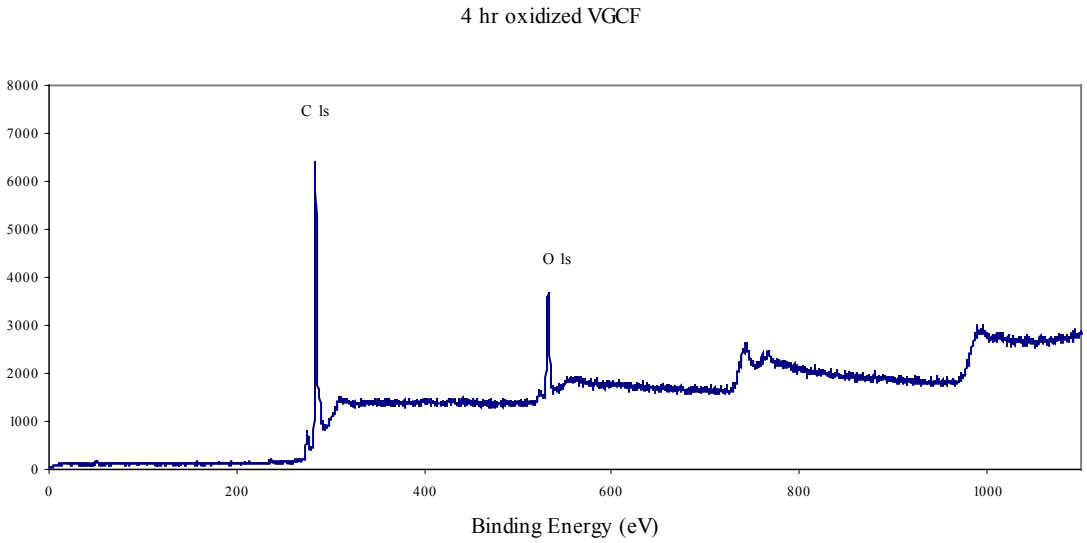

Figure 3.40 XPS survey spectra of VGCF (oxidized for 4 hr) taken at a 30° take-off angle.

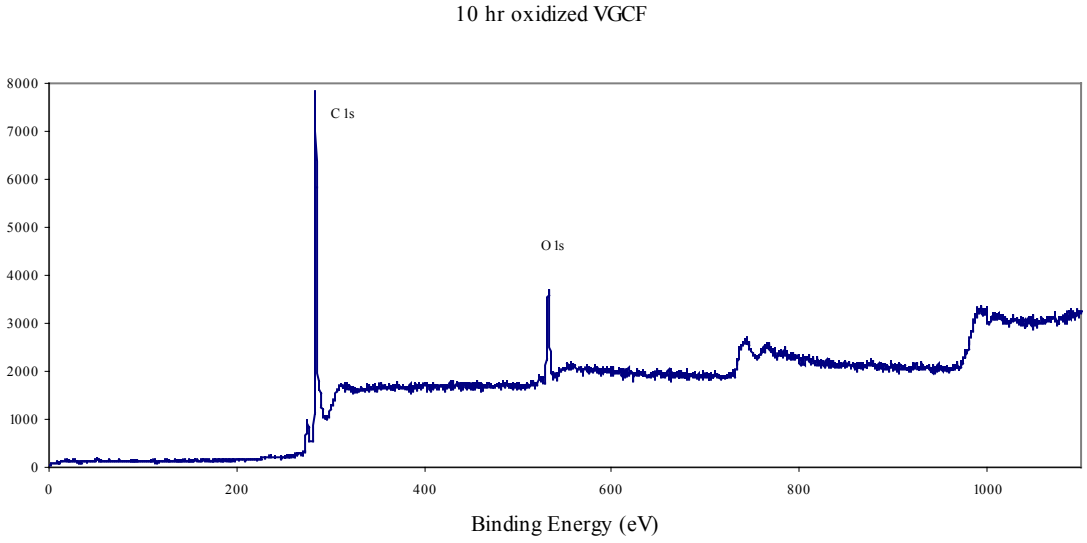

Figure 3.41 XPS survey spectra of VGCF (oxidized for 10 hr) taken at a 30° take-off angle.

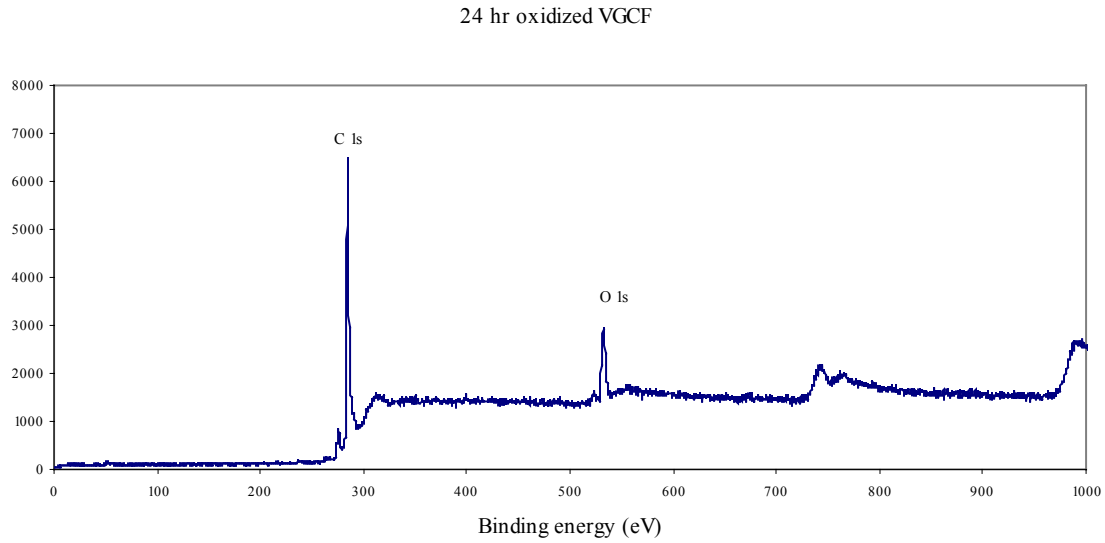

Figure 3.42 XPS survey spectra of VGCF (oxidized for 24 hr) taken at a 30° take-off angle.

Scanning Electron Microscope (SEM) studies

SEM pictures were taken using Leo/Leica/Cambride S360 SEM. Figure 3.43 shows the fractured end of an unoxidized VGCF/Epoxy resin composite. One can see the ends of the VGCFs at the fractured end. Figure 3.44 shows the same sample at a magnification of 10 K. Figure 3.45 shows a press-molded surface picture of the same unoxidized VGCF/Epoxy resin composite. The three-dimensional random arrangement of the VGCFs is obvious from these pictures. Figure 3.46 shows the fractured end of a composite sample containing VGCFs, which has been oxidized for 20 minutes. Figures 3.47 and Figure 3.48 show the fractured end of a VGCF (oxidized for 90 min)/epoxy resin composite. Figure 3.48 is taken at a higher magnification (10K) compared to Figure 3.47 (2.14K magnification).

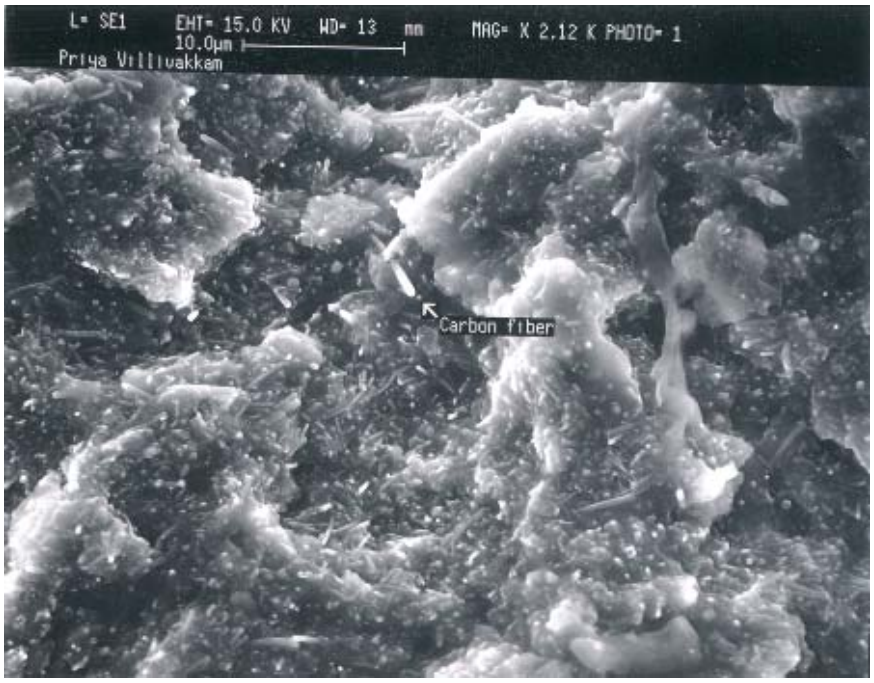

Figure 3.43 The fractured end of an unoxidized VGCF/Epoxy resin composite.

Figure 3.44 The fractured end on unoxidized VGCF/Epoxy resin composite at a magnification of 10K.

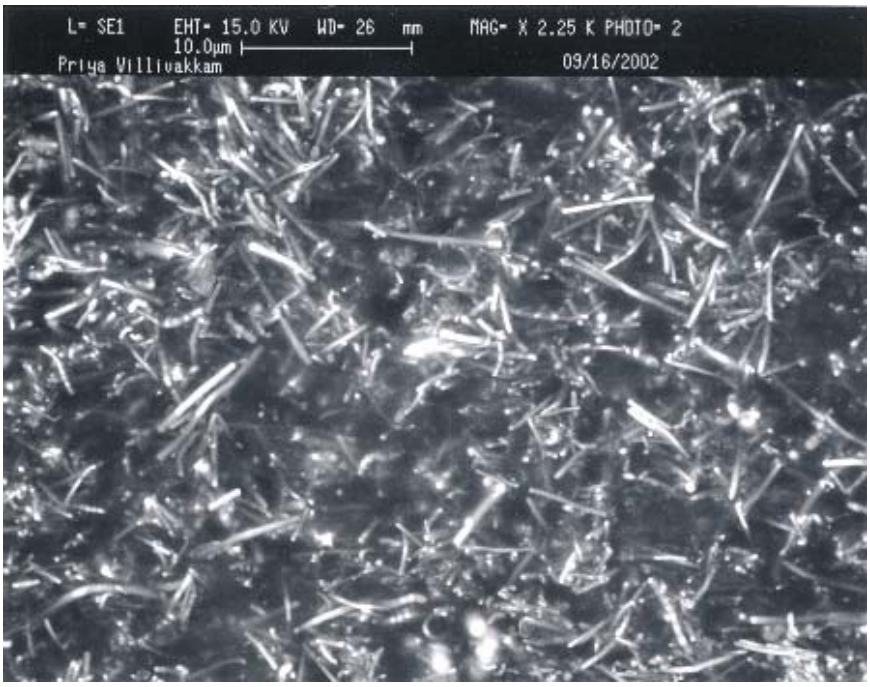

Figure 3.45 The press molded surface picture of the same unoxidized VGCF/Epoxy resin composite.

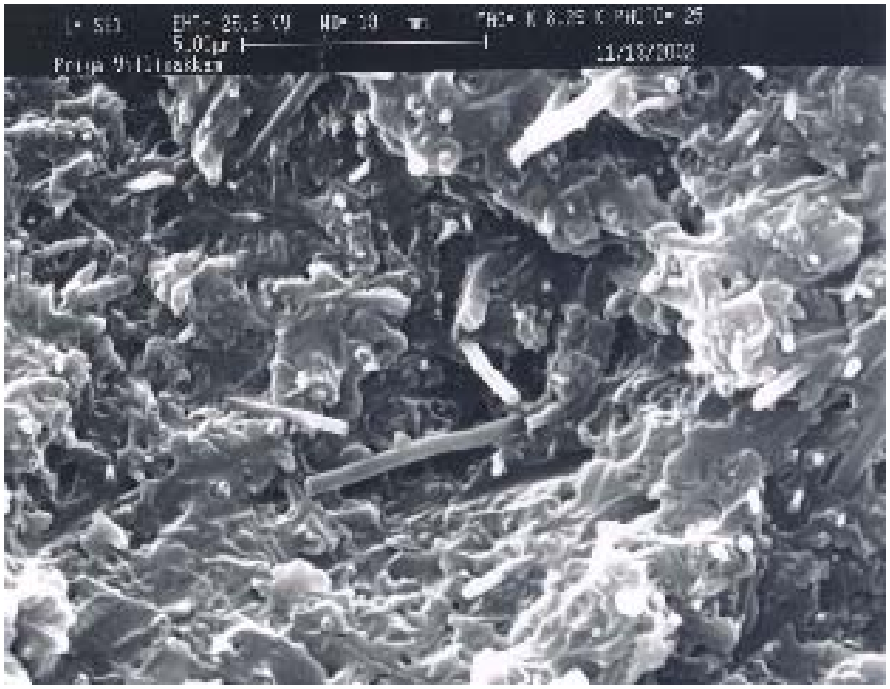

Figure 3.46 The fractured end of a VGCF (oxidized for 20 min)/epoxy resin composite.

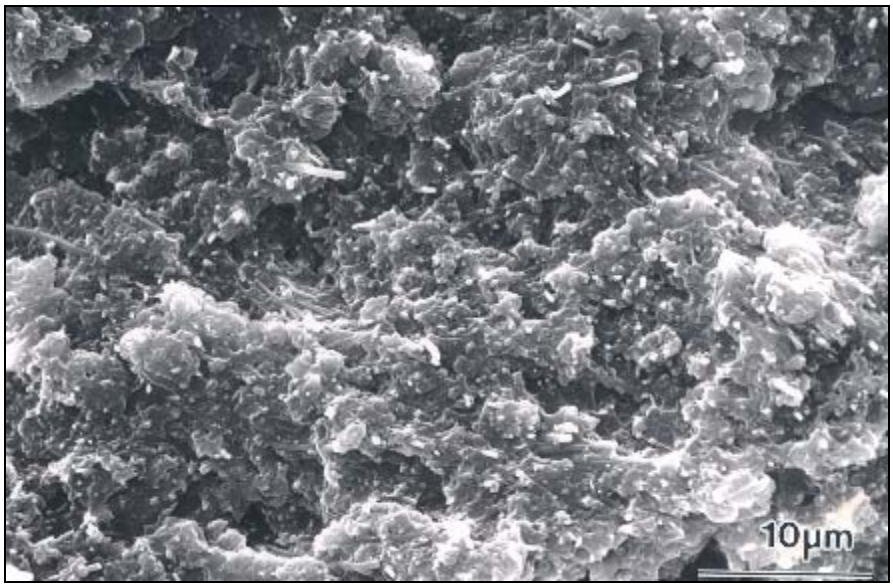

Figure 3.47 The fractured end of a VGCF (oxidized for 90 min)/epoxy resin composite at a magnification of 2.14 K.

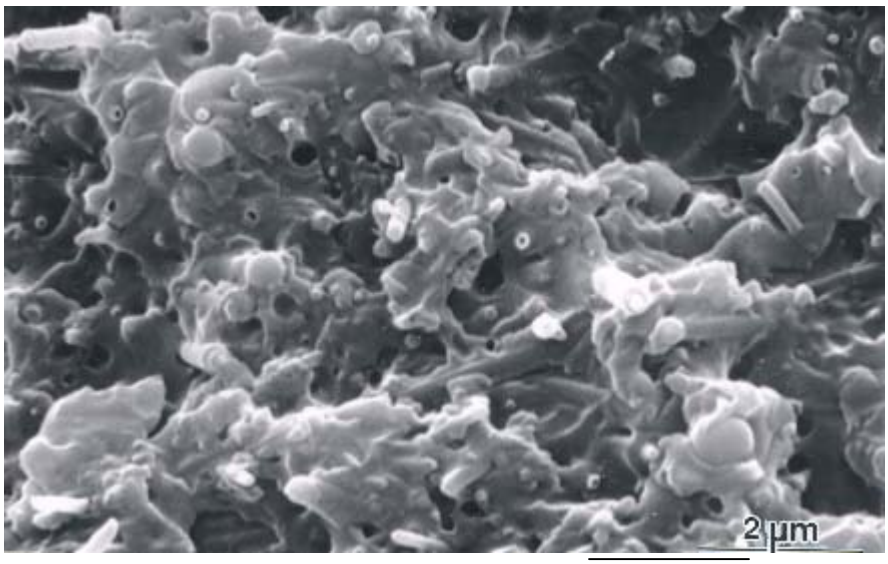

Figure 3.48 The fractured end of a VGCF (oxidized for 90 min)/epoxy resin composite at a magnification of 10 K.

Comparing the composite containing unoxidized VGCFs (Figure 3.43) with a composite made from oxidized VGCFs (Figure 3.47) demonstrates that fiber pullout was much more prominent with unoxidized VGCF (Figure 3.43). This is clearly seen when the magnification was increased to 10 K (Compare Figure 3.44 with Figure 3.48). In the unoxidized VGCF/epoxy resin composite, the fibers were randomly distributed in the matrix resin as nested groups. The adhesion between the fibers and the resin was limited. However, oxidation caused the further introduction of oxygen-containing surface functional groups, which altered the fiber-resin interface interaction and contributes to the improvement in adhesion of the oxidized fibers to the resin. The bonding strength between carbon fibers and resins does not depend on chemical bonds alone [41] but also depends on dispersion forces and mechanical interlocking of the fibers. The failure mode of the composite depends strongly on the fiber surface treatment. Untreated VGCFs failed by frictional debonding and pull-out from within the epoxy matrix (Figure 3.49a) whereas in the oxidized VGCFs, the adhesion between the fibers and resin was so strong that the matrix failed perpendicular to the fiber axis (Figure 3.49b). The fiber pull out in the unoxidized fiber-containing composite was much greater than that of the oxidized fiber-containing composite. Also there was less epoxy resin present on the pulled out fibers (unoxidized) compared to those fewer oxidized fibers, which were observed to extend from the matrix in composites made with oxidized VGCF. Figure 3.46 gives further evidence of a better adhesion between the oxidized VGCFs and the polymer matrix. TEM studies show how the fibers are distributed in all directions within the resin.

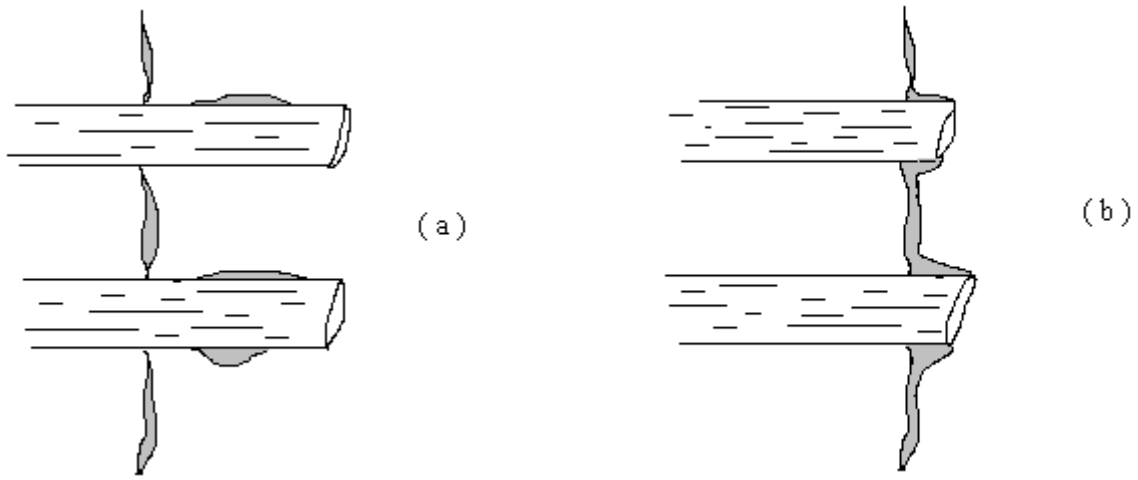

Figure 3.49: Schematic representation of the fractured surface of: a) An unoxidized VGCF-containing composite b) An oxidized VGCF-containing composite.

Transmission Electron Microscope (TEM) studies

TEM pictures were taken using a JOEL JEM-100CX II TEM. All the composite samples shown here contained only 5-weight % of fibers. Composites containing 19-volume % of fibers (equal to 29.4 weight % of fibers) proved too hard to cut using the glass and diamond knives available at the TEM center. Figure 3.50 shows a clump of unoxidized VGCFs. The fibers are entangled and have some surface-to-surface attractions. Overall it is clear that they are both tangled and held together like a 'bird's nest'. This nesting is an important variable when blending fibers with polymers or resins, making it difficult or, perhaps, nearly impossible to completely disperse VGCF in a random fashion. Figure 3.51 clearly shows a bamboo morphology for some of these fibers (unoxidized VGCF). This morphology has often been observed [96,97] and is mixed with cylindrical fibers, which can be rather linear or curved or corkscrew-shaped.

Figure 3.52 shows an unoxidized VGCF/Epoxy resin composite at a magnification of 2000X. As is evident from the picture, the fibers were not evenly distributed throughout the resin matrix. Instead, higher fiber concentration nests or clumps were observed. However, these clumps were clearly infused with resin. Other regions of the resin showed lower fiber concentrations and the nested, fiber-rich regions were not uniformly distributed within the epoxy resin. Figure 3.53 shows a VGCF (oxidized for 30 min)/epoxy resin composite at a magnification of 1400X. At this lower magnification several nest-like regions were evident. These nests ranged from ~ 5 to 45 μm in diameter. The clumps of fibers seen here further prove that an uneven distribution of the fibers existed at the microscale in the epoxy resin matrix. At the macroscale, the fiber distribution would appear to be homogeneous.

Figure 3.54 shows a single strand of a VGCF (oxidized for 20 min) at a magnification of 20,000X. Figure 3.55 shows the finer details within the fibers. The hollow nature of the VGCFs can be seen in these TEMs (Figure 3.51 and Figure 3.52). This TEM photograph was developed on zooming further into the strand of fiber shown in Figure 3.54.

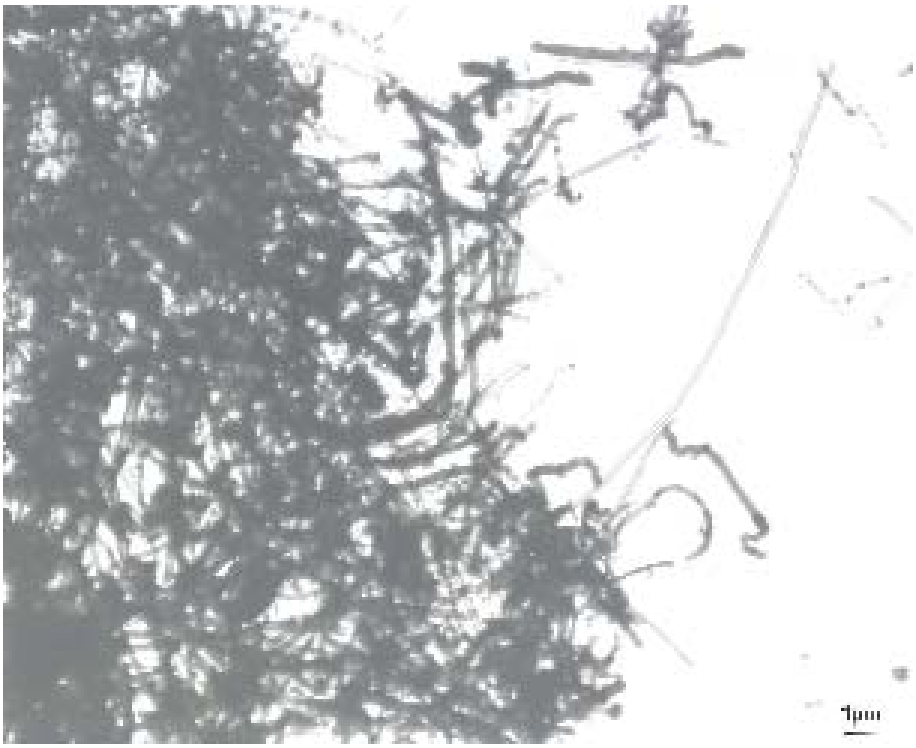

Figure 3.50 A clump of unoxidized VGCFs. Magnification is 2000X.

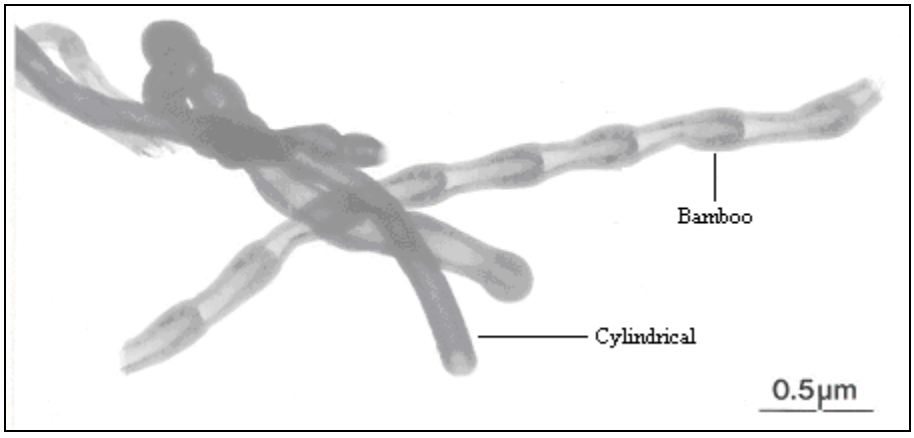

Figure 3.51 The bamboo vs cylindrical morphology of unoxidized VGCF. Magnification is 20000X.

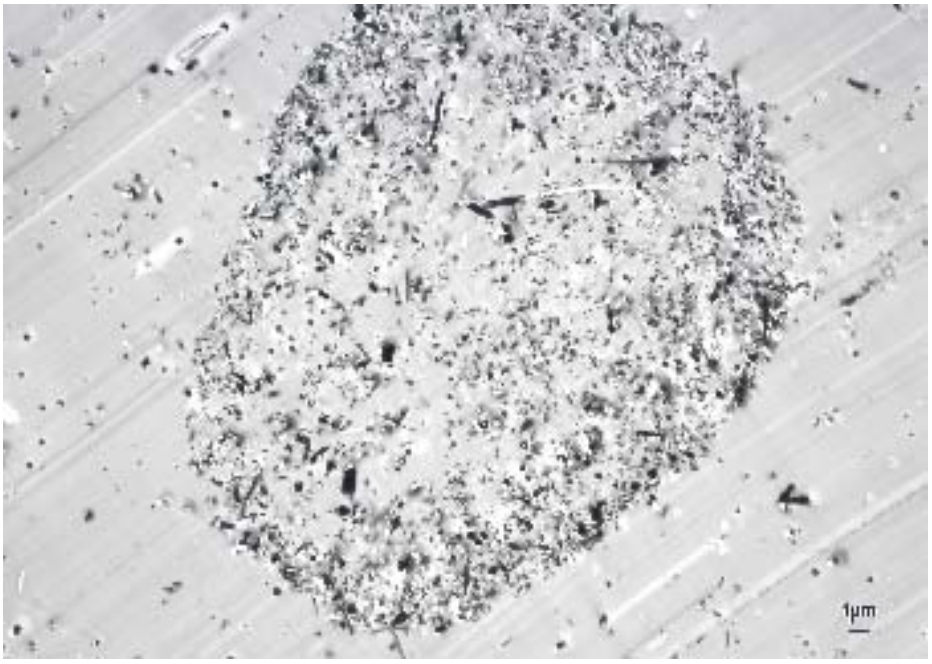

Figure 3.52 Unoxidized VGCF/Epoxy resin composite. A nest region with high concentration is present in matrix with a surrounding region of lower fiber density. Magnification is 2000X.

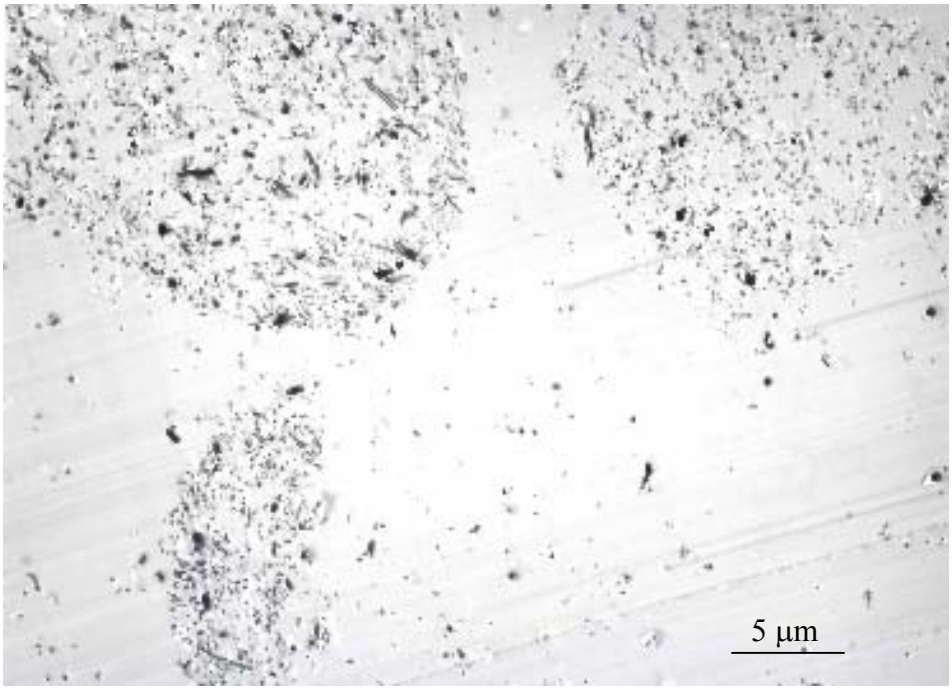

Figure 3.53 VGCF (oxidized for 30 min)/epoxy resin composite. Several nested regions

are evident. Magnification is 1400X.

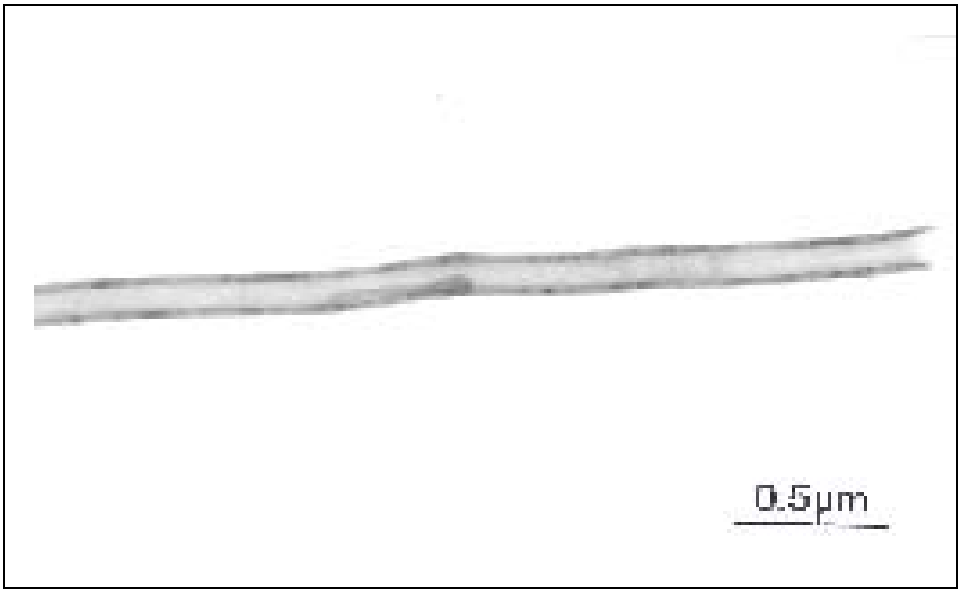

Figure 3.54 A single strand of a VGCF oxidized for 20-minute showing the hollow center of the fiber. Magnification is 20,000X.

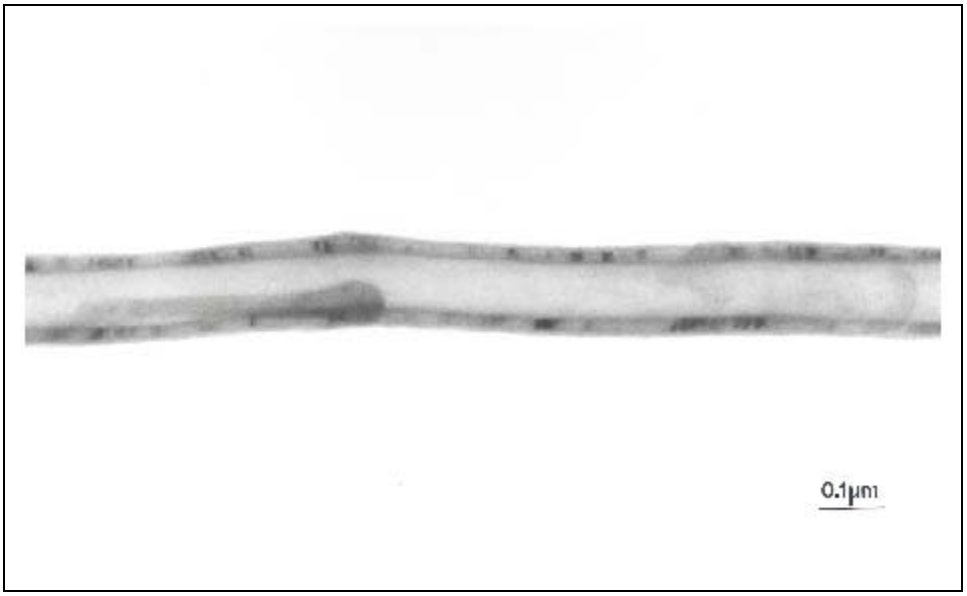

Figure 3.55 Finer details within the fibers are visible. Magnification is 20000X.

Electromagnetic interference (EMI) shielding measurements

Electromagnetic interference shielding measurements were made by Mr. Jun Xu on VGCF/ Derakane 411-45 vinyl ester type of composites. These measurements were performed to see how the EMI properties of vinyl ester/VGCF composite would differ if the fibers employed were oxidized (versus composites made with unoxidized VGCF). Oxidation creates a thicker layer of oxygenated carbon products on the surface. This, in turn, binds to resin. Thus, fiber-to-fiber contacts could involve a more insulating type of interaction through these surface regions, whereas unoxidized fibers may have contacts, which allow better electrical conductivity between fibers. Thus, the conductivity of equal wt% fiber composites containing unoxidized fibers might be higher than those containing oxidized fibers. Thus, EMI differences may exist.

Vinyl ester/oxidized VGCFs (VGCFs oxidized for 90 min) composites were provided to Jun Xu. A Hewlett Packard 8753D Network Analyzer was employed for EMI studies. Figure 3.56 shows the electric and magnetic field losses for unoxidized VGCF/ Derakane 411-45 vinyl ester composites containing 7-weight % fiber loading. Figure 3.57 shows the electric and magnetic field losses for the corresponding VGCF (oxidized for 90 min)/Derakane 411-45 vinyl ester composite containing 7 weight % fiber loading. A decrease in the shielding effectiveness up to almost 400 MHz was observed in the VGCF (oxidized for 90 min)/Derakane 411-45 vinyl ester composite. Figure 3.58 shows the electric and magnetic field losses for unoxidized VGCF/ Derakane 411-45 vinyl ester composite containing 15-weight % fiber loading. Figure 3.59 shows the electric and magnetic field losses for a VGCF (oxidized for 90 min)/ Derakane 411-45 vinyl ester

composite containing 15-weight % fiber loading. These results also showed a decrease in shielding effectiveness in the VGCF (oxidized for 90 min)/Derakane 411-45 vinyl ester composite.

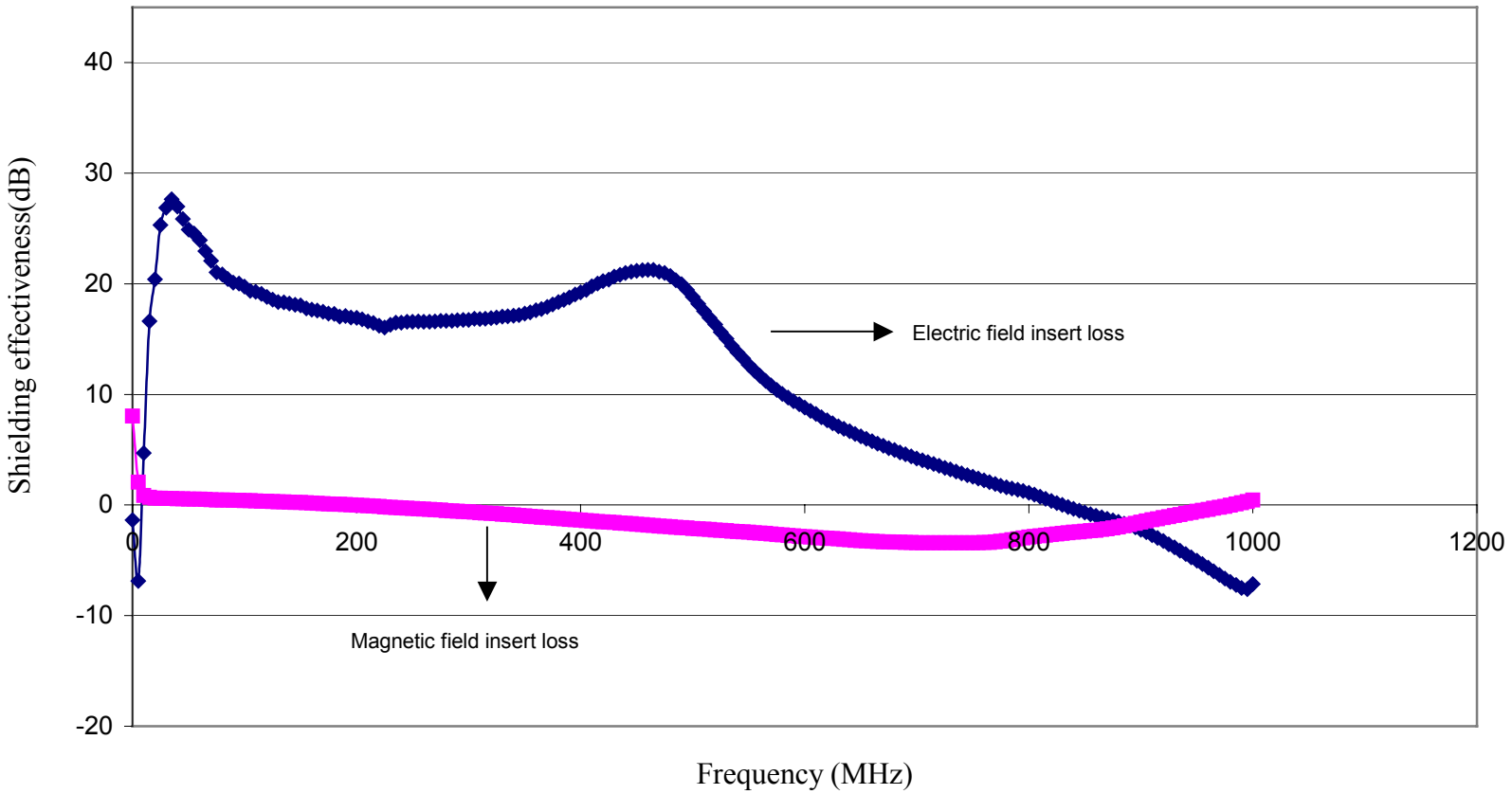

Figure 3.56 Electric and magnetic field losses for unoxidized VGCF/Derakane 411-45 vinyl ester composites containing 7-weight % fiber loading.

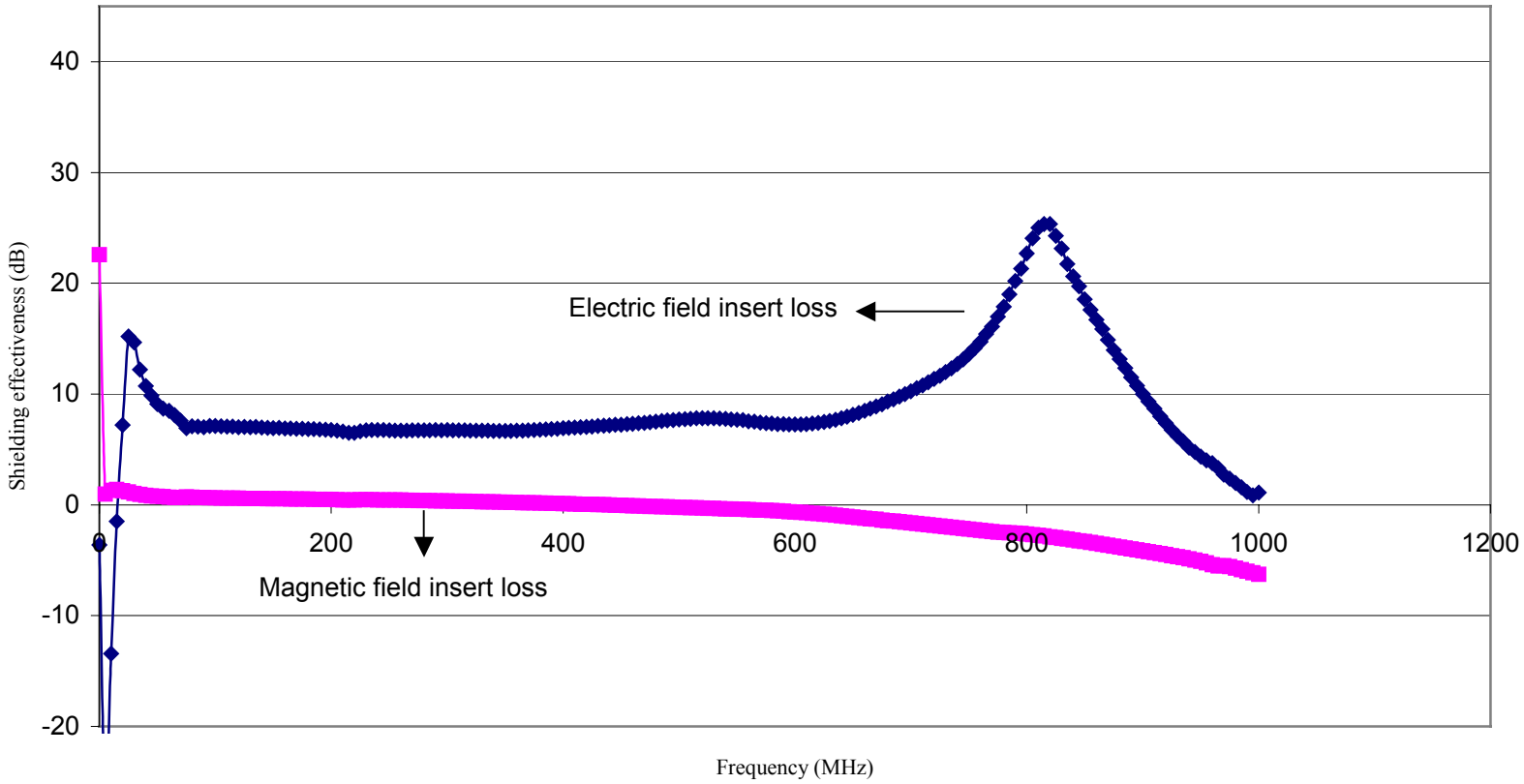

Figure 3.57 Electric and magnetic field losses for VGCF (oxidized for 90 min)/Derakane 411-45 vinyl ester composites containing 7 weight % fiber loading

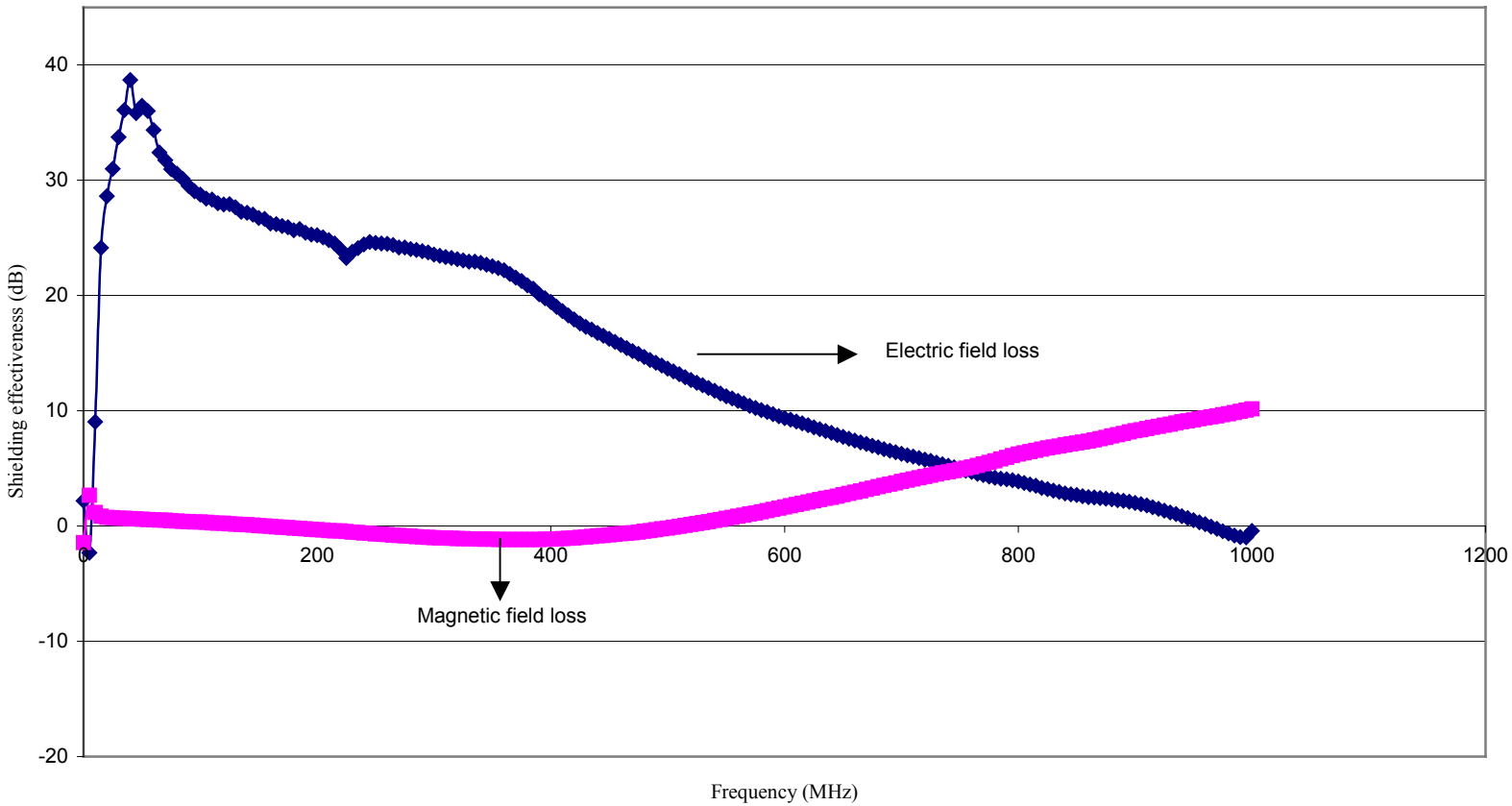

Figure 3.58 Electric and magnetic field losses for unoxidized VGCF/ Derakane 411- 45 vinyl ester composites containing 15-weight % fiber loading.

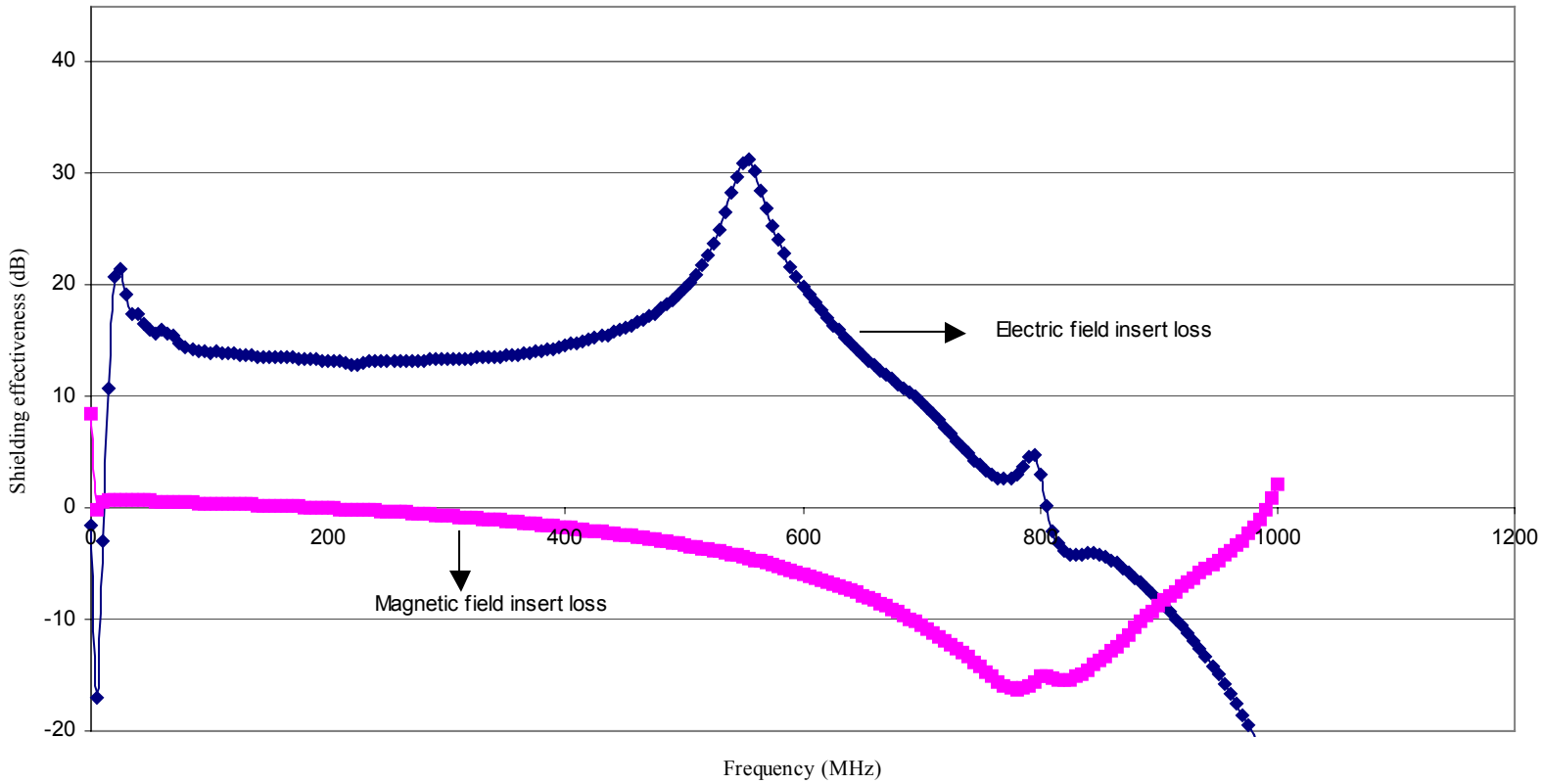

Figure 3.59 Electric and magnetic field losses for VGCF (oxidized for 90 min)/Derakane 411-45 vinyl ester composites containing 15 weight % fiber loading.

The volume electrical resistivities of these samples are compared in Table 3.12. A huge difference in the resistivities of the samples with oxidized fibers is clear. Their resistivities are ~ 10^{13} higher than when the unoxidized fibers were used at the same weight %.

Table 3.12 Volume electrical resistivities of VGCF/Derakane 411-45 vinyl ester composites.

Sample ID	Volume electrical resistivities (Ω cm)
Unoxidized VGCF/ Derakane 411-45 vinyl ester composites containing 7-weight % fiber loading	3.83×10^{2}
VGCF (oxidized for 90 min)/Derakane 411-45 vinyl ester composites containing 7-weight % fiber loading	9.02×10^{15}
Unoxidized VGCF/ Derakane 411-45 vinyl ester composites containing 15-weight % fiber loading	7.41×10^{1}
VGCF (oxidized for 90 min)/Derakane 411-45 vinyl ester composites containing 15-weight % fiber loading	7.4×10^{14}

These results prove that the nitric acid oxidation of VGCFs caused the fibers to act as ‘insulators’ when dispersed in the cured resin. These oxidized fibers acted as if they had an insulating layer present on their surfaces which prevented the electron transfer between the fibers present in the matrix. Hence, the unoxidized fiber-containing composite exhibited a higher shielding effectiveness. The research on the EMI shielding effectiveness measurements is the subject of the MS thesis of J.Xu [82].

CHAPTER IV

CONCLUSIONS

VGCFs (PR-19-PS) have been oxidized in 69-71 wt% nitric acid (115°C) for various times (10 min to 24 h). Composites containing 19.2 volume percent (29.4 weight percent) of VGCFs were prepared and their flexural properties were measured. Flexural moduli and strengths did not change much when oxidized fibers were used. The maximum value of flexural strength was obtained using VGCFs oxidized for 30 min. The scatter in the moduli/strength data could be due to the significant number of voids present as indicated by void content measurements. Voids serve as stress concentration sites, acting as classical defects in the structure. The acidic functionality values obtained (calculated with the corresponding pH value of the blank solution at various time intervals) for fibers oxidized for various times were similar and showed little difference. However, the acidic capacity of the unoxidized fibers was less than that of the oxidized fibers. Surface wetability increased after oxidation based on their dispersion behavior when shaken with water.

Increasing the oxidation time gave only a small increase in fiber surface area to a limit (from 20.74 m^2/g for the unoxidized fibers to 25.78 m^2/g for fibers oxidized for 90 min) during N_2 BET measurements. Even after 10 h of oxidation, the surface area was not changed much (34.59 m^2/g for N_2 BET and 24.01 m^2/g for CO_2-DR). Larger surface area changes, from 20.95 m^2/g for unoxidized fibers to 67.47 m^2/g for fibers oxidized for

90 min, were obtained by CO_2 DR measurements. Surface areas from CO_2 DR were greater than N_2 BET suggesting some small size pores existed (<1 nm in diameter). Significant oxygen-containing surface functionality was present before oxidation and the amount of oxygen content increased initially with increasing nitric acid oxidation. The increase in surface area (as noted by our CO_2-DR measurements but not by Quantachrome's), the increase in acidic functions and the increase in surface oxygen atom percentage all occurred very rapidly (~10 min) during nitric acid oxidation at 115 ^{o}C. Beyond that period, further changes were minor. This is a sharp contrast to the behavior of PAN-based fibers.

Oxidation caused the disappearance of the O1s XPS peak IV (oxygen atoms in carboxyl groups) and the appearance of peak II (carbonyl oxygen atoms in esters, anhydrides and oxygen atoms in hydroxyls or esters). The amount of esters/anhydride, quinone groups (peak II and peak III) increased compared to the unoxidized VGCFs. Table 4.1 shows a comparison of VGCF vs PAN-based fibers after nitric acid oxidation (115 ^{o}C).

Table 4.1 Comparison of VGCF vs PAN-based fibers after nitric acid oxidation.

Details	HNO_3 oxidized PAN fibers	HNO_3 oxidized VGCFs
Wetability of fibers in water	Exhibits good wetability on oxidation	Exhibits good wetability on oxidation
Fiber weight loss on oxidation	The weight loss increased with oxidation	No such increase was observed
Surface area by N_2 BET	Continuously increased on oxidation (29-fold increase after 105 min)	Slightly increased with the increase occurring in the first 10 min.
Surface area by CO_2 – DR	Greatly increased on oxidation (>10 fold) compared to unoxidized fibers	Modest increase suggested in first 10 min.
Oxygen content at surfaces by XPS	Showed small increase	Greatly increased (>3 fold)

The surface morphology of VGCFs is different from those of PAN based carbon fibers. The internal structure of the large (1 to 10μm dia), Pyrograf I^{TM}-type VGCFs resembles a tree trunk containing concentric rings of CVD pyrolytic carbon (Figure 1.3) with an outside layer showing a glassy fracture (without parallel lines) formed from the pyrolytic phase [95]. Small (~ 200 nm diameter) Pyrograf III^{TM}-type VGCFs exhibit a pyrolytic (turbostratic) outer layer of CVD-deposited carbon, which surrounds the central highly organized graphitic filament. This central filament is hollow and its walls are

composed of well organized parallel planes of graphite wrapped in cones along the fiber axis. These graphite planes intersect the hollow center of the fiber at a highly oblique angle. This same type of filament structure also exists in the Pyrograf I^{TM} fibers. However, the thickness of the surrounding CVD layer in these fibers is far greater than that of the Pyrograf III^{TM} fibers.

PAN-based fibers on the other hand consist of long primary stacked units of graphite sheets lying parallel to the fiber axis and separated by elongated pores. The sheets bend and twist in various ways, sometimes intersecting the fiber surface to expose lateral planes among the more dominant basal surface planes. These lateral planes are the sites of progressive oxidations, which eventually destroy, PAN fibers. In contrast, VGCFs are remarkably oxidation resistant. Apparently, no lateral plane oxidation can proceed very far below the surface. The turbostratic layer is a highly oxidation resistant morphology. Previous work on VGCFs by Darmstadt et al. showed that due to the small diameter (0.2 μm) of VGCFs, surface treatment on VGCFs influenced not only the surface but also the bulk chemistry and structure [33a]. However, it appears that the VGCFs are more resistant to oxidation (compared to PAN fibers).

Composites were prepared containing VGCFs and epoxy resin. Transmission electron microscope (TEM) studies showed that many of the VGCFs were nested together in specific domains within the resin matrix. Uniform dispersion of the fibers in the resin is a problem, which has to be overcome in the future to obtain better results. This may require high shear mixing in a twin-screw extruder or brabender or some other

special pre-dispersion methods. Another major problem is the three-dimensional random fiber orientation.

APPENDIX

ALL THE DATAS USED IN TABLES

APPENDIX

Three point bend test results

Composite ID	Flexural Modulus (MPa)	Flexural Strength (GPa)
Unoxidized VGCF/epoxy composite	5342.57 5173.90 7154.61	113.55 91.69 108.21
VGCF (oxidized for 10 min)/epoxy composite	6311.99 8639.66	84.54 103.87
VGCF (oxidized for 20 min)/epoxy composite	3589.38 5058.25 3292.47	93.07 111.51 97.45
VGCF (oxidized for 30 min)/epoxy composite	3151.10 4091.15 3498.82 3991.03	119.63 113.32 97.89 109.66
VGCF (oxidized for 60 min)/epoxy composite	6364.80 6356.01 7039.98	82.61 84.71 95.13
VGCF (oxidized for 90 min)/epoxy composite	4001.06 4682.28 5627.49	95.61 112.35 99.522

Base uptake values

The acidic capacities of the VGCF samples calculated with the pH value (11.28) of the blank solution at various time intervals

Sample ID	Time (hr)						
	1	2	3	4	7	12	24
Unoxidized	26.25	24.65	33.76	36.53	47.52	46.41	46.41
VGCF(10 min oxidized)	95.26	95.26	95.27	95.26	95.27	95.27	95.27
VGCF(20 min oxidized)	95.24	95.22	95.24	95.25	95.25	95.25	95.26
VGCF(30 min oxidized)	95.27	95.27	95.27	95.27	95.27	95.27	95.27
VGCF(60 min oxidized)	94.07	91.39	92.82	93.19	94.25	94.76	95.13
VGCF(90 min oxidized)	95.27	95.27	95.27	95.27	95.27	95.27	95.27
VGCF(4 hr oxidized)	95.27	95.27	95.27	95.27	95.27	95.27	95.27
VGCF(10 hr oxidized)	95.27	95.27	95.27	95.27	95.27	95.27	95.27
VGCF(24 hr oxidized)	95.27	95.27	95.27	95.27	95.27	95.27	95.27

Base uptake values

The acidic capacities of the VGCF samples calculated with the corresponding pH value of the blank solution at various time intervals.

Sample ID	Time (hr)						
	1	2	3	4	7	12	24
Unoxidized	26.25	22.48	27.4	26.17	33.34	26.82	21.77
VGCF(10 min oxidized)	95.26	93.09	88.9	84.9	81.08	75.67	70.62
VGCF(20 min oxidized)	95.24	93.05	88.87	84.89	81.06	75.66	70.61
VGCF(30 min oxidized)	95.27	93.1	88.91	84.91	81.09	75.68	70.63
VGCF(60 min oxidized)	94.07	89.22	86.47	82.83	81.07	75.17	70.48
VGCF(90 min oxidized)	95.27	93.1	88.91	84.91	81.09	75.68	70.63
VGCF(4 hr oxidized)	95.27	93.1	88.91	84.91	81.09	75.68	70.63
VGCF(10 hr oxidized)	95.27	93.1	88.91	84.91	81.09	75.68	70.63
VGCF(24 hr oxidized)	95.27	93.1	88.91	84.91	81.09	75.68	70.63

Void content and density measurements

Sample ID	Void Content (%)	Density (g/cc)
Unoxidized VGCF/Epoxy composite.	2.318	1.303
	2.318	1.303
	3.217	1.291
	2.543	1.300
	2.168	1.305
VGCF (oxidized for 10 min)/epoxy composite	2.617	1.299
	2.617	1.299
	2.393	1.302
	2.318	1.303
	2.318	1.303
VGCF (oxidized for 20 min)/epoxy composite	2.992	1.294
	2.018	1.307
	2.318	1.303
	2.468	1.301
	2.318	1.303
VGCF (oxidized for 30 min)/epoxy composite	2.543	1.300
	1.943	1.308
	1.943	1.308
	2.543	1.300
	2.243	1.304
VGCF (oxidized for 60 min)/epoxy composite	2.168	1.305
	1.493	1.314
	2.243	1.304
	1.793	1.310
	2.243	1.304
VGCF (oxidized for 90 min)/epoxy composite	1.943	1.308
	2.093	1.306
	1.718	1.311
	1.868	1.309
	2.168	1.305

CO_2 - DR surface area versus N_2 BET surface area

Sample ID	N_2 BET (m^2/g)		CO_2-DR (m^2/g)	
Unoxidized VGCF	20.74 21.81	38.02*	20.95 [d,*] 20.00 [d,*]	25.11 [b] 20.33 [a]
VGCF oxidized for10 min	22.96 23.57		58.99 60.09	
VGCF oxidized for 20 min	23.87 24.27		54.26 52.42	
VGCF oxidized for 30 min	28.18 27.33	23.01	68.00 66.73	73.53
VGCF oxidized for 60 min	24.98 24.97		42.24 41.36	
VGCF oxidized for 90 min	25.78 26.30		67.47 67.13	
VGCF oxidized for 10 h	34.59 [d]	34.63	24.01 [c,d] 22.22 [c,d]	33.25 [b] 26.92 [a]

[a] Surface area value obtained (at MSU) by assuming the cross sectional area of CO_2 to be 17 $Å^2$/molecule.
[b] Surface area value obtained (at MSU) by assuming the cross sectional area of CO_2 to be 21 $Å^2$/molecule.
[c] Surface area value obtained (at Quantachrome) by assuming the cross sectional area of CO_2 to be 17 $Å^2$/molecule.
[d] Surface area values obtained at Quantachrome.
* Surface area values for a different batch of VGCFs (PR-19-PS).

REFERENCES

[1] Hughes,T.V., and Chambers,C.R.,US Patent 405,480.

[2] Davies W.R., Slawson,R.J., and Rigby,G.R., *Nature*, **1953**, *171*, 756.

[3] Baker,R.T.K., and Harris,P.S. (1978) The formation of filamentous carbon, in Walker, P.L., and Thrower,P.A.,(eds.) *Chemistry and Physics of Carbon*, Dekker, New York, **1978**, *14*, 83-165.

[4] Hillert,M., and Lang,N. *Zeit.Krist.,***1958**, *111*, 24-34.

[5] Koyama,T. and Endo,M.,*O.Buturi*, **1973**, *42*, 690.

[6] Benissad,F., Gadelle,P., Coulon,M., and Bonnetain,L., *Carbon*, **1988**, *26*, 61-69.

[7] Tibbetts, G.G, *J.Cryst.Growth*, **1985**, *73*, 431-438.

[8] Koyama,T., and Endo,M., Japanese Patent No.1982-58, 966, **1983.**

[9] Hatano,M., Ohsaki,T., and Arakawa,K.,*Science of Advanced Materials and Processes*, **1985**, *30*, 1467-1476.

[10] Tibbetts, G.G, and Beetz Jr,C.P.,*J.Phys.D:Appl.Phys*., **1987**, *20*, 292-297.

[11] Oberlin.A., Endo.,M., and Koyama,T.,*J.Cryst.Growth*, **1976**, *32,* 335.

[12] Tibbetts, G.G., Endo, M., and Beetz C. P., Jr., *SAMPE J.*, **1986**, *22*, 30.

[13] Dresselhaus, M.S.,*Graphite Fibers and Filaments*, Springer-Verlag, New York: **1988**.

[14] Tibbetts, G.G, Doll,G.L., Gorkiewicz,D.W., Moleski,J.J., Perry,T.A., Dasch,C.J.,Balogh,M.J.,*Carbon*, **1993**, *31(7)*,1037-1047.

[15] Patton,R.D., Pittman,C.U., Jr., Wang,L., Hill,J.R., Day,A., *Composites Part A*, **1999**, *30(9)*,1081-1091.

[16] Madronero,A., Ariza,E., Verdu Brandl,M.W., Barda,C., *J Material Science*, **1996**, *31(23)*, 6189-6193.

[17] Benissad,F., Gadelle,P., Coulon,M., and Bonnetain,L.,*Carbon*, **1988**,*26*,425.

[18] Patton,R.D., Pittman,C.U., Jr., Wang,L.,*Proceedings of the 29th International SAMPE Technical Conference Series***, 1997,**77-87.

[19] Pittman,C.U.Jr., Wang,L., Patton,R.D., *Extended Abstracts of the 23rd Biennial Conference on Carbon*, **1997**, 298-299.

[20] *Chemical and Engineering News*, **1997**, *75(39)*, 23.

[21] Ruoff,R.S., Lorents,D.C.,*Carbon*, **1995**, *33(7)*, 925-930.

[22] Salvetat,J-P.,Bonard,J-M., Thomson,N.H., Kulik,A.J., Forro, L.,Benoit,W., Zuppiroli,L.,*Appl.Phys.A***, 1999**, *69*, 255-260.

[23] VanHattum, F.W.J., Serp,P., Figueiredo,J.L., Bernardo,C.A.,*Carbon*, **1997**, *35(6)*, 860-863.

[24] Chellappa.V.,Chiu,Z.W.,Jang,B.Z.,*Proceedings of the 26th SAMPE Technical Conference,* **1994**, *26*, 112-118.

[25] Shui,X.,Chung,DDL., *Proceedings of the 38th International SAMPE Technical Conference,* **1993**, 1869-1875.

[26] Ciminelli,D.L., Kearns,K.M., Ragland,W.R., *Proceedings of the 41st International SAMPE Symposium,* **1996**, 495-501.

[27] Kumar,S., Doshi,H., Srinivasarao,M., Park,J.O., and Schiraldi,D.A., *Polymer*, **2002,** *43*,1701.

[28] Patton,R.D., Pittman,C.U. Jr., and Wang,L., *Composites: Part A*, **1999**, *30A (9)*, 1081.

[29] Milewski,J., Handbook of Fillers and Reinforcement for Plastic, Van Nostrand Reinhold, New York: **1978**, 66.

[30] Tibbetts,G.G.,*Nato Science Series,Series E,Applied Sciences*, **2001**, 372.

[31] Mortensen,A., Masur,L.J., Cornie,J.A., and Fleming,M.C., *Metall.Trans.A*, **1989**, *20A*,2535-2547.

[32] Tibbetts,G.G., and McHugh,J.J., *Mater.Res.*, **1999**, *14*, 2871-2880.

[33] Darmstadt,H., Roy,C., Kaliaguine,S.,Ting, J-M. and Alig,R.L., *Carbon*, **1998,** *36(7-8)*, 1183-1190

[33a] Darmstadt,H., Summchen,L., Ting., J-M., Roland,U., Kaliaguine,S., and Roy,C., *Carbon*, **1997**, *35 (10-11)*, 1581-1585.

[34] Venner,J.G., *Kirk-Othmer Encyclopaedia of Chemical Technology*, John Wiley and Sons,Inc.,New York: **1992**, *1*, 1.

[35] Fitzer,E., and Weiss,R.D.V.I.,Verlag, **1981**, 45.

[36] Ishida,H.,*Interfaces in PolymerCeramic and Metal Matrix Composites*,Elsevier, New York, **1988**.

[37] Ishida,H,*Controlled Interphases in Composite Materials*, Elsevier,New York, **1990**.

[38] Plueddemann,E.P.,*Interface in Polymer Matrix Composites,* Academic Press, New York, **1974**.

[39] Donnet, J.B., and Bansal, R.C., *Carbon Fibers*,2nd edn., Marcel Dekker,New York: **1990**.

[40] Hughes,J.D.H., *Composite Sci.Technol.*, **1991**, *41*, 13.

[41] Yosomiya,R., Morimoto,K., Nakajima,A., Ikada,Y., and Suzuki,T.,*Adhesion and Binding in Composites*,Marcel Dekker,New York, **1990**.

[42] Fitzer,E.,Jaeger,H., and Weiss,R.,*Extended Abstracts Program-16th Biennial Conference,Carbon*, **1983**, 471-472.

[43] Subramanian,R.V., and Jakubowski,J.J., *Polym.Eng.Sci.,* **1978**, *18(7)*, 590.

[44] Subramanian,R.V., Sundaran,V. and Patel,A.K.,*33rd Annual tech.Conference*,Society of Plastics and Industrial,Reinforced Plastics Composites Institute, Section 20, **1978**,1-8.

[45] Bell,J.P., Chang,J., Rhee,H.W., and Joseph.R.,*Polym.Composites,* **1987**, *8(1)*, 46.

[46] Wimolkiatisak, A.S. and Bell. J.P.I, *J.Appl. Polym. Sci.*, **1992**, 46, 1899.

[47] Gerald,J.F., *Polym.Eng.Sci.*, **1988**, *28(9),* 568.

[48] Gardner,S.D., Singamsetty,C.S.K., Booth G., He,G.R.,Pittman,Jr.,C.U.,*Carbon*, **1995**, *33(5),* 587.

[49] Pittman, C.U., Jr., He,G.R., Wu,B.H., Wang, L.C. and Gardner,S.D.,*Proceedings of the International Conference on Composite Interfaces*,ICCI-V,ed.H. Ishida, Gotenborg, Sweden, **1994**, 19-2.

[50] Li,W., "Bonding diisocyanates and elastomeric interphases to surface functionalized carbon fibers.Effects of surface treatments on composites", M.S.Thesis, Mississippi State University,MS, **1995**.

[51] Wu,Z.,Pittman, C.U., Jr., Gardner,S.D.,*Carbon*, **1995**, *33(5)*, 604.

[52] Wu,Z.,Pittman,Jr.,C.U., Gardner,S.D.,*Carbon*, **1996**, *34(1)*, 59.

[53] Leon y Leon,C.A., Radovic,L.R., in *"Chemistry and Physics of Carbon"*, Thrower P.A.ed., Marcel Dekker, New York :1974, *124*, 213

[54] Donnet,J.B.*Carbon*, **1968,** *6*, 161.

[55] Donnet,J.B. and Bansal, R.C.*Carbon Fibers,* Marcel Dekker, Inc., New York, NY, **1984**, Chapter III

[56] Hughes,D.J. *Composites Science and Technology*, **1991**, *41*,13.

[57] Wu,Z., "Reactions on carbon fiber surfaces:Grafting small polymers and model compounds onto epoxide and carboxyl-functionalized fiber surfaces", MS Thesis, Mississippi State University, **1994**.

[58] IUPAC, International Committee for Characterization and Terminology of carbon, *Carbon*, **1982**, *20*, 445; **1983**, *21*, 517; **1985**, *23*, 601.

[59] Cooper,G.A., and Mayer,R.M.*J.Mater.Sci.,***1970**, *6*, 60.

[60] Marshall,P., and Price, *J.Composites,* **1991**, *22*, 338.

[61] Bennet,S.C. and Johnson,D.J,. *Proc. 5th London Carbon and Graphite Conf*, **1978**,*1*,337.

[62] Byrne,J.F., and Marsh,H., in *"Porosity in Carbon: Characterization and Applications"*, J.W.Patrick, Halsted Press, Great Britain, **1995**, Chapter I.

[63] Marsh,H., *Carbon*, **1991**, *29*, 703.

[64] Darmstadt,H., Roy,C., Kaliaguine,S., Ting, J.M.,and Alig, R.L., *Carbon*, **1997,** *35(10-11)*,1581-1585.

[65] Serp.P.,Figueiredo,J.L., *Carbon*, **1997**,*35(5)*,675-683.

[66] Kowbel,W. and Shan,C.H., *Carbon*, **1990**,*28*,287-299.

[67] Gardner,S.D., Singamsetty,C.S.K., Booth,G.L., He.,G.R., Pittman,C.U., Jr., *Carbon*, **1995**,*33(5)*, 587-595.

[68] Polovina, M., Babic, B., Kaluderovic,B. and Dekanski,D., *Carbon*, **1997**, *35(8),* 1047-52.

[69] Zielke, U, Huttinger,K.J., and Hoffman,W.P., *Carbon, **1996**,* 34*, 983.*

[70] Purslow.D., *Composites*, **1986**, *17*, 289.

[71] Shorthall, J.B. and Yip.H.W.C. *J.Adhesion*, **1976**,*8*,155.

[72] Brunauer, S., Emmett, P.H., and Teller,E., *J.Am.Chem.Soc.,* **1938**, *60*, 309

[73] Dubinin,M.M., and Radushkevich,L.V., *Proceedings Academy of SciencesI,* USSR, **947**, *55*, 331.

[74] Dubinin,M.M. in *"Progress in Surface and Membrane Science",* Cadenhead,D.A.ed., Academic Press, New York, **1975**, *9*, 1

[75] Langmuir,I., *J.of Am.Chem.Soc.,* **1912**, *38*, 2221.

[76] Gregg,S.J. and Sing,K.S.W. *Adsorption,Surface Area and Porosity*,2nd edn, London: Academic Press, **1982.**

[77] Sing,K.S.W., Everett,D.H., Haul,R.A.W., Moscou,L., Pierotti,R.A., Rouquerol,J., and Siemieniewska,T., *Pure and App.Chem.*, **1985**, *57*, 603.

[78] ASTM D 790-92 standard test method for the flexural properties of unreinforced and reinforced plastics and electrical insulating materials, **1978**, 66.

[79] Jiang, W., "Electrochemical oxidation of carbon fibers: Properties, surface chemistry and morphology", Ph.D Dissertation, Mississippi State University, **1999**,15

[79a] Pittman, C.U., Jr., Jiang,W., Yue,Z.R., Leon y Leon, C.A., *Carbon*, **1999**, *37*, 85-96.

[80] Dubinin, M.M., *Chemistry and Physics of Carbon*, 2, Marcel Dekker, New York, **1996**, 51.

[81] Marsh, H., and Rand, B., *J. of Colloid Interface Sci.,* **1970**, *33*, 101.

[82] Xu,J., "Electrical and electromagnetic interference (EMI) shielding properties of vapor grown carbon fiber (VGCF) composites",M.S Thesis, Mississippi State University, **2003**.

[83] Moulder,J.F., Stickle,W.F., Sobol,P.E., and Bomben,K.D., in *Handbook of X-ray photoelectron spectroscopy,* Chastain, J.ed, Perkin-Elmer corporation, Eden Prairie,MN, **1992**, 183.

[84] Scanning electron microscopy course E8223, Fall 2002.

[85] Transmission electron microscopy course E8144, Spring 2002.

[86] Bernhard,K.E. "Principles of Electromagnetic Compatibility," Artech House, Inc Dedham, Massachusetts, **1983**.

[87] Chung, D. D. L., *Carbon***, 2001**, *39*, 279-286.

[88] Kodali, V. P., "Engineering Electromagnetic Compatibility: Principles, Measurement, and Technology," Institute of Electrical and Electronics Engineers, Inc., New York, **1996.**

[89] Paul, C.R., "Introduction to electromagnetic compatibility," John Wiley & Sons, Inc., New York, **1992**.

[90] Dixon, D. S. ,Masi, J.,*Proceedings of the IEEE International Symposium on Electromagnetic Compatibility,* Denver, CO, **1998**,1035-1040.

[91] Thomas, C.R., *Proc.5th Con. On Carbon and Graphite,* **1978**, *1*, 520.

[92] Fitzer, E., *Carbon*, **1975**, *13*,149.

[93] Koresh, J.E., Kim, T.H., Walker, D.R.B., and Koros, W.J., *J. of the Chemical Society, Faraday Trans.*, **1989**, *85*, 4311.

[94] Marcilla-Gomis,A., Garcia-Cortes, A.N and Martin-Martinez, J.M., *Carbon,* **1996**, *21*,1531.

[95] Madronero, A., Ariza, E., Verdu, M., Brandl, W., Barda, C., *J Mater. Sci.*, **1996**, *31(23)*, 6189-6193.

[96] Baird,T., Fryer,J.R., Grant, B., *Nature (London)*,**1971**, *233*, 329.

[97] Baird,T., Fryer,J.R., Grant, B., *Carbon*, **1974**, *12*, 591.

[98] Nguyen,C., Do,D.D., *Carbon*, **2001**, *39*, 1327-1336.